LAKEHEAD UNIVERSITY
DEPARTMENT OF NATURAL RESOURCE MANAGEMENT

Long-term relationship between soil carbon dynamics, hydrology, and microbiome in peatlands around North America's largest historical point source pollutant of toxic metals, metalloids, and sulfur (Sudbury, Ontario, Canada)

BY
SAMANTHA MITCHELL

Submitted in partial fulfillment of the degree of
MASTERS OF SCIENCE IN NATURAL
RESOURCE MANAGEMENT – FORESTRY

COMMITTEE MEMBERS:
DR. FLORIN PENDEA (SUPERVISOR)
DR. NATHAN BASILIKO (SUPERVISOR)
DR. COLIN MCCARTER (COMMITTEE MEMBER)
DR. AMANDA DIOCHON (EXTERNAL EXAMINER)

Abstract

Peatlands are major long-term carbon (C) sinks whose stability depends on tightly coupled soil carbon dynamics, hydrology, and microbial communities, yet these relationships can be profoundly disrupted by industrial pollution. In the 1970s, Sudbury (Ontario) was North America's largest point source of sulfur dioxide (SO_2) and toxic metal and metalloid (TMM) emissions, generating a deposition gradient that provides a natural experiment for examining the long-term consequences of atmospheric contamination on peatland ecosystems. Using radiocarbon-constrained peat cores from three poor fen sites - two proximal to the smelter centre (Laurentian, Transplant), one distal (Cartier) - this thesis integrates high-resolution geochemical analyses and paleoecological reconstruction to evaluate how industrial disturbance altered carbon accumulation and restructured microbial assemblages.

Geochemical profiles (Corg, Cinorg, N, S, Ca, P, and nine key metals/metalloids) reveal distinct smelter-derived signatures, including pronounced enrichments of Cu, Ni, Pb, As, Cd, Zn, and S at or below the Industrial Isochron (1880–1975 CE), accompanied by Ca depletion and coincident increases in N and P. Long-term apparent rates of carbon accumulation (LARCA) show a paradoxical response: heavily polluted fens exhibit industrial-era peaks in apparent C accumulation but lower Holocene-scale mean LARCA relative to a minimally impacted site with intact *Sphagnum* cover, indicating a cumulative long-term carbon deficit attributable to enhanced decomposition and export from older catotelm strata. Stratigraphic and geochemical evidence suggests vertically divergent effects of pollution, including suppressed microbial decomposition and enhanced apparent C preservation in shallow horizons under extreme metal–acid stress, coupled with enhanced decomposition and C loss in deeper peat driven by acidification, sulfate migration, and destabilization of humic-Fe-S complexes.

Stratigraphically constrained cluster analysis (CONISS), canonical correspondence analysis (CCA), variation partitioning, permutational multivariate analysis of variance (PERMANOVA), and indicator species analysis were used to characterise microbial community change relative to geochemical gradients. Pre-industrial testate amoebae (TA) assemblages at all three sites were dominated by sphagnophilous taxa, particularly *Hyalosphenia subflava*, indicating long-term hydrological stability. Pronounced community restructuring coincident with the Industrial Isochron was evident at the two smelter-proximal sites, where disturbance-tolerant TA taxa (*Cyclopyxis arcelloides* type, *Centropyxis cassis* type, *Phryganella acropodia* type) displaced wet-affinity forms. The distal reference site exhibited comparatively muted change. Geochemical variables explained a significant proportion of total community variance (20%; CCA $p < 0.001$), with carbon composition emerging as the strongest unique predictor (adj. $R^2 = 0.057$), exceeding the independent contribution of toxic trace metals (adj. $R^2 = 0.019$). Critically, no discrete post-industrial recovery assemblage was detected at either proximal site: industrial-era taxa persist in surface samples and CONISS does not resolve a recovery zone distinct from the disturbance interval. These findings indicate that passive recovery following emission reductions has not reversed the microbial legacy of industrial contamination and that active restoration intervention may be required to re-establish pre-disturbance ecological conditions.

Keywords: Peatland degradation, Carbon dynamics, Industrial pollution, Testate amoebae, Community ecology, Paleoecology, Sudbury, Heavy metals, Ecosystem recovery, Smelter emissions

Acknowledgements

Over the past two and a half years I have been honoured to work with some incredible individuals, both on the ground in Sudbury and back in the lab in Orillia. I am grateful for the guidance, conversations, support, feedback and good times shared with everyone who has been a part of my master's experience. I want to specifically thank those who have offered feedback and guidance throughout my research; Dr. Colin McCarter, Dr. Peter Beckett, Dr. Pete Whittington, Dr. Ellie Goud. I also thank Dr. Amanda Diochon for the feedback and review of my manuscript.

I want to give a special thanks to my supervisors, Dr. Florin Pendea and Dr. Nathan Basiliko, who have been immensely supportive and encouraging of this work and my personal development as a researcher. I am deeply grateful for their financial support (NSERC Alliance, Dr. Basiliko; Faculty Residual Research Fund, Dr. Pendea)

I want to thank my lab-mates, present and past, who have made this entire experience that much more meaningful. Along with Dr. Pendea, my lab mates have assisted me with data collection in the field and processing of materials in the lab. Specifically I want to thank Lily Edmunds, Evelyn McCloy, Ally Haak, and Brin Schat.

I am grateful, as well, for everyone involved in the Sudbury restoration project, those who I have had the honour of working alongside, as well as those who began this work many years ago. I want to thank all of my fellow students for their dedication to this research – may you all succeed in your future endeavours! In particular, I want to thank Rachel Kendall for the site-specific vegetation data they provided.

Lastly, I want to thank my friends and family for their continued support. To my mother and father, I thank them for their encouragement and love, and to my brother, I thank him for his help, both in the field and in life.

I want to acknowledge that funding was received from NSERC (CGS-M), the Ontario Graduate Scholarship, the WCS Weston Family Boreal Fellowship, and the International Peatland Society.

I acknowledge that this research was conducted on the traditional lands of the Atikameksheng Anishnawbek and Wanapitei First Nation, who have lived on and stewarded these lands since time immemorial. I acknowledge that these communities were adversely impacted by the industrial activities we discuss. I acknowledge that the history of these lands is Indigenous history, and that this area was habited during all time periods we discuss. I acknowledge that lab work and thesis writing was completed on the traditional territory of the Anishinaabeg, specifically the Ojibwe and Chippewa peoples.

The data analyses were performed by the author and writing represents original writing. ChatGPT (v. 5.2) was used to summarize the main findings into a conclusion chapter, to remove repetitions and reporting redundancies within the writing, and to help identify unclear sections. GenAI was also used responsibly to troubleshoot R codes, when necessary.

Table of Contents

List of Tables

List of Figures

List of Appendices

Chapter 1 – Thesis Introduction

1.1 Research Objectives and Questions

Peatlands are globally significant long-term carbon sinks whose stability depends on the tight coupling among hydrology, peat chemistry, and microbial processes (Limpens et al., 2008; Arsenault et al., 2023; McCarter et al., 2020; Waddington et al., 2014; Furukawa et al., 2025). Although the impacts of industrial pollution on peatland chemistry and vegetation have been documented, less is known about how prolonged sulfur and toxic metals and metalloids (TMMs) deposition alters carbon accumulation trajectories, vertical geochemical mobility, and microbial community structure over centennial timescales (Bindler et al., 2006; Payne et al., 2012; Martínez Cortizas et al., 2007).

The Sudbury region (Ontario), characterized by a well-documented history of smelting emissions followed by substantial remediation, provides a natural experiment for investigating these long-term impacts of industrial pollution (Gunn et al., 1995, 2001; Gignac and Beckett, 1986; Pennington and Watmough, 2015; Seward et al., 2023). Distinct spatial and temporal contamination gradients preserved within peat stratigraphy enable analysis of carbon dynamics, pollutant redistribution, and biological response across pre-industrial, industrial, and post-industrial periods.

This thesis addresses the following overarching questions;

1. How, and to what, extent has prolonged sulfur and TMM deposition altered long-term carbon accumulation, stoichiometric balance, and vertical pollutant redistribution within peatland profiles, and how have these processes mediated post-depositional carbon loss?

2. How have microbial communities responded to industrial pollution, and are these responses driven primarily by direct metal toxicity or by indirect changes in peat carbon composition?

3. Has ecosystem recovery occurred following emission reductions, or do peatland carbon and microbial systems exhibit persistent legacy effects?

1.1.1 Chapter 2 Peat Carbon Dynamics and Geochemical Forcing

Chapter 2 quantifies long-term carbon accumulation trajectories and evaluates the vertical mobility of sulfur and TMMs within peat profiles. By combining radiocarbon-constrained chronologies with detailed elemental analyses, this chapter assesses whether industrial pollution altered carbon storage through:

- Acidification-driven enhancement of deeper peat decomposition and carbon export,
- Suppression of microbial activity and apparent surface carbon preservation during peak contamination,
- Shifts in peat stoichiometry indicative of nutrient enrichment and base-cation depletion.

1.1.2 Chapter 3 Microbial and Hydrological Response to Industrial Disturbance

Chapter 3 examines testate amoebae as bioindicators of microbial and hydrological change under industrial stress. Using stratigraphy constrained ordination, variation partitioning, and indicator species analysis, this chapter evaluates:

- The magnitude and timing of community restructuring associated with industrial deposition,
- The relative importance of direct trace-metal toxicity versus indirect alteration of peat carbon chemistry,
- Evidence for ecosystem recovery or persistence of industrial-era assemblages following emission reductions.

1.2 Background and Literature Review

1.2.1 Overview of Canadian Peatland Biology

Peatlands are a unique type of wetland system where the rate of net primary productivity (NPP) exceeds the rate of decomposition of organic matter (Wieder et al., 2006). This imbalance results in the accumulation of peat, a dense, carbon-rich organic material formed from the partially decomposed remains of plant life (Lourenco et al., 2022). Peatlands in Canada are predominantly located in the boreal and subarctic zones (Frolking et al., 2011) and, in addition to storing vast amounts of carbon (Tarnocai, 2009), provide other ecosystem services such as enhance biodiversity and water quality improvement (Martin-Ortega et al., 2014; Renou-Wilson et al., 2019).

The Canadian Wetland Classification System (1997) identifies peatlands as bogs, fens, and sometimes swamps. These classifications are based on surface morphology, water quality and quantity, underlying mineral soil, and vegetation communities (Kroetsch et al., 2011; Clymo, 1987). Bogs are described as ombrotrophic, meaning they receive hydrologic and mineral inputs via atmospheric precipitation only (Shotyk, 1996). This is in contrast to fens (minerotrophic

systems) which, in addition to precipitation, receive hydrologic inputs from surface waters and surrounding uplands via runoff (Gorham and Janssens, 1992). Raised peatland swamps – sometimes referred to as forested peatlands - are similar to transitional bogs but have minerotrophic ground water influence (Canadian Wetland Classification System, 1997).

1.2.2 Controls on Carbon Storage and Decomposition in Peatlands

The capacity of peatlands to function as long-term carbon sinks is governed by a tightly coupled set of hydrological, biological, and geochemical controls that regulate the balance between organic matter production and decomposition (Frolking et al., 2011). Central to this regulation is the position and stability of the water table, which is a primary control on redox conditions that determines the relative dominance of aerobic and anerobic decomposition pathways, and consequently, the balance between carbon dioxide and methane emissions (Koskinen et al., 2025; Belyea and Clymo, 2001; Mitsch et al., 2013). Persistent saturation promotes anoxic conditions in deeper peat layers, suppressing aerobic microbial activity and slowing the breakdown of organic material, thereby favouring long-term carbon accumulation (Boonman et al., 2024; Dickopp et al., 2018; Holden and Burt, 2003; Clymo, 1987).

Vegetation exerts a parallel control on carbon dynamics by influencing both the quantity and chemical composition of organic matter entering the system (Ward et al., 2013; Gong et al., 2020). Peat-forming mosses, particularly species of *Sphagnum,* are especially influential due to their low decomposability, and capacity to modify their surrounding chemical environment (Rydin et al., 2006). Through cation exchange and the release of organic acids, *Sphagnum* lowers pH and reduces nutrient availability, creating conditions that further inhibit microbial activity (Andersen et al., 2010). In contrast, increased dominance of vascular plants introduces more

labile organic substrates, enhancing oxygen transport to deeper layers which can accelerate decomposition (Robroek et al., 2016).

Carbon storage in peatlands is also shaped by post-depositional processes within the peat profile. Over time, buried organic matter undergoes humification and chemical transformation, and its stability depends on anoxic conditions (Chambers et al., 2011). Changes in porewater chemistry can alter the solubility and reactivity of organic compounds, potentially stimulating dissolved organic carbon (DOC) production and export from older peat layers (Dieleman et al., 2016).

1.2.3 Sulfur and Toxic Metals in Peatlands: Retention, Mobility, and Risk

Peatlands are highly effective sinks for TMMs due to the abundant chemical binding sites provided by their absorption properties and high organic matter content (Piaszczyk et al., 2025). Industrial mining activities introduce sulfur dioxide (SO_2), TMMs and particulate matter that can be accumulated within organic layers (Bindler et al., 2006). Once deposited, these pollutants can become immobilized through complexation with humic substances, adsorption to mineral particles, or precipitation under reducing conditions (Vodyanitskii et al., 2015).

However, pollutant retention within peatlands is not necessarily permanent. The mobility of TMMs is controlled by hydrological and geochemical parameters, including pH, redox potential, organic ligand availability, and water-table position (Osborne et al., 2024). Acidification can increase the solubility of pH sensitive metals such as Ni, Cu, Zn, and Pb, facilitating their downward transport through porewaters (Tipping et al., 2003). Water table position and frequency of fluctuations can influence metal mobility through downwashing (Hansson et al., 2015; Novak et al., 2011) and, more significantly, through the regulation of redox conditions

within the peat profile (Broder and Biester, 2015; Novak and Pacherova, 2008). Redox conditions refer to the oxidation of peat (Boonman et al., 2024) which occurs when water tables are low and peat is exposed to air (Souter and Watmough, 2016). Drought induced drawdown creates a reducing environment where the concentration of protons can raise metal solubility and cause rapid post-drought releases of Cu, Ni, and Co (Souter and Watmough, 2016). Organic ligands become more soluble as pH rises which allows certain metals to form soluble metal-dissolved organic matter (DOM) complexes that are able to move with porewater (McCarter et al., 2024).

Sulfur deposition plays a particularly important role in mediating these transformations. Elevated sulfuric acid inputs can lower porewater pH, enhance certain cation leaching, and alter iron-sulfur cycling, thereby influencing both metal mobility and organic matter stability (Steinmann and Shotyk, 1997). Under certain conditions, sulfate reduction and the formation or dissolution of Fe-S minerals may destabilize humic-metal complexes, increasing the solubility of dissolved organic carbon and modifying substrate availability for microbial communities (Sitte et al., 2010).

1.2.4 Testate Amoebae as Bioindicators in Peatlands

Microbial communities are important in helping to regulate peatland biogeochemistry by mediating the transformation of-plant derived organic matter into mineral, dissolved, and gaseous forms of carbon and nutrients (Wilkinson and Mitchell, 2010; Lamentowicz et al., 2013; Jassey et al., 2013; Kuuri-Riutta et al., 2022; Wanner et al., 2020). As a result, changes in microbial assemblages often provide early signs of altered peatland function. Testate amoebae

(TA) are a particularly useful microbial bioindicator, especially when it comes to reconstructing historical ecosystem change (Birks et al., 2010; Parmar et al., 2016).

These unicellular, shell-bearing protists inhabit the water films surrounding peatland vegetation and have distinct taxa that exhibit well-defined ecological preferences along gradients of pH, nutrient status, and metal concentration, allowing assemblage composition to be linked to environmental conditions (Nasser et al., 2016; Swindles et al., 2016; Booth et al., 2025; Gu et al., 2025; Mitchell et al., 2008). By examining shifts in TA composition through stratified peat layers, it is possible to infer historical changes in hydrology, acidity, and nutrient availability that are otherwise difficult to reconstruct from geochemical data alone (Ndayishimiye et al., 2025; Gu et al., 2025; Wanner et al., 2020).

Elevated metal concentrations and acidifying inputs can alter TA community structure directly through toxicity, and indirectly by modifying vegetation cover, organic matter quality, and microbial metabolic pathways (Asada and Warner, 2009; Patterson et al., 1996; Reinhardt et al., 1998). The biological responses to these pollutants reflect broader ecosystem-level processes, including the balance between aerobic and anaerobic conditions that govern carbon mineralization and methane production.

1.2.5 The Sudbury Region as a Natural Experiment

The Greater Sudbury Area (Ontario, Canada) has long been a globally important setting for studying long-term ecological effects of industrial mining pollution, specifically copper and nickel ore smelting, on boreal peatlands (Newman et al., 2023; Luke et al., 2015). Situated on a meteorite impact known as the Sudbury Basin (Roussell and Long, 1998), the region contains

exceptionally rich nickel and copper deposits that have driven over a century of intensive mining and smelting (Souter and Watmough, 2016; Potvin and Negusanti, 1995).

In the early nineteenth century, mining practices involved open air smelting, releasing large quantities of sulfur dioxide and TMMs into the atmosphere (Gunn et al., 1995). At the height of industrial activity in the mid-twentieth century, emissions from the three smelters (Copper Cliff, Falconbridge, and Coniston) were considered one of the largest point sources of SO_2 globally (Potvin, 2007; Chan and Lusis, 1985). These pollutants, along with anthropogenic land use change (e.g. logging and drainage), caused widespread vegetation loss and soil degradation (Saarinen, 2013; Gignac and Beckett, 1986; Seward et al., 2023; McCarter et al., 2024; Freedman and Hutchinson, 1980).

Regulatory changes beginning in the 1970s began a transition toward environmental restoration (Potvin and Negusanti, 1995; Sickles II and Shadwick, 2015). The construction of the Inco Superstack and introduction of emission controls reduced sulfur dioxide outputs by roughly 90% (Gunn et al., 1995). The Sudbury Regreening Program was also established during this time, which involved the application of lime (chiefly calcium carbonate, $CaCO_3$), N-P-K fertilizers, and extensive revegetation in the most impacted landscapes (Gunn, 1995). In most regional ecosystems (e.g. uplands, lakes) studies have found measurable recovery, but the same cannot be said for peatlands.

Chapter 2 – Impacts of smelter pollution on soil carbon dynamics in peatlands around North America's largest historical point source pollutant of toxic metals, metalloids, and sulfur.

2.1 Introduction

Peatlands are one of the few long-term terrestrial carbon (C) sinks currently sequestering ~100 Mt of C annually (Strack, 2008) and are an estimated persistent store of 547,000 Tg of C (Yu et al., 2010), largely deposited since the Last Glacial Maximum in the Northern hemisphere (Gorham et al., 2012). Northern peatlands, which cover ~10% of the land surface in boreal and subarctic regions (Frolking et al., 2011), have exerted a net negative radiative forcing effect (cooling) on global climate throughout the Holocene due to sustained C sequestration (Frolking et al., 2006; Chaudhary et al., 2017). Yet future terrestrial surface-atmosphere coupling in a warming climate may drive these systems to switch into a positive radiative forcing mode (Baird et al., 2009; Chaudhary et al., 2017; Qiu et al., 2020; Zhao and Zhuang, 2023), although the timing and extent of such transitions remain uncertain (e.g., Frolking et al., 2011; Charman et al., 2013; Chaudhary et al., 2017; Heffernan et al., 2020). An important source of uncertainty in estimating the future climate feedbacks of northern peatlands is disturbance, both natural (e.g., fire, pathogen outbreaks) and anthropogenic (e.g., intentional drainage, peat extraction, pollutant loading), with the latter factor often contributing to an increase in severity of natural disturbance and driving profound changes in ecosystem functions (Turetsky and St. Louis, 2006; Andersen et al., 2010; Berger et al., 2017; Vitt and Wieder, 2009).

In Canada, boreal peatlands stretch across the country from British Columbia to Newfoundland and Labrador (McDonough et al., 2022). Although many Canadian peatlands remain relatively pristine, resource extraction (e.g. timber, oil, minerals) can have substantial impacts on these systems (Müller and Joos, 2021; Munford et al., 2023). Extraction activities alter microbial and vegetation communities (Payne and Mitchell, 2009; Andersen et al., 2010; Kaila et al., 2012; McCarter et al., 2021; Coggins et al., 2006) and disrupt natural peatland functions, including hydrology and nutrient cycling (Volik et al., 2020; Rooney et al., 2011; Bourgeau-Chavez et al., 2020; Nwaishi et al., 2015). Additionally, mineral resource extraction and processing often contribute pollutants such as sulfur and toxic metal and metalloids (TMMs), which can degrade peatland health and reduce their capacity to sequester carbon effectively (Smieja-Król et al., 2010; Newman et al., 2023; Luo et al., 2023). These impacts may be further exacerbated by climate-change-driven changes in temperature, precipitation patterns, and seasonal cycles (Martínez Cortizas et al., 2007; Baird et al., 2009).

In the early 1970s, Sudbury, Ontario, was one of the world's largest emitters of TMMs and sulfur dioxide (SO_2) (Gunn et al., 1995). Modern smelting in the region began with the opening of the Copper Cliff smelter in the 1880s, which emitted high levels of copper (Cu), nickel (Ni), lead (Pb), sulfur (S) and toxic metalloids such as arsenic (As) causing soil and plant toxicity and creating barren landscapes (Saarinen, 2013; Freedman and Hutchinson, 1980). Although pollution has decreased due to clean air legislation in the 1970s and 1990s in North America that implemented improved infrastructure and technology (Gunn, 1995; Gunn et al., 1995; Potvin and Negusanti, 1995; Sickles II and Shadwick, 2015), regreening efforts in Sudbury have focused on restoring forested uplands, leaving peatlands to recover naturally (Gunn et al., 1995). However,

the extent of recovery to peatland processes, such as carbon sequestration or net climate cooling, remains poorly resolved partly due to lingering TMMs and S (Pamer, 2008; Seward et al., 2023).

The ability of peatlands to sequester pollutants or carbon depends on complex hydrological, biological, geomorphological, and chemical interactions that are fundamental to peatland functions, yet are sensitive to pollution and other disturbances (Munford et al., 2023; McCarter et al., 2024). In particular, understanding the vertical distribution of S and metal pollutants and their role in the long-term carbon cycling is critical to assessing the trajectory of Sudbury peatlands and for identifying where mitigation efforts are needed. This chapter investigates the potential interactions between historical S and TMMs deposition and long-term carbon accumulation in three Sudbury peatlands; two sites near the smelters that had lost *Sphagnum* mosses, and one distal to the industrial centre that was minimally impacted in terms of vegetation and contemporary pore water chemistry (Gignac and Beckett, 1986; Seward et al., 2023). Using high-resolution peat geochemistry (C_{org}, C_{inorg}, S, N, Ca, P, Pb, Na, Fe, Sr, Zn, Cu, Ni, As, Cd) and ^{14}C dating, we seek to determine whether and to what extent TMMs and sulfur contaminants have affected peat C chemistry and accumulation rates in these systems. In addition, we compare the mobility of pollutants along the peat profiles from heavily polluted and minimally impacted peatlands and evaluate changes that may have occurred to their C stocks.

2.2 Study Location and Environmental History

The Greater Sudbury Region (Fig. 1) occupies a ~200,000 ha area on the Canadian Shield in central Ontario (Canada) and is located within the traditional lands of the Atikameksheng Anishinaabek and Wanapitei First Nation. During the industrial period (1880-1975 CE) the region underwent rapid development of mining and smelting operations, which led to economic growth but had adverse environmental effects (Souter and Watmough, 2016; Potvin and Negusanti, 1995). Sudbury's industrial activities have affected local ecosystems, including

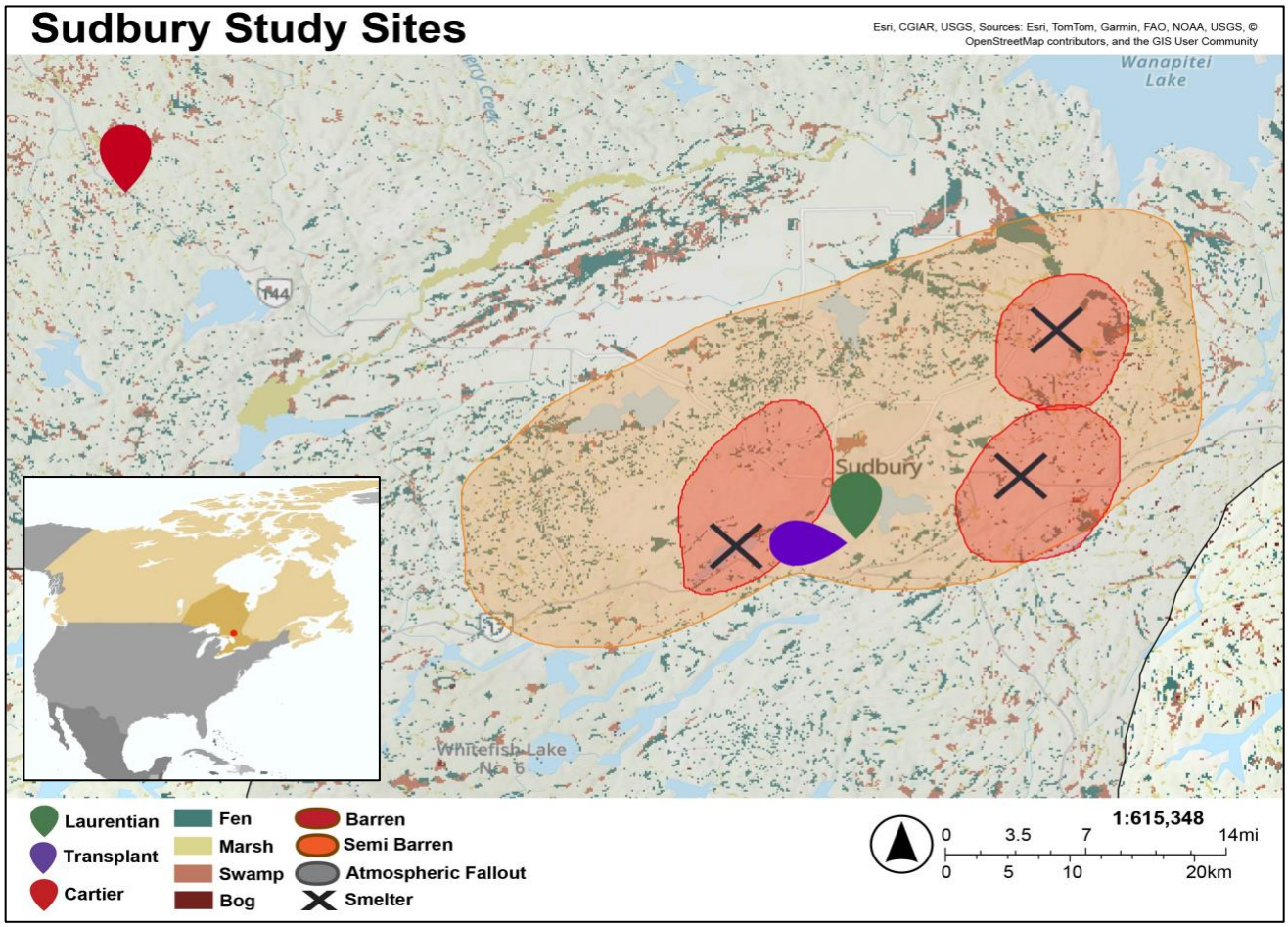

Figure 1 *Location map of Greater Sudbury Region, wetland distribution, study sites, and the landscape legacy of the historical industrial activity. Barren is defined bare, blackened rock completely denuded of soil. Semi-barren is bare rock with some remaining vegetation and soil; atmospheric fallout is defined by lower levels of pollutant loading. Statistics on wetland distribution are presented in Table 1.*

peatlands, through sulfur dioxide emissions (Potvin, 2007; Chan and Lusis, 1985; Gunn et al., 1995). Moreover, the deposition of TMMs like nickel and copper has likely further degraded vegetation and microbial communities, leading to reduced species diversity, altered ecosystem structure (notably with the elimination of *Sphagnum* mosses) and compromised ecological functions such as water retention and carbon cycling (Gunn et al., 1995; Gignac and Beckett, 1986; Seward et al., 2023; Luke et al., 2015; McCarter et al., 2024).

The industrial legacy of the area has created three upland landscape units characterized by varying levels of historical disturbance: The areas proximal to the smelters and ore roasting yards - called the Barrens - were defined as areas generally devoid of plant life and had mineral soil pH below 4.3 (Lautenbach et al., 1995). In a few places across the Barrens, in addition to bare, blackened rock there were a few native species such as *Betula papyrifera*, *Acer rubrum*, *Quercus rubra*, *Populus tremuloides, Vaccinium spp.*, *Deschampsia cespitosa*, and *Polytrichum commune* (Watkinson et al., 2022). Surrounding the Barrens, the Semi-Barrens supported a greater abundance of vegetation, consisting of the same species found in the Barrens along with additional acid- and fire-tolerant plants (Watkinson et al., 2022). Beyond this, the Atmospheric Fallout Zone experienced lower pollutant loading, allowing local vegetation to remain comparatively less disturbed.

Following major mitigation of the local atmospheric pollution, the region underwent a large-scale restoration process commencing in 1978 that featured dolomitic limestone applications, N-P-K fertilization, herb seeding and tree planting (Watkinson et al., 2022). To date, over 10 million trees and shrubs have been planted in over 3000 ha of barren and semi-barren land in the Sudbury region (VETAC, 2024). The Sudbury Regreening Program has focused on reclamation

and afforestation of the forests and lakes, while the region's wetlands have remained relatively untouched. Although operational-scale reclamation efforts are not yet underway, there have been comprehensive studies of impacts to the abundant peatlands in the region. Generally, despite restoration efforts in the uplands and cascading impacts that have improved aquatic ecosystem health, the vegetative cover in peatland of Barren and Semi-Barren areas remains altered, notably with no *Sphagnum* cover in the 1980s (and only modest recolonization by the 2010s and 2020s) and abundant ericaceous shrubs (Barrett and Watmough, 2015; Gignac and Beckett, 1986; Seward et al., 2023). While the exact mechanism of how pollution eliminated *Sphagnum* is not yet known, metal concentrations correlate tightly with *Sphagnum* abundance (Gignac and Beckett, 1986; Seward et al., 2023). As of 2025, the surface peat in these sites is highly humified relative to sites outside of the semi-barren zone, with speculation about enhanced decomposition rates that may have occurred after *Sphagnum* communities (that inhibit heterotrophic microbes) collapsed, along with a potential role for sulfate loading, which may have stimulated anaerobic respiration (Luke et al., 2015).

2.2.1 Regional Climate

The climate in the Greater Sudbury area is continental with an average total annual precipitation of 903 mm (Environment Canada, 2025). The average daily minimum and maximum temperatures between 1981 and 2024 were -17 ºC and -8 ºC in January and 13 ºC and 25 ºC in July. Wind direction is north in winter and spring, southwest in summer, and south in autumn (Environment Canada, 2025). The growing season in this region is 125 - 145 days, defined by the average last spring frost of May 17th, and the average first fall frost of September 26th (Government of Ontario, 2024).

In the region of eastern Canada literature has documented two major Holocene climate variability periods; the Holocene Thermal Maximum (HTM) followed by a period of Neoglacial cooling (Wu et al., 2023; Porter et al., 2019; Keizer et al., 2015). The Holocene Thermal Maximum was a warm and wet interval that peaked globally around ~12,900-5,700 Cal yrs BP but was delayed in NE North America by 1,000-2,000 years due to cooling from the Laurentide Ice Sheet (Rensson et al., 2012; Porter et al., 2019; Magnan and Garneau, 2014). The HTM was followed by a period of Neoglacial cooling which occurred from around ~5,000-950 Cal yrs BP (Mangan and Garneau, 2014; Wu et al., 2023; Kjær et al., 2022). This interval is described by cool and dry conditions, often divided into older and younger phases, with the younger referring to the Little Ice Age (LIA) that occurred between ~400-200 Cal yrs BP (Keizer et al., 2015). The Neoglacial cooling period was also intersected by short, mildly warm events such as the Medieval Warming Phase (MWP) from ~1150-850 Cal yrs BP (Keizer et al., 2015; Kjær et al., 2022).

2.2.2 Regional Geology

Situated in the southern province of the Canadian Shield, the Sudbury area comprises the Sudbury Structure (Pearce, 1976), also known as the Sudbury Basin, a large, oval-shaped geological feature formed approximately 1.85 billion years ago as a result of a massive meteorite impact event during the Paleoproterozoic era (Rousell and Long, 1998; Ames et al., 2002). It is one of the largest and best-preserved impact structures on Earth and is also a globally significant mining district, particularly for nickel and copper (Grieve and Therriault, 2000; Ames et al., 2002). The Sudbury Structure combines several geological complexes including the *Sudbury Igneous Complex* (a 2.5 km-thick, differentiated melt sheet composed of granophyre, quartz

gabbro/norite, norite and mafic norite), *Footwall Breccias and Inclusion-bearing Norite,* and the *Whitewater Group* as an overlying sedimentary structure (Rousell and Card, 1998).

Along with the meteorite impact, the region's geology has been influenced via ice sheets on several occasions during the Precambrian area about 2.4 billion years ago, with the most recent glaciation event occurring during the Quaternary period (Saarinen, 2013; Lazorek et al., 2006). The Laurentide Ice sheet covered large parts of North America and much of Ontario – including the Greater Sudbury Region (Saarinen, 2013). The ice sheet began to retreat from the Sudbury area approximately 10,000 years ago, after which ensured a period of deglaciation processes that included scouring of underlying Precambrian Shield, the formation of various glacial, glaciolacustrine and meltwater related landforms (e.g. kettle lakes, eskers) and the deposition of silt and sand sediments by glacial streams (Saarinen, 2013; Dirszowsky, (2020).

2.2.3 Regional Hydrology

The Sudbury area lies entirely within the Georgian Bay (Lake Huron) watershed (Ontario Ministry of Natural Resources and Forestry, 2025). The regional drainage system is dominated by the French and Spanish Rivers, with water flowing in a NE-SW orientation. All of the study sites are located within Sudbury's Drinking Water Source Protection (DWSP) zone, which includes three watersheds; Vermillion River, Wanapitei River, and Whitefish River.

2.2.4 Regional Vegetation and Wetland Distribution

The Greater Sudbury Region straddles the transition zone ecotone between the Boreal Forest zone in the north, to the Great Lakes - St. Lawrence Forest regions (Rowe, 1972) in the south

(Ontario Ministry of Natural Resources, 2021). The regional vegetation includes typical Great Lakes-St. Lawrence Forest species such as *Pinus resinosa*, *Pinus strobus*, *Acer saccharum*, and *Betula papyrifera*, as well as southern boreal species such as *Pinus banksiana* and *Picea glauca* (Sherman and Beckett, 2003). Along with forests, this region has three broad ecological systems including wetlands, rock barrens, and lakes (City of Greater Sudbury, 2013). Wetlands in this boreal landscape are numerous and scattered (Fig. 1) occupying 12% (23,445 ha) of the Greater Sudbury Area (Ontario Ministry of Natural Resources and Forestry, 2025) with over 33,000 ha of wetlands (dominated by fen and bog systems) found within the City of Greater Sudbury (Munford et al., 2023). The wetland area of the Greater Sudbury Area (Table 1) comprises fens (64%), swamps (23%), marshes (12%) and a few bogs (1.3%).

Table 1 *Wetland distribution statistics for the Greater Sudbury Region (Ontario). Outlining the total area (ha, %) of total Wetlands and wetland subtypes (fen, swamp, marsh, bog) within the region. As well as outlining the area (%) that each wetland subtype occupies within the total Wetland area (Ontario Ministry of Natural Resources and Forestry, 2025).*

Type	Area (ha)	Area (%)	Wetland Area (%)
Total	200,351	-	-
Wetland	23,445	12	-
Fen	14,984	7	64
Swamp	5,268	2.6	23
Marsh	2,893	1.4	12
Bog	299	0.2	1.3

2.3 Fieldwork

2.3.1 Site selection

Three sites were selected (Fig. 1, Table 2) with two proximal to former smelter centres (Transplant and Laurentian, local names), and one minimally impacted (Cartier North, local name; note Cartier North has been previously referred to as Cartier in past publications), situated at the NW edge of the Atmospheric Fallout area. Although the two sites proximal to the industrial centre are both within the Semi-Barrens and have similar age and peat depth, they differ in surface hydrology. All chosen sites were identified as poor fen systems, following the Canadian Wetland Classification System (National Wetlands Working Group, 1997).

The Transplant site is a 0.7-ha isolated depression in bedrock largely fed by rainfall and limited runoff from surrounding slopes. It is a heavily degraded peatland (Barrett and Watmough, 2015; Gignac and Beckett, 1986) with wetland vegetation dominated by *Chamaedaphne calyculata, Kalmia angustifolia, Eriophorum virginicum*, *Rhynchospora fusca*, *Eriophorum vaginatum*, and *Odontoschisma fluitans.* The wetland is surrounded by both planted and naturally re-established trees such as *Betula papyrifera*, *Populus tremuloides*, *Acer rubrum*, *Pinus banksiana* and various ericaceous shrubs such as *Vaccinium angustifolium*.

The Laurentian site occupies 2.29 ha (Szkokan-Emilson et al., 2013) slightly above the elevation of a large lake (Lake Laurentian). In contrast to the Transplant site, Laurentian formed through the paludification of a former riparian system is well coupled to the surface hydrology, receiving a small intermittent brook at headwaters and being drained by a similar system downstream (Szkokan-Emilson et al., 2013). It has a heavy degradation status (Barrett and Watmough, 2015;

Gignac and Beckett, 1986) with wetland vegetation dominated by *Carex echinata*, *Chamaedaphne calyculata, Odontoschisma fluitans, Mylia anomala,* and *Warnstorfia fluitans.* The peatland margins support some sparce *Sphagnum* hummocks although within the peatland *Sphagnum* is absent. The site is surrounded by a variety of slope features largely vegetated with species established during the decades following major local air quality improvements in the 1970s such as, *Betula papyrifera*, *Populus tremuloides*, *Acer rubrum*, *Pinus banksiana* and various ericaceous shrubs such as *Vaccinium angustifolium*.

The Cartier North site is a 3.74 ha, minimally impacted peatland (Barrett and Watmough, 2015; Gignac and Beckett, 1986) with wetland vegetation dominated by *Sphagnum* species (*S. fallax, S. fuscum, S. divinum complex ,* and *S. rubellum)* and several vascular taxa such as *Rhododendron groenlandicum, Chamaedaphne calyculata, Carex oligosperma, Kalmia angustifolia, Kalmia polifolia, Larix laricina, Picea mariana,* and *Eriophorum vaginatum.* The surrounding upland is forested with *Picea mariana, Picea glauca,* and *Larix laricina*. While the atmospheric deposition was minimal in this peatland, it is currently impacted by a road (west), rail line (east) and a power line running through the middle of the peatland.

2.3.2 Coring

Soil cores were retrieved from the deepest part of each site with a McCauley corer (half cylinder barrel with a 5 cm diameter) to the depth of refusal (Table 2). Soil cores were sealed in PVC pipes lined with plastic film on site and transported to the lab where they were kept at 4^{o}C until processing. For the topsoil with live, often woody rhizosphere the McCauley blade was ineffective, and thus, 30 x 30 cm monoliths (~ 30-50 cm depth) were cut with a serrated knife and subsequently wrapped in plastic film. Peat parameters (pH and water table depth) and live

vegetation (presence/absence) were recorded along a continuous transect from the core locus to the edge of the peatland.

Table 2 *Study details for Transplant, Laurentian, and Cartier North sites. Including coordinates, peatland type, the distance (km) from the center of the three regional smelting smokestacks, and the total core depth (cm) taken.*

Site	Coordinates	Type	Distance from smelting centre (km)	Core Depth (cm)
Transplant	46.45327°N, 80.97439°W	Poor Fen	8.8	296
Laurentian	46.45539°N, 80.96765°W	Poor Fen	8.3	304
Cartier N	46.66272°N, 81.52039°W	Poor Treed Fen	50.9 (NW)	369

2.4 Laboratory Analyses

2.4.1 Sample Preparation

Peat cores were cut into 1-cm-thick subsamples every 2 cm to a depth of 60 cm, and every 10 cm thereafter. Samples of known volume were oven-dried at 50°C to constant weight and subsequently ground to a fine powder with a mortar and pestle. Bulk density (g cm^{-3}) was calculated as the dry weight (g) divided by the sample volume (cm^3). From each depth increment, two subsamples were prepared; one for CHNS analysis and one for acid digestion and Inductively Coupled Plasma Optical Emission Spectroscopy (ICP-OES).

Macrofossils for radiocarbon dating were collected from the remaining peat samples at various intervals throughout the core using a dissecting microscope. They were cleaned with DI water, air dried and stored at 4°C until shipped to the radiocarbon lab.

2.4.2 Peat Composition Analysis

Due to the advanced state of peat humification in the cores from the Transplant and Laurentian sites, the standard macrofossil sample pre-treatment (Mauquoy et al., 2010) was modified as follows. Peat samples (2-4 cm^3) every 2 cm to a depth of 60 cm, and every 10 cm, thereafter, were dispersed in warm 5% KOH solution for 15 minutes and then washed over a 125-micron nylon mesh sieve. The retained material was placed in Petri dishes and examined under a low power (×10 – ×50) stereo-zoom microscope. We used a semi-quantitative analysis of the peat samples in which we assigned ordinal ranks (1 = rare, 2 = occasional, 3 = frequent, 4 = common, and 5 = abundant; Walker and Walker, 1961; Barber, 1981) to major macrofossil categories using diagnostic cell structure features of identifiable plant detritus. The macrofossil groups were gyttja (mixture of mineral detritus and amorphous or colloidal organic matter interspersed with submergent plant parts mainly from Nymphaeaceae, Hydrocharitaceae, and Isoetaceae), herbaceous undifferentiated (a mix of Poales and forbs), ligneous undifferentiated (wood xylem, bark, tree seeds and leaves), Ericaceous (Ericaceae leaves, seeds, and roots), Carr (*Alnus* twigs, leaves, and seeds), Poales (Cyperaceae, Poaceae, and Juncaceae leaves, stems, seeds, and roots), Bryidae (brown moss leaves, stems, and rhizoids), and *Sphagnum* moss (leaves, stems, and rhizoids). Identification of macrofossil groups follows Lévesque et al. (1988) and Schweingruber et al. (2020).

2.4.3 Elemental Analyses: Carbon (C), Nitrogen (N), and Sulfur (S)

Total organic and inorganic C, N, and S were analyzed using an ELVario cube CHNS analyzer (DIN/ISO 10694) at the Lakehead University Environmental Laboratory (2025). For estimates of C_{org} concentration by mass (%) a portion of the ground sample was acidified (10M HCl) to purge

carbonates before combustion. The unacidified portion of the sample was used to estimate total C, N and S (% by mass). Inorganic C was estimated by subtracting C_{org} from total C. Dry bulk density (BD) estimates (g cm^{-3}) and C_{org} concentration by mass (%) were used to calculate soil C_{org} density (g cm^{-3}) for each soil increment and cumulative C_{org} stocks (kg m^{-2}).

2.4.4 Elemental Analyses: Metals, Metalloids, and select Non-Metals

Samples from the same depths as for the CHNS analysis were analyzed for a suite of metals, metalloids, and several non-metallic elements [copper (Cu), nickel (Ni), lead (Pb), sulfur (S), arsenic (As), cadmium (Cd), aluminum (Al), boron (B), beryllium (Be), calcium (Ca), cobalt (Co), chromium (Cr), iron (Fe), potassium (K), magnesium (Mg), manganese (Mn), molybdenum (Mo), sodium (Na), phosphorous (P), selenium (Se), silicon (Si), strontium (Sr), titanium (Ti), thallium (Tl), vanadium (V), and zinc (Zn)]. Prior to analysis, samples underwent a microwave digestion with a 3:1 ratio of HNO_3:HCL, done in 40 mL glass vials at the Lakehead University Environmental Laboratory. The microwave used was a CEM Mars Xpress Microwave with HTV Vessel turntable. A maximum of 0.230 g of dried, homogenized sample was weighed into a 40 mL glass vial. Concentrated nitric acid (3.75 ml) and 1.25 mL of concentrated hydrochloric acid was added to the sample and let sit overnight for pre-digestion. Samples are then microwaved, ramping up to 90ºC over approximately 4 hours. Samples are then cooled, brought to 40 mL with distilled deionized water, and inverted to mix. Approximately 10 mL of the sample is filtered through a 0.45 um filter and then run through an Agilent 5900 ICP-OES analyser.

2.4.5 Radiometric Dating and Age-Depth Modelling

Accelerated Mass Spectrometry (AMS) radiocarbon measurements were obtained exclusively on macrofossils including seeds, twigs, and leaves. AMS radiocarbon analyses were performed by Beta Analytic Inc. (Miami, USA) and the André E. Lalonde AMS Lab at University of Ottawa (Canada). Quoted errors represent one relative standard deviation statistics (68% probability) and counting errors are based on the combined measurements of the sample, background, and modern reference standards. Radiocarbon ages were corrected for isotopic fractionation and were calibrated using the IntCal20 curve (Reimer et al., 2020). Calibrated ranges are reported as two standard deviations. Age-depth models for all cores were derived using the *rbacon* package in the R platform (Blaauw and Christen, 2011), which divides a dated sequence into many short sections for which accumulation rates (in yr cm^{-1}) are modelled. The accumulation rate of any individual section "*i*" depends both on the adjacent radiocarbon age estimates and, to a certain degree, on the accumulation rate of previous section (*i*-1). In this way, a "memory" of accumulation rate throughout time is obtained, that seeks to reflect environmental conditions that might change gradually over time.

2.4.6 Calculation of Carbon Accumulation

An important metric in evaluating the role of peatlands as C sinks is the Long-term Apparent Rate of organic Carbon Accumulation (LARCA) as a measure of millennial-scale C sequestration potential in wetlands (Clymo et al., 1998). This measure depends on the net primary productivity of the system and the post-genetic decomposition losses via gas emissions and dissolved and particulate C exports. In practice, LARCA is measured based on the rate of peat accretion (cm yr^{-1}), peat C_{org} concentration, and bulk density. The rate of peat accretion is,

in turn, based on the median modelled radiocarbon age interval between adjacent depths. In this study, LARCA was modeled after Hughes et al. (2013) and calculated as:

$$LARCA = r * p * 10{,}000$$

Where LARCA = areal apparent accumulation of dry mass per year (g C_{org} m^{-2} yr^{-1}), r = rate of peat accumulation (cm yr^{-1}), and p = organic carbon density (g cm^{-3}).

2.5 Results

2.5.1 Chronostratigraphy and Accumulation Rates

Twenty-six AMS radiocarbon age measurements (ten at Transplant, seven at Laurentian, and nine at Cartier; Table 3) were used to construct age-depth models and derive peat soil accumulation rates at each site (Fig. 2). The modelled ages for each depth and the macrofossil group determinations from core materials provided a biostratigraphic framework since peat formation began at each site (Fig. 2). To facilitate inter-site comparisons, we define three chronostratigraphic units at all sites, namely the *Pre-disturbance* stratigraphy (peat deposited prior to 1880 CE), the *Industrial Isochron* (1880 to 1975 CE), and the *Recovery* stratigraphy (last ca. 50 years). We define the Industrial Isochron of this region as the start of industrial activities (mining and smelting), which began in the late 1800s. The end of the Industrial Isochron and the beginning of the Recovery period are marked as 1975 CE, when substantial environmental policies began to be implemented, specifically regulations on pollution from smelting and mining.

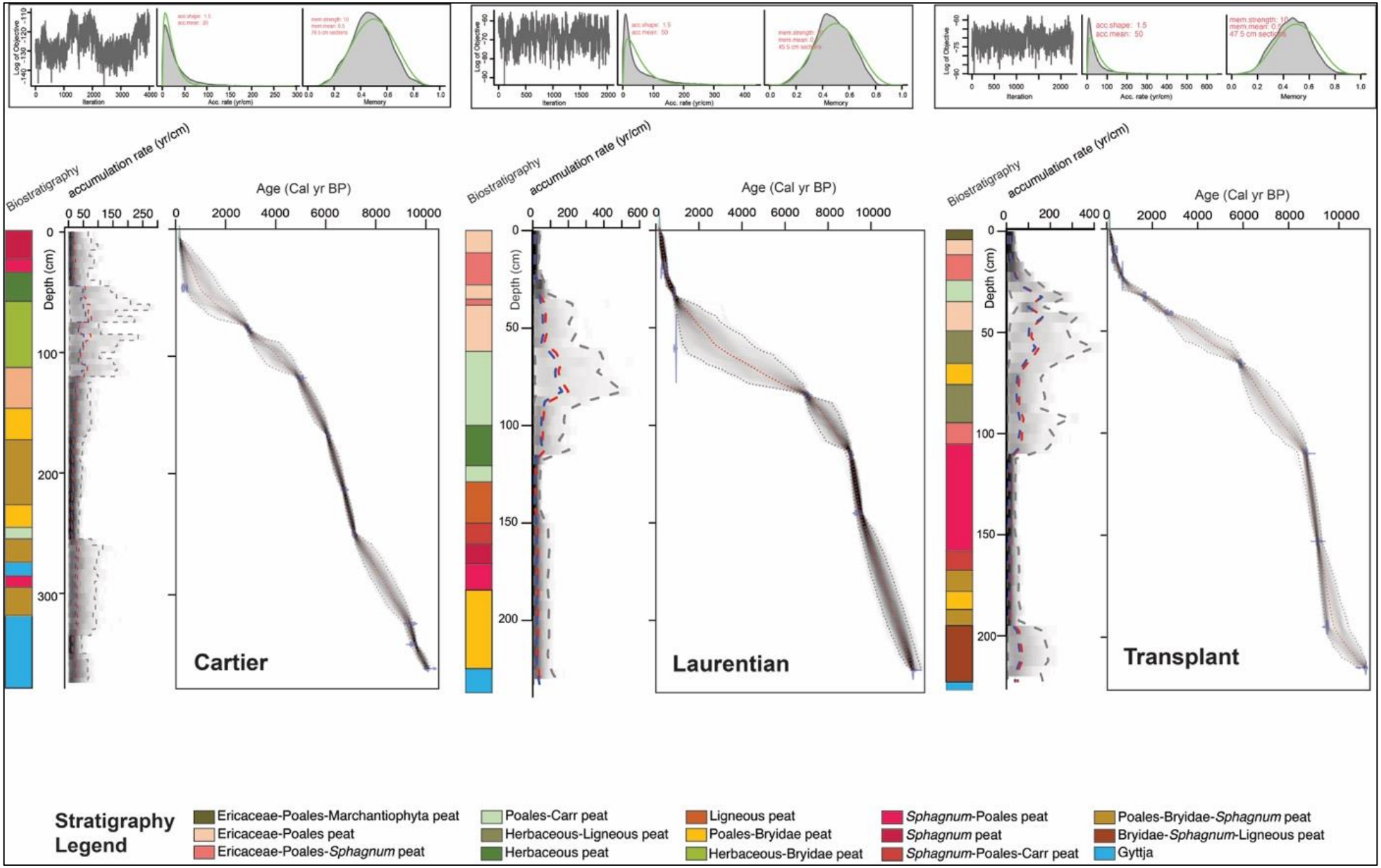

Figure 2 *Peat stratigraphy and age-depth models for three peatlands in the Greater Sudbury Region (ON), Canada. The age-depth relationships were derived from macrofossil-based radiocarbon age determinations (Table 3) and depth using the rbacon package in the R platform (Blaauw and Christen, 2011)*

2.5.2 The Pre-disturbance Period

The basal Pre-disturbance stratigraphy of all sites consists of lacustrine silty clays (1-3% C_{org}) and organo-mineral gyttja (3-17% C_{org}), which started to accumulate before ca. 10,000 cal. years BP through a progressive infilling of postglacial lakes/ponds (Fig. 2). The average sediment accumulation rates during this phase were 25 ± 8 years cm^{-1} at Cartier, 29 ± 3 years cm^{-1} at Laurentian, and 74 ± 14 years cm^{-1} at Transplant.

Peatland initiation (C_{org} >17%) started early and synchronously at the Transplant and Laurentian sites (ca. 11,200 cal. years BP), while at Cartier North it began much later (ca. 9,400 cal. years BP) following a protracted period of lake infilling and paludification (Fig. 2). The first peats deposited at Transplant and Laurentian were minerotrophic, largely constituted of plant remains from brown mosses (Bryidae) and graminoids (Poales). The first *Sphagnum* communities appear early at Transplant but do not become dominant in the macrofossil record until ca 9,100 cal yr BP, whereas at Laurentian dominantly *Sphagnum* peats are deposited continuously between 9,900 and 9,000 cal yr BP (Fig. 2). The peat accumulation rate during this *Sphagnum* phase was high and ranged from 16.6 years cm^{-1} at Transplant to 27.5 years cm^{-1} at Laurentian. The initial *Sphagnum* peats at Transplant and Laurentian are replaced, ca. 9,000 - 8,200 cal years BP, by various combinations of herbaceous, Ericaceous, carr, ligneous, and brown moss peats (Fig. 2), which continue to accumulate until ca. 1,000-500 cal yr BP at a much lower accumulation rate (95.5 years cm^{-1} at Transplant and 73.8 years cm^{-1} at Laurentian). *Sphagnum* communities reappear towards the end of the Pre-disturbance phase, largely within a dominantly Ericaceous system, first at Laurentian (ca. 1000 cal yr BP) and then at Transplant (ca. 500 cal yr BP), although their remains are a minor component of the peat deposited during this time (Fig. 2). The

last Pre-disturbance peat deposited at both Transplant and Laurentian is a mixture of Ericaceous, Poales, and *Sphagnum* materials and marks a substantial increase in the accumulation rate (23-33 years cm^{-1}).

At the Cartier site, the Pre-disturbance peat stratigraphy is slightly different than at the other two sites as herbaceous materials are generally more abundant while *Sphagnum* is a relatively minor constituent. Between ca. 9,500 and 7,500 cal years BP, peat deposition includes a mixture of Poales, Bryidae and *Sphagnum* biomass in varying proportions (Fig. 2), with a brief return to gyttja deposition 8,150-8,500 cal year BP. Peat accumulation rate averages 30 years cm^{-1}. The appearance of a carr component in the peat ca. 7,500 cal yr BP marks the beginning of a period of high accumulation rates (average 16 years cm^{-1}) when peat was dominated by Poales and Bryidae, with or without minor *Sphagnum* materials. The latest part of the Pre-disturbance stratigraphy (5,800-230 cal yr BP), peat composition is more diverse and includes herbaceous mixtures of graminoids and forbs as well as Ericaceous shrubs in addition to Bryidae mosses and minor *Sphagnum* components. This period is defined by the lowest peat accumulation rate, averaging 50 years cm^{-1}, although at the end of the Pre-disturbance period (ca. 1650 CE) the accumulation rate increases dramatically (7 years cm^{-1}).

2.5.3 The Industrial Isochron and the Recovery Period

The beginning of the industrial disturbance (i.e., the Industrial Isochron) is marked by a virtually synchronous (1830-1860 CE) shift from Ericaceous-Poales- *Sphagnum* to Ericaceous-Poales peats at both Transplant and Laurentian, with the latter site remaining unchanged through to the present day (Fig. 2). At Transplant, the Ericaceous-Poales peat is enriched with a liverwort component (Marchantiophyta) beginning ca. 1945 CE, similar to the community extant at the site

today. The accumulation rate during the Industrial Isochron (1880-1975 CE) and the Recovery period (1975 CE to present) is similar at both Transplant and Laurentian, averaging 15- (SD = 0.015) and 13- (SD = 0.018) years cm^{-1}, respectively.

At the Cartier site, a *Sphagnum*-Poales peat started to develop prior to the beginning of the Industrial Isochron (ca. 230 cal yr BP or 1720 CE), with *Sphagnum* progressively increasing towards present. There are no obvious changes in peat stratigraphy between the end of the Pre-disturbance period, the Industrial Isochron, and the Recovery period, and the accumulation rate averages ~9 (SD = 0.011) years cm^{-1}.

2.5.4 Carbon – Nitrogen Chemistry (C_{org}, LARCA, C_{inorg}, C/N)

Organic (C_{org}) and inorganic C (C_{inorg}) concentrations, and organic C to N ratios (C_{org}/N) of peats at each site are illustrated in Figs. 3 to 5 and a chronostratigraphic descriptive statistic breakdown is available in Appendix 6.

Organic C concentration increased progressively at all sites during the paludification of the postglacial lakes/ponds from <1% during the early lacustrine gyttja deposition to ~45% at the end of the peatland initiation, a process completed by 10,200 cal yr BP at Transplant, 9,600 cal yr BP at Laurentian, and 7,900 cal yr BP at Cartier. For the remainder of the Pre-disturbance period, peat C_{org} remained relatively stable (42 to 52%) at all sites.

The Industrial Isochron is marked by a decrease in C_{org} values below 40% at Laurentian and Cartier, while at Transplant an apparent decrease in C_{org} concentrations starts prior to the Industrial Isochron. During the Recovery period, C_{org} concentrations increase slightly although they remain below the Pre-disturbance maximum. Total C_{org} stocks (Table 4) are 152 kg m^{-2} at Transplant, 147 kg m^{-2} at Laurentian, and 130 kg m^{-2} at Cartier.

Table 3 *Radiocarbon Accelerator Mass Spectrometry (AMS) age determinations for three peatland stratigraphies in the Greater Sudbury Region (ON), Canada. Radiocarbon ages were calibrated using IntCal20 curve (Reimer, et al., 2020) and subsequently incorporated into the age-depth models (Fig. 2)*

Site	BETA / Lalonde ID#	Depth (cm)	Sample Material	Radiocarbon age (yr BP)	2σ probability cal age (yr BP) 1st	2nd
LAU-19	UOC-25007	19	Charred wood	100 +/- 20	258-223 (25.7%)	140-32 (69.7%)
LAU-23	UOC-25022	23	Wood, charcoal	185 +/- 15	287-265 (20%)	218-164 (50.7%), 158-145 (8.3%), 24 – (16.4%)
LAU-34	664904	34	*Picea mariana*	590 +/- 30	648 - 582	570 - 539
LAU-62	UOC-25008	62	wood	715 +/- 15	678-654 (95.4%)	n/a
LAU-117	UOC-25009	117	wood	7690 +/- 25	8540-8415 (95.4%)	n/a
LAU-147	UOC-25010	147	charcoal	7930 +/- 25	8983-8911 (16.8%)	8900-8876 (4.1%), 8870-8825 (12%), 8813-8638 (61.7%), 8615-8606 (0.8%)
LAU-228	664905	228	*Carex spp.*	9830 +/- 30	11271 - 11195	n/a
TR-SM-10	UOC-25021	10	wood	110 +/- 15	258-223 (24.4%)	140-32 (71%)
TR-SM-15	UOC-24999	15	wood	120 +/- 15	263-220 (23.1%)	144-26 (72.4%)
TR-SM-23	UOC-25000	23	Wood, sedge, seed	420 +/- 20	515-460 (95.4%)	n/a
TR-SM-33	UOC-25001	33	Charcoal, wood	1600 +/- 20	1530-1412 (95.4%)	n/a
TRANS-41	664906	41		2420 +/- 30	2515 - 2351	2697 - 2637
TR-SM-66	UOC-25002	66	charcoal	4970 +/- 20	5741-5647 (77.4%)	5635-5603 (18%)
TR-SM-110	UOC-25003	110	Sedge, rhizomes	7810 +/- 25	8642-8537 (95.4%)	n/a
TR-SM-153	UOC-25004	153	Charred wood	8140 +/- 25	9256-9243 (1.3%)	9196-9182 (1.9%), 9134-9002 (92.3%)
TR-SM-195	UOC-25005	195	seed	8450 +/- 25	9530-9435 (95.4%)	n/a
TR-219						
CART-43	664908	43	wood	60 +/- 30	140 - 32	257 - 224
CART-78	UOC-25013	78	Sedge, wood, seed, leaf	2800 +/- 20	2960-2850 (95.4%)	n/a
CART-121	UOC-25014	121	wood	4530 +/- 20	5312-5261 (25.8%)	5245-5235 (1.4%), 5189-5052 (68.3%)
CART-171	UOC-25015	171	wood	5610 +/- 20	6443-6419 (12.1%)	6410-6310 (83.3%)
CART-218	UOC-25016	218	wood	6200 +/- 20	7167-7148 (8.2%)	7135-7001 (87.2%)
CART-255	UOC-25017	255	wood	6600 +/- 20	7565-7536 (22.8%)	7514-7430 (72.6%)
CART-334	UOC-25018	334	Conifer seed	8890 +/- 30	10175-9900 (95.4%)	n/a
CART-352	664909	352		8960 +/- 30	10226 - 10116	10066 - 10006
CART-373	UOC-25019	373	Seed, stem, leaf	9470 +/- 25	10770 - 10646	10992 - 10978

Average Long-term Apparent Rate of C_{org} Accumulation (LARCA) since peat inception varied from 16.7±11 g C_{org} m^{-2} yr^{-1} at Transplant and 17.6±10 g C_{org} m^{-2} yr^{-1} at Laurentian to 19.6±11 g C_{org} m^{-2} yr^{-1} at Cartier. At Transplant and Laurentian, LARCA displays a distinctly bimodal variability over time (Figs 3, 4), while at Cartier (Fig. 5) LARCA is unimodal. At Transplant and Laurentian, LARCA increases sharply during the peatland initiation process and displays a broad first peak during the early to mid-Holocene period (ca. 9,500 to 8,200 cal yr BP) when LARCA

values range between ~20 to 50 g C_{org} m^{-2} yr^{-1}, while at Cartier, the only LARCA peak (~20 to 40 g C_{org} m^{-2} yr^{-1}) is broad and appears later, during the mid Holocene (7,800 to 5,600 cal yr BP). Early LARCA peaks generally align with the Holocene Thermal Maximum, which occurred in NE North America around 10,000-5,700 Cal yr BP (Rensson et al., 2012). All sites experience decreasing LARCA values during the mid to late Holocene (ca. 5,000 to 2,000 cal yr BP) – a period described by Neoglacial cooling (Rensson et al., 2012) - when values drop to <5 g C_{org} m^{-2} yr^{-1}.

The beginning of the Industrial Isochron at Transplant and Laurentian is marked by substantial variability in LARCA (~20-50 g C_{org} m^{-2} yr^{-1}), followed by a general decrease thereafter. However, this second LARCA peak is preceded by progressively increasing values in peats deposited well before the beginning of the Industrial Isochron. At Cartier, the existence of this second peak is not apparent, although LARCA features some minor, short lived variability in peats deposited between 2,700 and 600 cal yr BP.

Inorganic C concentrations vary between 0.1 and 5% at all sites without a clear temporal pattern. However, Pre-disturbance averages are lower (2% at Cartier, 2.1% at Transplant, 2.3% at Laurentian) than those during the Industrial Isochron (3.2% at Cartier, 3% at Transplant, 3.9% at Laurentian) and the Recovery period (4.1% at Cartier, 2.3% at Transplant, 4.4% at Laurentian).

Peat C_{org}/N exhibit a generally non-monotonic increase over time at Cartier, with the lowest values recorded in older peats (13) and the highest at the surface (95), a brief but sharp decrease (23) at the end of the Industrial Isochron notwithstanding. At Transplant and Laurentian, C/N follow a broad bimodal pattern with increasing values during the early peatland development (13

to 60), a decrease in the peat deposited during the late Pre-disturbance and Industrial Isochron periods (60 to 17), and finally a second increase during the Recovery period (17 to 34).

2.5.5 Metals, Metalloids, and Key Non-Metallic Elements

Table 4 *Stocks of organic carbon and select metal, metalloid, and sulfur over the top 100 cm at the three peatland sites (Transplant, Laurentian, Cartier N) in the Greater Sudbury Region (ON).*

(g m^{-2})	Cu	Ni	As	Cd	Pb	Zn	Ca	Na	P	Fe	S	C_{org} Stocks (kg/m^2)
Laurentian	139	254	6.5	0.49	18	11	4251	46	287	1938	1716	147
Transplant	169	277	6	0.5	29	11	3626	53	376	2524	1734	152
Cartier N	9.5	4.8	1.1	0.73	5.7	7.2	930	39	111	467	758	130

The geochemical profile of the peat cores at each site is presented in Fig 3, 4, and 5 and includes key toxic metals and metalloids (TMM) and total S related to the historical smelting (Ni, Cu, Pb, Cd, As, Fe and Zn), as well as several critical elements namely Ca, N, P, and Na.. Complete ICP-OES geochemical assays are included in Appendix 4.

Toxic Metals and Metalloid loadings were generally highest at the Laurentian site in peat formed prior to the Industrial Isochron (Cu: 1,550 µg g^{-1}, Ni: 1,569 µg g^{-1}, As: 48 µg g^{-1}) except Cd and Zn, which are highest at Cartier (Cd: 9.7 µg g^{-1}, Zn: 73 µg g^{-1}) and Pb, which had highest concentrations at Transplant (Pb: 163 µg g^{-1}), all either during or slightly below the Industrial Isochron. During the Recovery Period, TMMs concentrations decreased considerably (on average by 61%), although remained within the same geographical patterns as for maximum values. The stocks for the top 100 cm of each core share a slightly different story; Transplant had the highest stocks for Cu (139 g m^{-2}), Ni (277 g m^{-2}), Pb (29 g m^{-2}), and is tied with Laurentian for the highest stocks of Zn (11 g m^{-2}). Laurentian had the highest stocks only for As (6.5 g m^{-2}), and Cartier only for Cd (0.73 g m^{-2}). Iron reaches the highest concentrations at Transplant (13,340µg g^{-1}) slightly below the Industrial Isochron, followed by the Cartier site (10,621µg g^{-1})

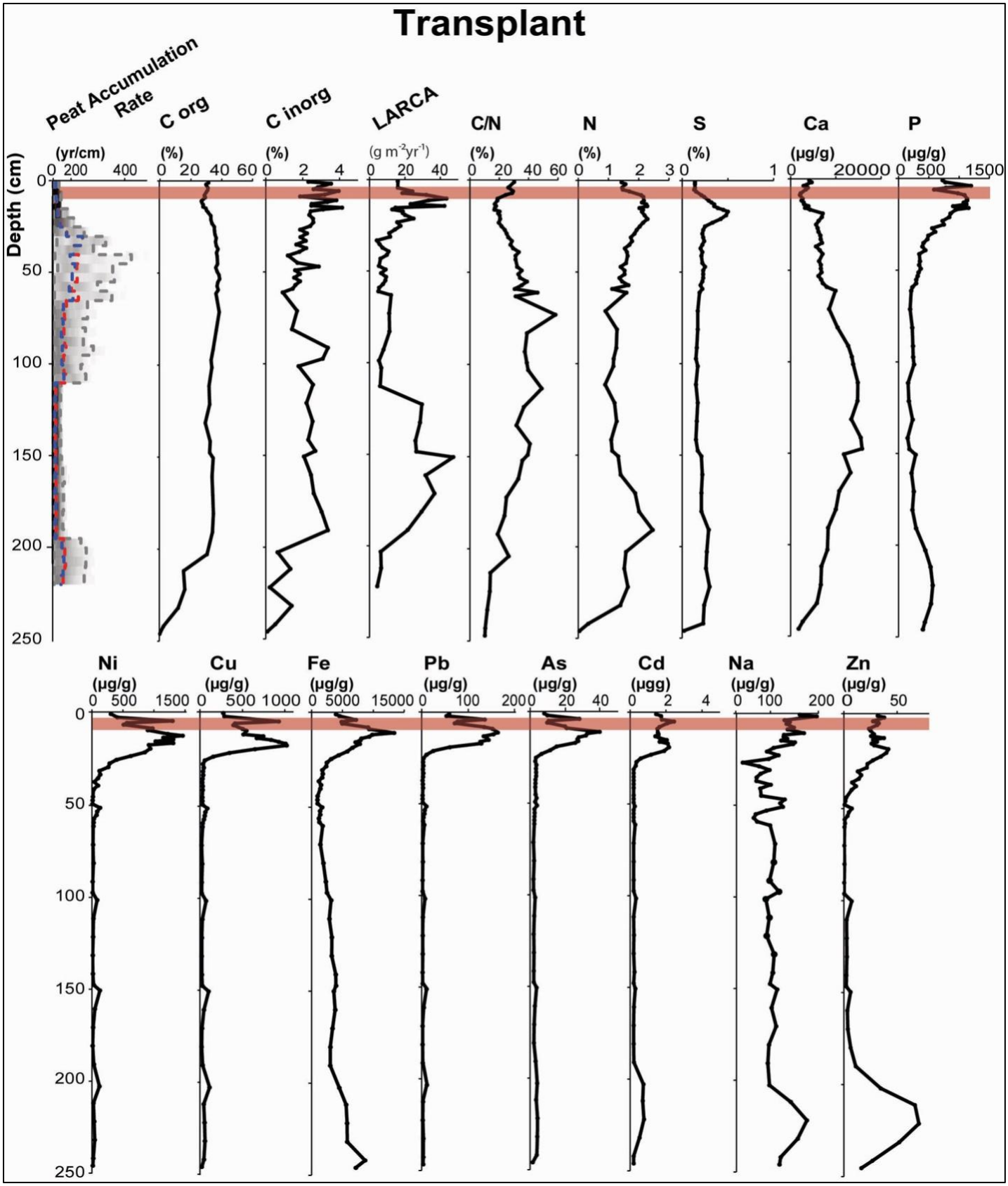

Figure 3 *Peat accumulation rate, Long-term Apparent Rate of organic Carbon accumulation (LARCA), and peat geochemistry (major elements, metals, and metalloids) at the Transplant peatland, a heavily degraded peatland in the Greater Sudbury Region (ON), Canada. The red shade stripe represents the Industrial Isochron (1880 to 1975 CE). The density shading (grey) features peat accumulation rates, with darker shades representing higher accumulation rates. Average and median peat accumulation rates are marked with dashed curves, red and blue, respectively.*

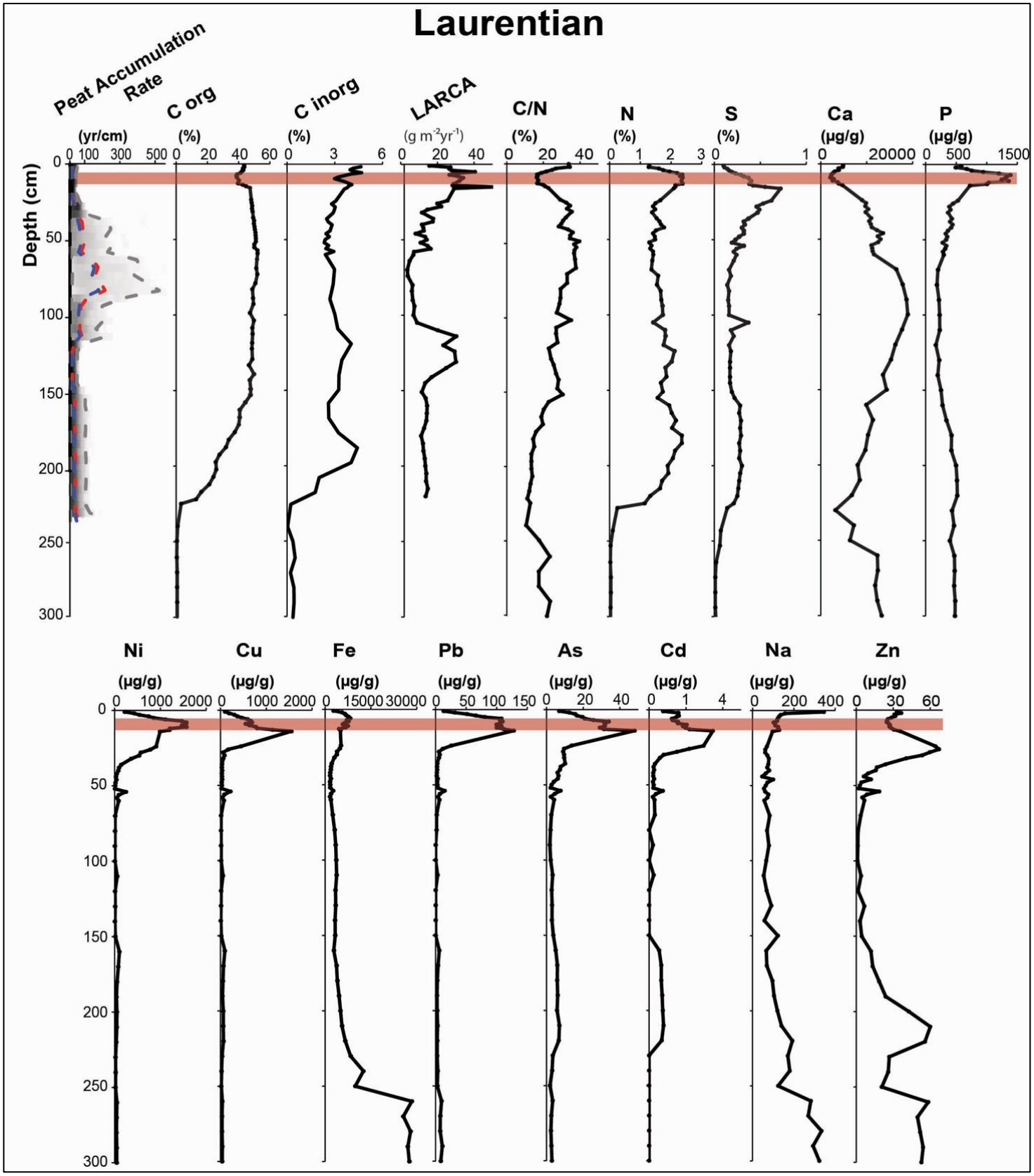

Figure 4 *Peat accumulation rate, Long-term Apparent Rate of organic Carbon accumulation (LARCA), and peat geochemistry (major elements, metals, and metalloids) at the Laurentian peatland, a heavily degraded peatland in the Greater Sudbury Region (ON), Canada. The red shade stripe represents the Industrial Isochron (1880 to 1975 CE). The density shading (grey) features peat accumulation rates, with darker shades representing higher accumulation rates. Average and median peat accumulation rates are marked with dashed curves, red and blue, respectively.*

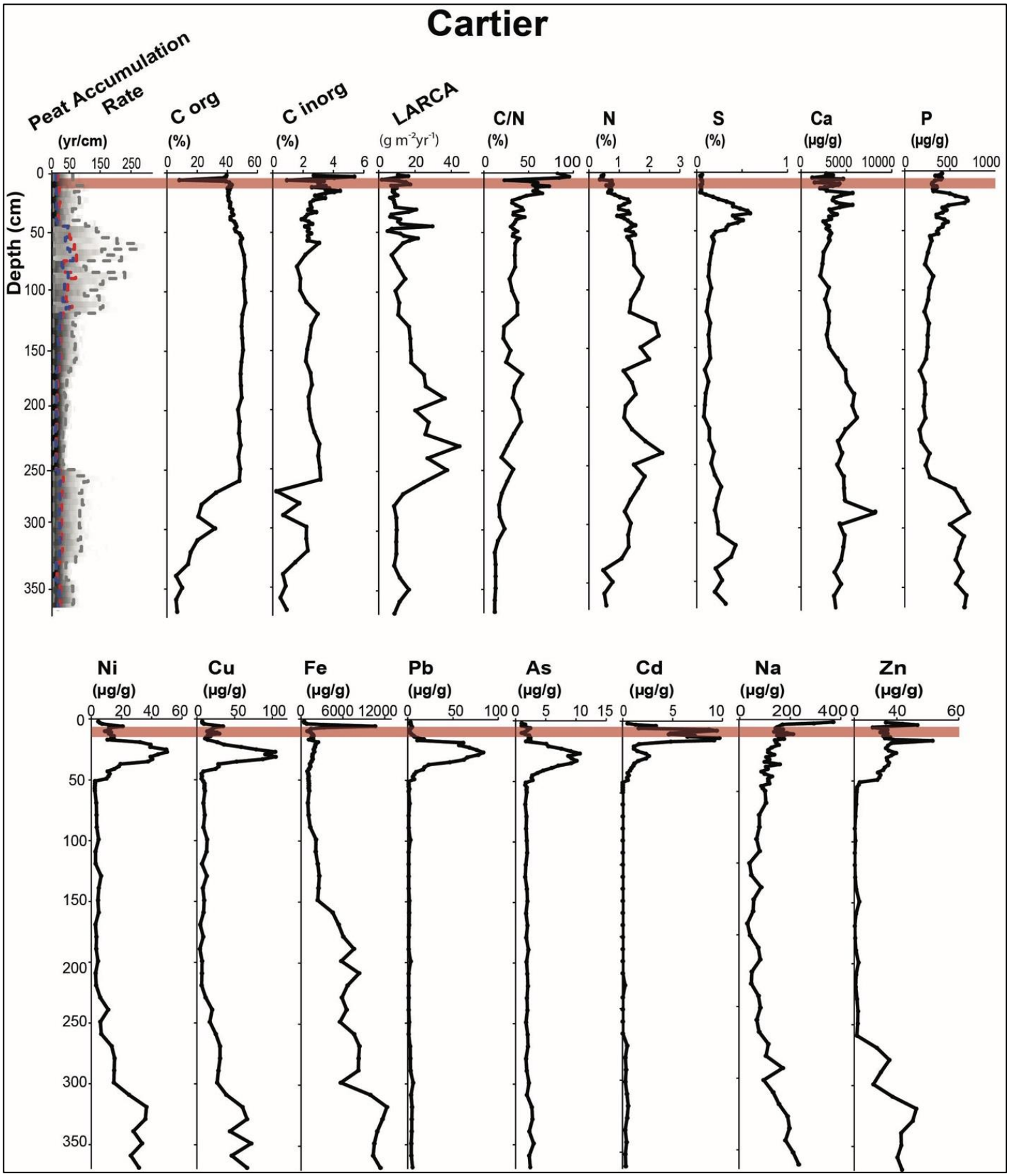

Figure 5 *Peat accumulation rate, Long-term Apparent Rate of organic Carbon accumulation (LARCA), and peat geochemistry (major elements, metals, and metalloids) at the Cartier peatland, a minimally impacted peatland in the Greater Sudbury Region (ON), Canada. The red shade stripe represents the Industrial Isochron (1880 to 1975 CE). The density shading (grey) features peat accumulation rates, with darker shades representing higher accumulation rates. Average and median peat accumulation rates are marked with dashed curves, red and blue, respectively.*

and Laurentian (8,222 μg g^{-1}), both within the Industrial Isochron peat. Transplant had the highest stocks for Fe (2524 g m^{-2}).

Sulfur concentration patterns follow closely those of Cu and Ni (Figs. 3 to 5) with the Laurentian site recording the maximum concentration (7744 μg g^{-1}) slightly below the Industrial Isochron horizon, followed by Cartier (6842 μg g^{-1}), and Transplant (5304 μg g^{-1}). However, the total S loading for the upper 100 cm of peat shows that Cartier accumulated the least amount of S (758 g m^{-2}), while Laurentian accumulated 1716 g m^{-2} and Transplant 1734 g m^{-2}.

Calcium concentrations in peat were highest at the Laurentian site (Ca: 18,926 μg g^{-1}) in peat formed well before the Industrial Isochron, a temporal pattern shared with the other two sites. However, there is a distinct, well-constrained decrease of both these elements during the Industrial Isochron and a recovery thereafter (Figs. 3 and 4). This pattern is absent at Cartier (Fig. 5), where Ca exhibits a decreasing but highly variable pattern since 6,600 cal yr BP. Laurentian had the highest stocks for Ca (4251 g m^{-2}).

Phosphorus concentrations reach maximum values at Laurentian (1387 μg g^{-1}) and Transplant (1193 μg g^{-1}) during the Industrial Isochron, while at Cartier values are substantially lower (693 μg g^{-1}) attained well below the Industrial Isochron. Transplant had the highest stocks for P (376 g m^{-2}).

Finally, Na concentrations are highest at Cartier (370 μg g^{-1}) followed by Laurentian (345 μg g^{-1}) and Transplant (173 μg g^{-1}) all attained during the Recovery Period. Transplant had the highest stocks for Na (53 g m^{-2}).

2.6 Discussion

2.6.1 Vertical Translocation of Metals and Sulfur in Peatland Soils

The peat profiles from the three study sites reveal distinct geochemical signatures that reflect both industrial atmospheric deposition and longer-term pedogenic processes. Sharp increases in Cu, Ni, Pb, Cd, As, Zn, and total S near or slightly below the Industrial Isochron at both Laurentian and Transplant indicate substantial smelter-derived inputs, consistent with historical emissions patterns of the Sudbury smelting complex (Chan and Lusis, 1985; Gunn et al., 1995; Keller et al., 1998). Sodium is the only metal that peaks during the Recovery Period, probably a reflection of de-icing road salt treatment in the last 50 years (Pearson et al., 2001). The minimally impacted Cartier site, though still showing 19th–20th century enrichment, exhibits considerably lower absolute loadings, reinforcing the interpretation that the elevated concentrations at these sites are attributable to the local point-source industrial deposition.

The juxtaposition of sharp industrial-era concentration peaks with more diffuse enrichments extending tens of centimeters downward is consistent with limited but measurable post-depositional mobilization of many TMMs in acidic, poor-fen peat systems. Elevated sulfuric acid inputs from smelting and industrial emissions can decrease porewater pH and, in turn, increase the solubility and subsequent downward transport of pH sensitive trace metals (i.e., Ni, Cu, Pb, and Zn), especially where porewaters are dominated by dissolved organic ligands and mineral buffering is weak (Nieminen et al., 2002; Rausch et al., 2005; Novák and Pacherová, 2008; Novák et al., 2005) and mean hydraulic gradients are downward. At multiple Central and Northern European sites with industrial histories broadly similar to Sudbury, downward redistribution of S and sulfate has been demonstrated through depth offsets between deposition

histories and peat S maxima (e.g., Novák et al., 2005), and through strong covariance between S and mobile metals in pollution-era peat profiles (e.g., De Vleeschouwer et al., 2009). In these acidic, organically buffered systems, metals such as Ni, Cu and Zn are readily mobilized likely via organic complexation, changing redox conditions, and leaching, producing vertically-smoothed profiles (Shotyk et al., 1996; Rausch et al., 2005, Novák and Pacherová, 2008). Collectively, these findings suggest that atmospheric sulfur enrichment and associated acidification can promote modest downward migration of sulfur and co-transport of dissolved, mobile trace metals, particularly in poor fens and ombrotrophic bogs where groundwater-derived base cations are scarce and pH is governed largely by organic acids (Shotyk, 1996; Bourbonniere, 2009).

In addition to aqueous leaching, several studies have documented limited gravity-driven downward movement of metal-bearing particulates in some peatlands. Fine atmospheric particles and metal-rich organo-mineral aggregates containing Pb, Zn, Cu, Ni, and As can be retained and redistributed within surface peat layers, with prolonged residence making them susceptible to gravitational relocation and porewater-driven movement (i.e., colloidal transport) that blurs sharp depositional peaks (Smieja-Król et al., 2010; Shotyk, 1988; Kalmykova et al., 2010). Although much weaker than solute-mediated transport, this process can contribute to the smearing of industrial-era pollution signals and partially explain downward offsets in some metal concentration peaks observed in the Sudbury peatlands.

A key question is whether the deeper maxima of several metals (especially Ni, Cu, As, Fe, and S) in the Laurentian and Transplant profiles (Fig. 3 & 4) represent downward migration of pollution-derived contaminants or reflect inherited geochemical inputs from the initial organo-mineral stages of peat formation, when these wetlands were broadly connected with surface

hydrology. The presence of elevated metal concentrations in the basal gyttja and minerotrophic peats at all sites points to a significant terrigenous component linked to the mineralogy of the Sudbury Igneous Complex (Ames et al., 2002; Grieve and Therriault, 2000). These deeper strata therefore suggest a plausible geogenic source for some of the elevated metal concentrations in the lower catotelm via upward diffusion into the peat (Reeve et al., 2001), even in the absence of anthropogenic forcing. However, detailed hydrogeochemical and peatland development exploration and numerical modelling would be needed to test this hypothesis.

A striking geochemical signal emerging from Laurentian (Fig. 4) and, to a lesser extent, from Transplant (Fig. 3) is the paired pattern of a modest but distinct Ca depletion together with marked enrichments in N and P, features largely absent at the minimally impacted site Cartier (Fig. 5). Because these values derive from bulk peat concentrations, the elevated N and P need not indicate increased nutrient storage; rather, they reflect a combination of external industrial-era inputs and post-depositional concentration effects driven by enhanced peat degradation. Prolonged exposure to smelter-derived sulfate from elevated atmospheric SO_2 and the resulting acidification would have intensified base-cation leaching, with Ca among the most readily mobilized under chronic acid deposition (Likens et al., 1996). At the same time, regional increases in atmospheric NOx deposition (Dentener et al., 2006; Vet et al., 2014) and P-bearing industrial dust and combustion aerosols (Tipping et al., 2014; Schillereff et al., 2021) likely imposed a gradual nutrient load on these otherwise oligotrophic systems. Equally important, however, is the mechanism of apparent enrichment through selective carbon loss. Chronic sulfur and metal stress in the Sudbury region reduced *Sphagnum* productivity or eliminated it (Gignac and Beckett, 1986; Rochefort and Vitt, 1990) but also stimulated microbial mineralization, likely through the promotion of sulfate-reducing pathways that oxidize organic matter to CO_2 (e.g.,

Nedwell and Watson, 1995) and through sulfuric acid-driven destabilization of humic–metal complexes that increases the chemical lability of peat organic matter (Tipping et al., 2003). Under such conditions, carbon was preferentially lost relative to nutrient elements, a pattern well documented in current peat litter decomposition studies (Moore et al., 2007), leading to progressively higher bulk concentrations of N and P even in the absence of substantial additions to their total pools. The broad, progressive rise in N and P toward the Industrial Isochron - and the discrete peak during it – thus likely reflects the overlap of enhanced nutrient deposition and acrotelm redistribution, with decomposition-driven concentration. Taken together, the Ca depletion coupled with N–P enrichment forms a clear industrial-era stoichiometric overprint, indicating that Laurentian and Transplant have undergone fundamental shifts in nutrient balance and post-genetic carbon loss, in sharp contrast to the relatively stable oligotrophic stoichiometry maintained at Cartier.

2.6.2 "Chemical" Fens – A Novel Ecosystem with a Soil Carbon Paradox

Viewed through the lens of long-term apparent rates of carbon accumulation (LARCA), the three Sudbury peatlands present a deceptively simple picture. Mean LARCA values range from 16.7±11 and 17.6±10 g C_{org} m^{-2} yr^{-1} at Transplant and Laurentian to 19.6±11 g C_{org} m^{-2} yr^{-1} at the minimally impacted Cartier peatland. The Cartier value is close to the time-weighted Holocene mean of ~22 g C m^{-2} yr^{-1} derived from global peatland syntheses (Yu et al., 2010; Loisel et al., 2014) and lies midway within the broader 15–25 g C m^{-2} yr^{-1} range typical of northern peatlands (Treat et al., 2016). In contrast, the lower LARCA values at Laurentian and Transplant signal a small but non-trivial long-term carbon deficit relative to both the regional reference site and global expectations. The LARCA patterns observed below 1 metre within the

peat profiles may be explained through the influence of Holocene paleoclimate variability on peat accumulation, namely the Holocene Thermal Maximum and Neoglacial cooling period.

Peatland initiation occurs when effective precipitation (precipitation less evapotranspiration) and other hydrologic inputs are high enough to keep the water table at or near the surface, creating saturated, low-pH conditions that favour *Sphagnum* growth (Magnan and Garneau, 2014). The Holocene Thermal Maximum was a warm-wet interval that occurred globally around 12,900-5,700 Cal yrs BP but was delayed in NE North America by 1-2 ka due to forced cooling from the Laurentide Ice Sheet (Rensson et al., 2012; Porter et al., 2019; Magnan and Garneau, 2014; Wu et al., 2023). The higher temperatures and precipitation characteristic of the HTM likely would have raised water tables, promoting rapid *Sphagnum* growth and thus increase peat accumulation rates (Magnan and Garneau, 2014). Following was a period of Neoglacial cooling, occurring in eastern Canada from ~5,0000-950 Cal yrs BP, it was a period of reduced temperatures and drier conditions (Magnan and Garneau, 2014; Wu et al., 2023). These drier conditions likely would have lowered water-table depths, increased hydrologic variability, and reduced *Sphagnum* growth, leading to slower peat accumulation rates (Magnan and Garneau, 2014).

Peat accumulation rates are a direct driver of long-term carbon accumulation as the amount of organic matter being stored depends on how quickly peat layers are established (Magnan and Garneau, 2014; Wu et al., 2023). High *Sphagnum* productivity – as seen during the HTM – increases peat formation, leading to periods of rapid peat buildup and therefore higher rates of carbon sequestration. In contrast, reduced *Sphagnum* growth – as seen during the period of Neoglacial cooling – slows both peat and carbon accumulation.

Age–depth relationships reinforce this interpretation. The upper metre of peat at Transplant accumulated over ~7,920 years and at Laurentian over ~7,500 years, compared with only ~3,970 years at Cartier. For comparable peat thickness, the impacted poor fens are therefore almost twice as old as the minimally disturbed one. If LARCA represents the long-term balance between carbon inputs and losses, the combination of older ages and lower mean LARCA at the polluted sites implies either slower long-term net carbon addition or post-depositional carbon loss, or a combination thereof. The depth of this deficit, together with the physical condition of the peat, points to older catotelm strata as the locus of carbon loss. All three peatlands initiated as minerotrophic fens, and macrofossil evidence indicates broadly similar early vegetation despite a later oligotrophication at Cartier. The key distinction is therefore not initial trophic status but prolonged exposure to acidifying metal–sulfur pollution at Laurentian and Transplant.

Studies from Central European industrial peatlands show that heavy SO_2 deposition can drive a smear-front migration of sulfate and associated metals into older peat layers, coupled with pH reduction, dissolution of existing mineral phases, and formation of secondary Fe–S minerals (Smieja-Król et al., 2010; Cabała et al., 2013). As this chemically reactive front moves downward, it increases the solubility of humic substances and stimulates release of dissolved organic carbon (DOC). Experimental and field studies in peatlands demonstrate that sulfate inputs and acidity stimulate DOC production and export by accelerating sulfur and iron cycling and increasing organic matter solubility (Urban et al., 1989; Evans et al., 2012; Clark et al., 2012).

In the Sudbury fens, this suggests that intermediate, sub-lethal pollution zones (where decomposers were impaired but not eliminated) were chemically primed for enhanced decomposition of older, partially humified peat. The physical structure of the peat in Sudbury

peatlands supports this mechanism. The upper metre at Laurentian and Transplant shows signs of compression and structural collapse, with higher bulk density, as well as significant different hydrophysical properties to unimpacted poor fens (McCarter et al., 2024). Similar compaction patterns are characteristic of peatlands undergoing chemical degradation or oxidation-driven mass loss (Landry and Rochefort, 2012; Price and Schlotzhauer, 1999), beyond what self-weight consolidation alone would produce (Clymo and Pearce, 1995). This indicates that peat in horizons below the identified Industrial Isochron at the impacted sites likely experienced enhanced decomposition and carbon export.

In contrast to this decomposition impairment within deeper strata, the horizons below the sub-surface horizons at Laurentian and Transplant tell a different story. During the decades of extreme pollutant loading, TMMs toxicity and severe acidity may have suppressed microbial decomposers and extracellular enzyme activity, resulting in reduced decomposition and an industrial-era LARCA peak. In these near surface horizons, even modest productivity can yield elevated apparent accumulation when decomposition is greatly inhibited due to previous decomposition of the more labile organic matter. However, it is important to acknowledge that over short intervals, (i.e. decades) LARCA can be inflated by incomplete decomposition of young peat that has not reached mass-loss equilibrium (Clymo, 1984).

This vertical partitioning of pollution effects clarifies the paradox. Industrial pollution simultaneously enhanced peat decomposition throughout and below the Industrial Isochron and preserved more recent organic matter either through increased less labile organic matter inputs (i.e., shift towards woody vegetation, e.g., Gignac and Beckett, 1986), peat consolidation-moisture content feedback decreasing organic matter decomposition (c.f., Waddington et al., 2014; McCarter et al., 2020; Furukawa et al., 2025), periodic suppression of microbial activity

due to elevated pollution concentrations (e.g., Vile et al., 2003a; Vile et al., 2003b), or, most likely, a combination of all three. The result is a peat column in which late-Holocene LARCA is inflated by potentially suppressed surface decay, yet long-term LARCA is depressed by cumulative losses from deeper layers.

The Holocene LARCA trajectories reinforce this interpretation. Cartier exhibits a unimodal pattern, peaking during the early to mid-Holocene, consistent with regional climate-driven C accumulation found across eastern Canada and northern peatlands more broadly (Loisel et al., 2014; Morris et al., 2018). Laurentian and Transplant show the same early-Holocene peak, confirming shared climatic controls, but also exhibit a second, industrial-era peak. Such a resurgence in apparent accumulation is difficult to attribute to climate alone and aligns instead with pollution-induced arrest of decomposition. Thus, the Sudbury fens functioned as vertically stratified chemical reactors, experiencing two contrasting carbon regimes over time and depth:

1. *Reduced decomposition and high apparent C_{org} accumulation* in upper horizons under extreme metal-acidity stress, peat consolidation, and vegetation shifts; and

2. *Enhanced decomposition and carbon export* in peat exposed to migrating metal-sulfur fronts and altered redox conditions.

Together, these mechanisms explain why Laurentian and Transplant show both an industrial-era LARCA peak *and* a long-term carbon shortfall. In our view, this is the most likely scenario capable of resolving this soil carbon paradox and highlights how anthropogenic chemical forcing can generate divergent carbon dynamics within a single peat profile, underscoring the vulnerability of deep, aged peat to industrial disturbance.

Integration of Chapters 2 and 3

Chapter 2 shows that industrial sulfur and TMM deposition fundamentally altered carbon accumulation trajectories. Despite extreme enrichment in Ni, Cu, Pb, As, and S, the proximal "chemical" fens had exhibited elevated apparent carbon accumulation during the industrial period, even as their long-term carbon storage is reduced relative to the minimally impacted site. This pattern reveals a soil carbon paradox: contamination appears to coincide with enhanced surface accumulation while ultimately contributing to a cumulative carbon deficit. Resolving this paradox requires examining the processes that regulate organic matter preservation and decay.

Microbial assemblages regulate the conversion of plant derived inputs into dissolved mineral, and gaseous carbon forms and are therefore central to long-term peatland carbon balance. Industrial sulfur deposition can modify porewater acidity and redox conditions, while TMMs may directly inhibit enzymatic activity or restructure microbial food webs. At the same time, base-cation buffering capacity and background mineral inputs influence the chemical environment in which these assemblages operate. These pollutants alter microbial metabolism directly through toxicity, and indirectly through changes in peat carbon composition.

Chapter 3 builds on these concepts by examining how microbial community structure responds to the geochemical characteristics identified in Chapter 2. Through stratigraphically constrained ordination and partitioning of variance among TMMs and sulfur enrichment, buffering capacity, and carbon composition, Chapter 3 reviews the relative importance of direct metal and sulfur toxicity versus indirect substrate-mediated controls on testate amoebae assemblages. It further assesses whether microbial communities exhibit evidence of recovery following reductions in atmospheric emissions or whether industrial-era restructuring persists in surface peat.

Chapter 3 – Persistent microbial restructuring in industrially contaminated peatlands: testate amoeba stratigraphies from the Sudbury smelting region.

3.1 Introduction

Peatlands are globally significant ecosystems, storing more carbon per unit area than any other terrestrial biome and regulating both local and regional hydrology (Yu et al., 2011; Gorham, 1991). These long-term carbon sinks exert a net cooling effect on global climate throughout the Holocene through sustained carbon accumulation (Frolking et al., 2006; Chaudhary et al., 2017). Their hydrological function is equally critical: by maintaining high water tables and slow decomposition rates, peatlands stabilise carbon stores, regulate runoff, and buffer watersheds during drought and flooding (Waddington et al., 2014). However, these functions are highly sensitive to atmospheric disturbance and climate-mediated drying (Weltzin et al., 2003; Lund et al., 2012; Furukawa et al., 2025). Lowered water tables promote peat mineralisation and carbon loss (Creevy et al., 2018), exacerbate wildfire severity (Turetsky et al., 2014), and alter vegetation communities in ways that restructure nutrient availability, energy budgets, and greenhouse gas fluxes (Turetsky and St. Louis, 2006; Andersen et al., 2010; Berger et al., 2017; Vitt et al., 2009). Anthropogenic pollutants and land-use change compound these climate-driven stressors, with the potential to shift peatlands from net carbon sinks to net carbon sources (Xu et al., 2018; Harris et al., 2021; Baird et al., 2009; Chaudhary et al., 2017; Qiu et al., 2020; Zhao and Zhuang, 2023).

Biological indicators provide a means of detecting and reconstructing past environmental changes in these systems (Birks et al., 2010; Parmar et al., 2016). Testate amoebae (TA) in

particular, are widely used paleoecological indicators due to their sensitivity to moisture, pH, trophic status, and pollutant loading, as well as their decay-resistant tests that preserve well in peat (Nasser et al., 2016; Swindles et al., 2016; Booth et al., 2025; Gu et al., 2025; Mitchell et al., 2008). Beyond their value as indicators, TA play integral roles in peatland functioning by regulating carbon and nutrient cycling (Wilkinson and Mitchell, 2010), contributing to microbial food web structure (Lamentowicz et al., 2013; Jassey et al., 2013), and influencing decomposition and photosymbiont-driven carbon uptake (Kuuri-Riutta et al., 2022; Wanner et al., 2020). Their community composition responds rapidly to acid deposition, TMMs, atmospheric pollution, drought, and warming, making them particularly informative in disturbed peatlands (Ndayishimiye et al., 2025; Gu et al., 2025; Wanner et al., 2020). Previous hydrological reconstructions have demonstrated that TA assemblages track changes in moisture gradients, with dry-indicator taxa (e.g., *Trigonopyxis* spp., *Assulina muscorum*) contrasting with wetter assemblages (e.g., *Amphitrema* spp., *Difflugia* spp.) (Booth et al., 2025; Swindles et al., 2016; Amesbury et al., 2018). Functional traits, such as mixotrophy or aperture position, have also been proposed as metrics for monitoring peatland degradation and restoration (Creevy et al., 2018; Marcisz et al., 2020).

A growing body of work has specifically examined the relationship between TA communities and atmospheric metal contamination. Experimental and field studies have shown that lead deposition reduces TA species richness and density (Nguyen-Viet et al., 2007, 2008), that *centropyxid* and agglutinated taxa dominate heavily polluted substrates (Asada and Warner, 2009; Patterson et al., 1996; Reinhardt et al., 1998), and that extreme atmospheric dust and metal deposition can restructure TA communities and functional traits in ways that may resemble or partially obscure hydrological change (Fiałkiewicz-Kozieł et al., 2015; Payne et al., 2012).

However, most of this work has focused on either modern communities or relatively short temporal windows. Long-term stratigraphic records that capture both the onset of industrial contamination and the subsequent post-industrial period remain rare, particularly from systems where the pollution source is well-characterised and the intensity was relatively large.

Sudbury, Ontario, provides an ideal system for addressing this gap (Chan and Lusis, 1985; Levasseur et al., 2023; McCarter et al., 2024). From the late nineteenth century through most of the twentieth century, Sudbury was one of the most extreme point sources of atmospheric pollution globally, emitting vast quantities of sulfur dioxide and toxic metals and metalloids (e.g. Ni, Cu, Pb, and As) from large-scale smelting operations (Gignac and Beckett, 1986; Saarinen, 2013; Gunn et al., 1995). These emissions produced highly acidic waters, barren landscapes, and widespread ecological collapse across the region (Keller et al., 1998; Gunn et al., 1995; Hutchinson and Whitby, 1977). Although significant improvements in smelting infrastructure following clean air legislation in the 1970s and 1990s have reduced emissions and facilitated large-scale regreening of forested uplands (Gunn, 1995; Gunn et al., 1995; Potvin and Negusanti, 1995; Sickles II and Shadwick, 2015), peatlands have largely been left to recover without active restoration (Newman et al., 2023; Gunn et al., 1995). Evidence increasingly suggests that peatland recovery has been slow or incomplete near smelters, with persistent contamination, altered vegetation and microbial communities, disrupted hydrology, and impaired carbon storage capacity (Pamer, 2008; Newman et al., 2023; Seward et al., 2023; McCarter et al., 2024). Despite more than a century of pollution and partial recovery, historical ecological and hydrological baselines remain largely unknown - a major barrier to assessing ecosystem resilience and informing targeted restoration.

The aim of this study is to reconstruct and compare past community change between peatlands distal and proximal to smelter centres using fossil testate amoeba assemblages in parallel with high-resolution geochemical profiles presented in a companion study (Mitchell et al., in preparation; hereafter Chapter 2). This study seeks to: (1) establish long-term pre-disturbance TA baselines, (2) characterise the nature and magnitude of community restructuring associated with industrial deposition, (3) evaluate the relative contributions of trace metal toxicity, sulfur enrichment, and peat substrate alteration as predictors of community change, and (4) assess whether microbial recovery has occurred following decades of reduced atmospheric emissions. Together, these objectives aim to provide critical context for understanding past ecosystem responses to extreme industrial pollution and for guiding future peatland restoration strategies in the Sudbury region.

3.2 Materials and Methods

3.2.1 Study Location and Environmental History

The Greater Sudbury Region (Fig. 1; see Chapter 2) occupies a ~200,000 ha area on the Canadian Shield in central Ontario, Canada, and is located within the traditional lands of the Atikameksheng Anishinaabek and Wanapitei First Nation. During the industrial period (1880–1975 CE) the region was a major centre of nickel and copper mining and smelting (Newman et al., 2023). Industrial emissions during this period resulted in substantial deposition of sulfur dioxide and associated metals, influencing the chemistry of surrounding terrestrial and wetland ecosystems (Potvin, 2007; Gunn et al., 1995; Seward, 2023; Seward et al., 2023; Gignac and Beckett, 1986).

The industrial legacy of the area has created three landscape units characterised by varying levels of historical disturbance. The areas proximal to the smelters and ore roasting yards, termed the Barrens, were defined as areas generally devoid of plant life with soil pH below 4.3 (Gignac and Beckett, 1986; Lautenbach et al., 1995). Between and around the Barrens, the Semi-Barrens supported more abundant vegetation (Watkinson et al., 2022). Beyond the Semi-Barrens, the Atmospheric Fallout zone was characterised by lower pollutant loading and consequently less disturbed vegetation.

Following the industrial period, despite large-scale restoration efforts focused on upland forests (Watkinson et al., 2022), the vegetative cover of Barren areas remains low and non-native species constitute most of the plant cover (Barrett and Watmough, 2015; Gignac and Beckett, 1986; Newman et al., 2023; Watkinson et al., 2022). Colonisation by native species and *Sphagnum* continues to be inhibited by legacy metal concentrations (Gignac and Beckett, 1986; Seward et al., 2023).

3.2.2 Regional Setting

The Greater Sudbury Region is located on the southern Canadian Shield and experiences a continental climate with a mean annual precipitation of ~903 mm (Environment Canada, 2025). Average temperatures range from −17.1°C in January to 25.2°C in July (Environment Canada, 2025). Sudbury lies within an ecotonal transition between the Boreal Forest and Great Lakes–St. Lawrence Forest regions (Rowe, 1972; Ontario Ministry of Natural Resources, 2021), supporting mixed coniferous and deciduous forests alongside extensive wetlands, lakes, and rock barrens (Sherman and Beckett, 2003; City of Greater Sudbury, 2013). The region falls within the Georgian Bay (Lake Huron) watershed and is primarily drained by the French and Spanish River

systems, with regional flow-oriented northeast–southwest (Ontario Ministry of Natural Resources and Forestry, 2025).

3.2.3 Site Selection

Three poor fen systems (National Wetlands Working Group, 1997) were selected (Fig. 1, Table 2; see Chapter 2) along the regional pollution gradient, with two proximal to former smelter centres (Transplant and Laurentian; colloquial, unofficial names) and one distal (Cartier North), situated at the northwest edge of the Atmospheric Fallout zone.

The Transplant site is a 0.7 ha isolated depression in bedrock, largely fed by rainfall and limited runoff from surrounding slopes. It is a heavily degraded peatland with wetland vegetation dominated by *Chamaedaphne calyculata*.

The Laurentian site occupies 2.29 ha (Szkokan-Emilson et al., 2013) slightly above the elevation of a large lake (Lake Laurentian). In contrast to Transplant, Laurentian formed through paludification of a former riparian system and remains coupled to the surface hydrology, receiving a small intermittent brook at headwaters and being drained by a similar system downstream. It is also heavily degraded , with wetland vegetation dominated by *Carex echinata*. The peatland margins support sparse *Sphagnum* hummocks, although within the peatland interior *Sphagnum* is absent.

The Cartier North site is a 3.74 ha, minimally impacted peatland with wetland vegetation dominated by *Sphagnum* species (*S. fallax*, *S. fuscum*, *S. divinum complex,* and *S. rubellum*) and several vascular taxa including *Rhododendron groenlandicum* and *Chamaedaphne calyculata*.

Sediment cores were retrieved from the deepest part of each site using a McCauley corer to the depth of refusal (Table 2; see Chapter 2). Cores were sealed in PVC pipes lined with plastic film

on site and transported to the laboratory where they were stored at 4°C until processing. For the uppermost horizons with live, often woody rhizosphere material where the McCauley blade was ineffective, 30 × 30 cm monoliths (~30–50 cm depth) were cut with a serrated knife and wrapped in plastic film. Sediment cores were subsampled at 1-cm-thick intervals every 2 cm to a depth of 60 cm and every 10 cm thereafter. Samples of known volume were oven-dried at 50°C to constant weight and ground to a fine powder. Bulk density (g cm^{-3}) was calculated as dry weight divided by sample volume.

3.2.4 Testate Amoeba Analysis

Samples were processed following a modified version of the protocol described by Booth et al. (2010). Subsamples were placed into 50 mL centrifuge tubes filled with deionised water and boiled for 20 minutes. The resulting suspension was sieved through a 300 µm mesh; the smaller fraction was then sieved through a 7 µm mesh, and the larger fraction was retained for macrofossil analysis. Sieved residues were centrifuged at 2500 rpm for 5 minutes and a subsample of the resultant material was transferred to a microscope slide for identification at 400× magnification.

A minimum count of 100 tests per sample was targeted following standard practice (Payne and Mitchell, 2009). Where preservation was sufficient, counts exceeded this threshold. However, test preservation declined substantially in deeper horizons at all three sites, particularly below the industrial isochron at Laurentian and Transplant. Samples yielding fewer than 50 identifiable tests were retained in stratigraphic diagrams but are plotted with open symbols to distinguish them from statistically robust counts. Sterile samples (TA sum = 0) and samples with fewer than 50 tests were not included in diversity calculations or in the response matrix for constrained ordination and variation partitioning (Laurentian n=7, Transplant n=4). Instead, these samples

were projected passively into CCA ordination space using their geochemical profiles as predictors, providing a visual indication of where these chemically characterised but biologically depauperate or unproductive horizons would fall relative to the environmental gradients structuring the viable assemblages. This approach ensures that the multivariate analyses are based on statistically adequate counts while preserving the spatial context of sterile or poorly preserved intervals as evidence of substrate conditions hostile to TA preservation or habitation.

Tests were identified to the species level where possible using the taxonomic keys of Booth and Sullivan (2007) and pooled into taxonomic groups following Amesbury et al. (2018). Relative abundance (%) of each taxon was calculated for each sample. All stratigraphic analyses and reconstructions were performed using the 'riojaPlot' package in R (Juggins, 2019).

3.2.5 Community Wetness Affinity (WT_index)

To provide an assemblage-level summary of hydrological preference, each taxon was assigned to one of four hydrological affinity categories - high water table (HWT), intermediate water table (IWT), low water table (LWT), or Degraded - based on published ecological optima (Amesbury et al., 2018; Booth et al., 2025; Swindles et al., 2016). The Degraded category encompasses taxa that are not characteristic of any specific water-table position in undisturbed peatlands but are instead associated with disturbed, minerotrophic, or heavily modified substrates where conventional moisture categories may not apply. A community wetness affinity index (WT_index) was then calculated for each sample as:

$$WT\_index = HWT + 0.5 \times IWT - LWT$$

Where HWT, IWT, and LWT represent the summed relative abundances of taxa assigned to high, intermediate, and low water-table categories, respectively. This index represents

community-level moisture preference rather than a quantitative reconstruction of water-table depth. Samples with fewer than 50 tests were excluded from WT_index calculations.

3.2.6 Peat Composition Analysis

Due to the advanced state of peat humification in the cores from Transplant and Laurentian, the standard macrofossil pre-treatment (Mauquoy et al., 2010) was modified. Peat samples at 2 cm intervals to a depth of 60 cm and at 10 cm intervals thereafter were dispersed in warm 5% KOH solution for 15 minutes and then washed over a 125 μm nylon mesh sieve. The retained material was placed in Petri dishes and examined under a low-power stereo-zoom microscope. A semi-quantitative analysis (Walker and Walker, 1961; Barber, 1981) classified identifiable plant detritus into major macrofossil categories using diagnostic cell structure features. Macrofossil groups comprised gyttja, herbaceous undifferentiated, ligneous undifferentiated, Ericaceous, Carr, Poales, Bryidae, and *Sphagnum* moss. Identification follows Lévesque et al. (1988) and Schweingruber et al. (2020).

3.2.7 Radiometric Dating and Age-Depth Modelling

Accelerator Mass Spectrometry (AMS) radiocarbon measurements were obtained exclusively on macrofossils including seeds, twigs, and leaves. AMS analyses were performed by Beta Analytic Inc. (Miami, USA) and the André E. Lalonde AMS Laboratory at the University of Ottawa (Canada). Calibrated ranges are reported as two standard deviations. Age–depth models for all cores were derived using the *rbacon* package in R (Blaauw and Christen, 2011). Full details of dating results and age–depth models are presented in Chapter 2.

3.2.8 Geochemical Predictors

High-resolution geochemical profiles of all three cores, including measurements of toxic trace metals and metalloids (Cu, Ni, Pb, Zn, Cd, As), lithogenic elements (Al, Ti, Fe, Mn, Cr, Co, V, Si), base cations and nutrients (Ca, Sr, Mg, P, %N), sulfur (%S), and carbon (%Corg, %Cinorg), are presented in Chapter 2.

To reduce the dimensionality of the geochemical dataset while retaining ecologically interpretable groupings, principal component analysis (PCA) was applied separately to four element groups. A toxic trace metal and metalloid composite (TMM_PC1) was derived from Cu, Ni, Pb, Zn, Cd, and As after $\log_{10}(x + 1)$ transformation. A residual lithogenic composite (OTHER_PC1) was derived from Al, Ti, Fe, Mn, Cr, Co, V, and Si, also $\log_{10}(x + 1)$-transformed. A base cation–nutrient composite (BASE_NUT_PC1) was derived from Ca, Sr, Mg, P, and %N on untransformed values. A carbon composition composite (CARBON_PC1) was derived from %Corg and %Cinorg, also untransformed. In each case, PCA was performed on centred and scaled variables using prcomp in R, and the first principal component (PC1) was retained as a composite index. Rows with more than one missing value (two for OTHER_PC1; zero for CARBON_PC1) were excluded from the PCA; remaining missing values within retained rows were imputed with column medians prior to scaling. Sulfur (%S) was retained as an independent predictor and was not included in any PCA grouping. Variable loadings and variance explained by PC1 for each composite are reported in Appendix 7.

3.2.9 Statistical Analysis

Stratigraphic zonation was performed independently for each core using constrained incremental sum of squares (CONISS; Grimm, 1987) applied to the TA relative abundance data. The number

of statistically significant zones was determined using the broken-stick model (Bennett, 1996). Where non-significant subclusters coincided with independently dated industrial boundaries and exhibited ecologically interpretable compositional shifts, they were retained as informal subzones and are identified as such in the text and figures.

Canonical correspondence analysis (CCA) was used to assess the relationship between TA community composition and grouped geochemical gradients across all three cores. The constrained model included five predictors: TMM_PC1, S%, BASE_NUT_PC1, CARBON_PC1, and OTHER_PC1. Significance of the overall model, individual axes, and individual terms was assessed via permutation tests (999 permutations). Variance inflation factors (VIF) were examined to evaluate multicollinearity among predictors.

Variation partitioning was conducted to isolate the independent and shared contributions of four geochemical gradients (TMM_PC1, S%, BASE_NUT_PC1, CARBON_PC1) to community composition, using adjusted R^2 values and permutation-based significance tests. This analysis did not utilize OTHER_PC1 as this predictor serves as a catch-all composite axis which summarizes the remaining geochemical variation, rather than representing an explanatory block.

Permutational multivariate analysis of variance (PERMANOVA) was applied to test for significant differences in community composition among pre-industrial, industrial, and post-industrial phases, with permutations stratified by core. Homogeneity of multivariate dispersion was evaluated using betadisper to distinguish centroid-position effects from dispersion effects.

Indicator species analysis was performed using the IndVal procedure of Dufrêne and Legendre (1997) to identify taxa significantly associated with disturbance phases, both globally (all cores

pooled) and within individual cores. Significance was assessed via permutation tests (1000 iterations; $\alpha = 0.05$).

All statistical analyses were conducted in R (R Core Team, 2024) using the 'vegan' (Oksanen et al., 2022), 'rioja' and 'riojaPlot' (Juggins, 2019, 2025), and 'indicspecies' (De Cáceres and Legendre, 2009) packages.

3.3 Results

3.3.1 Testate Amoebae Stratigraphy and Zonation

Cartier

Stratigraphically constrained cluster analysis resolved three statistically significant assemblage zones at 45 cm and 27 cm depth (ca. 375 and 177 cal yr BP, respectively).

CZ3 (70–45 cm; ca. 2400–375 cal yr BP). The basal zone is characterised by strong and sustained dominance of *Hyalosphenia subflava*, which averages 66.4% (median = 69.8%) and ranges from 41.2% to 87.8%, attaining its highest values in this interval. Subordinate but consistent components include *Trigonopyxis arcula* type (mean = 9.3%, range = 1.5–26.0%) and *Archerella flavum* (mean = 6.8%, range = 0–18.0%). Other taxa remain minor (<7%) throughout the zone. Assemblage composition is comparatively stable and clearly sphagnophilous-dominated.

CZ2 (45–27 cm; ca. 375–177 cal yr BP). CZ2 marks a distinct restructuring of the assemblage. *Cyclopyxis arcelloides* type becomes prominent, averaging 23.5% (median = 21.8%) and ranging from 8.3% to 39.7%. *Difflugia pulex* increases concurrently (mean = 16.9%, range = 4.5–29.5%),

while *Hyalosphenia subflava* declines to a mean of 15.8% (range = 6.3–27.0%). Dominance is more evenly distributed among taxa relative to CZ3, and no single taxon maintains overwhelming control of the assemblage.

CZ1 (27–0 cm; ca. 177 cal yr BP–present). The uppermost zone exhibits the greatest internal variability. *Hyalosphenia elegans* emerges as the most abundant taxon overall (mean = 21.4%, range = 0–63.9%), while *Difflugia pulex* remains prominent (mean = 15.6%, range = 0–36.4%). *Alabasta militaris* increases substantially (mean = 14.2%, range = 4.0–34.2%), and *Nebela tincta* type reaches up to 21.3%. Although maxima are high for several taxa, dominance fluctuates between samples rather than remaining consistent across the zone

Laurentian

Three primary zones were identified at 44 cm and 32 cm depth (ca. 1170 and 510 cal yr BP), with the uppermost zone further subdivided into two non-significant subclusters (LZ1a and LZ1b). Although these subclusters did not exceed the broken-stick significance threshold, they are retained because they correspond to independently dated industrial boundaries and exhibit ecologically interpretable compositional shifts consistent with the site's industrial history.

LZ3 (59–44 cm; ca. 2300–1170 cal yr BP). LZ3 is characterised by moderate but consistent dominance of *Hyalosphenia subflava* (mean = 34.8%, median = 33.3%, range = 22.2–50.0%). *Nebela tincta* type forms an important secondary component (mean = 18.4%, range = 5.9–33.3%), while *Difflugia pulex* averages 11.2% (range = 0–23.5%). The assemblage is relatively stable, with sphagnophilous taxa collectively forming the principal component of the community.

LZ2 (44–32 cm; ca. 1170–510 cal yr BP). In LZ2, *Hyalosphenia subflava* remains numerically dominant (mean = 43.6%, median = 50.0%), although the range broadens considerably (6.3–100%), the latter reflecting a single near-monospecific horizon. *Cyclopyxis arcelloides* type and *Trigonopyxis arcula* type increase modestly (means of 7.3% and 6.1%, respectively). Overall assemblage structure remains recognisable, but variability increases relative to LZ3.

LZ1a (32–19 cm; ca. 510–148 cal yr BP). LZ1a exhibits greater heterogeneity. *Cyclopyxis arcelloides* type (mean = 17.5%, range = 0–41.0%) and *Difflugia globulosa* type (mean = 14.8%, range = 0–41.3%) become prominent components, while *Hyalosphenia subflava* declines to a mean of 13.6% (range = 0–28.7%). Dominance is shared among several taxa, and assemblage structure becomes more evenly partitioned.

LZ1b (19–0 cm; ca. 148 cal yr BP–present). The uppermost subzone shows pronounced internal variability. *Difflugia globulosa* type attains a mean of 24.7% (range = 0–86.9%), while *Cyclopyxis arcelloides* type averages 18.2% (range = 0–35.0%). *Physochila griseola* also becomes prominent (mean = 14.9%, range = 0–84.2%). The high maxima in this interval reflect strong single-sample dominance events rather than uniform composition across the subzone.

Transplant

Three primary zones occur at 19.5 cm and 8 cm depth (ca. 330 and 40 cal yr BP), with TZ2 subdivided into two non-significant subclusters (TZ2a and TZ2b) retained for consistency with the industrial chronology, as described above for Laurentian

TZ3 (42–19.5 cm; ca. 2600–330 cal yr BP). TZ3 is dominated by *Hyalosphenia subflava*, which averages 59.6% (median = 68.0%) and ranges from 0% to 96.2%. Secondary taxa remain comparatively minor, including *Cyclopyxis eurystoma* (mean = 7.6%, max = 49.6%) and *Trigonopyxis arcula* type (mean = 5.3%, max = 20.0%). The interval is clearly sphagnophilous-dominated.

TZ2a (19.5–12 cm; ca. 330–119 cal yr BP). A marked shift occurs in TZ2a, where *Cyclopyxis arcelloides* type becomes overwhelmingly dominant (mean = 69.9%, median = 70.7%, range = 57.1–81.2%). Other taxa, including *Phryganella acropodia* type and *Hyalosphenia subflava*, remain present but subordinate (<7% on average).

TZ2b (12–8 cm; ca. 119–40 cal yr BP). Cyclopyxid dominance persists in TZ2b, though at slightly reduced mean abundance (53.3%, median = 55.3%, range = 21.4–81.2%). *Difflugia pulex* increases modestly (mean = 9.9%, max = 30.4%), while other taxa remain secondary.

TZ1 (8–0 cm; ca. 40 cal yr BP–present). In TZ1, assemblage composition shifts again. *Hyalosphenia subflava* (mean = 26.1%, range = 1.7–75.8%) and *Nebela tincta* type (mean = 20.3%, median = 22.7%, range = 0–42.6%) become the dominant taxa. *Difflugia pulex* remains an important component (mean = 12.8%, max = 35.1%). In contrast, *Cyclopyxis arcelloides* type declines markedly (mean = 7.5%). Dominance is less extreme than in TZ2, and composition varies between samples.

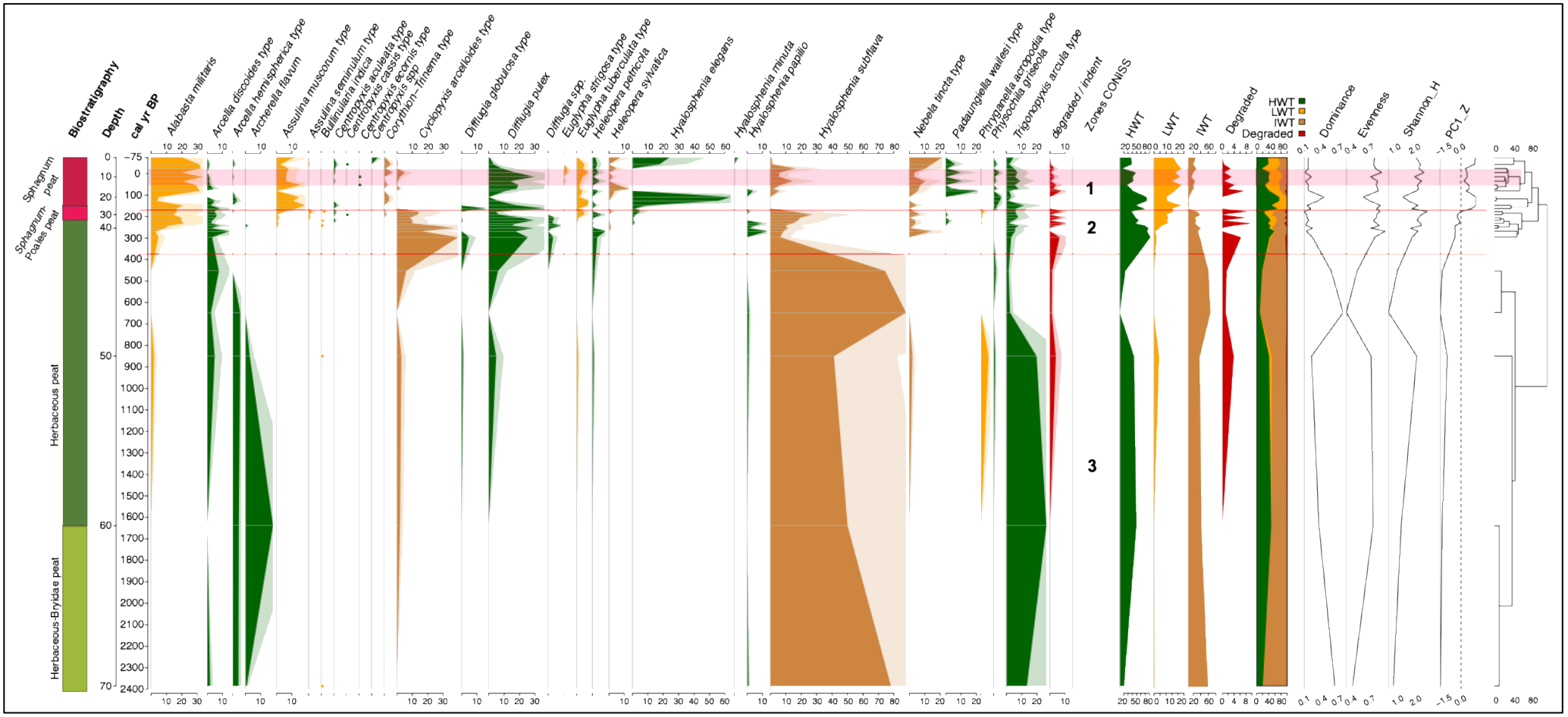

Figure 6 *Stratigraphic diagram of testate amoeba assemblages from the Cartier core over the last ~2400 calibrated years BP. Relative abundances are expressed as percentages of the total assemblage. Zones (CZ3–CZ1) were defined using CONISS; statistically significant zone boundaries are indicated and the associated dendrogram is shown at right. The industrial isochron interval (5–15 cm) is marked by horizontal red lines. Hydrological affinity groupings (HWT, IWT, LWT, Degraded) are displayed as summary panels. Diversity indices (Dominance, Evenness, Shannon H) and the first principal component of zonation (PC1_Z) are shown to the right of the taxa curves. Depth (cm) is plotted on the primary y-axis, with calibrated age (cal yr BP) on the secondary axis. The red shading is the radiocarbon-derived timespan of the Industrial Isochron (1,880-1, 975 CE). Biostratigraphy is presented here for substrate context and described in detail in Chapter 2 (page 34)*

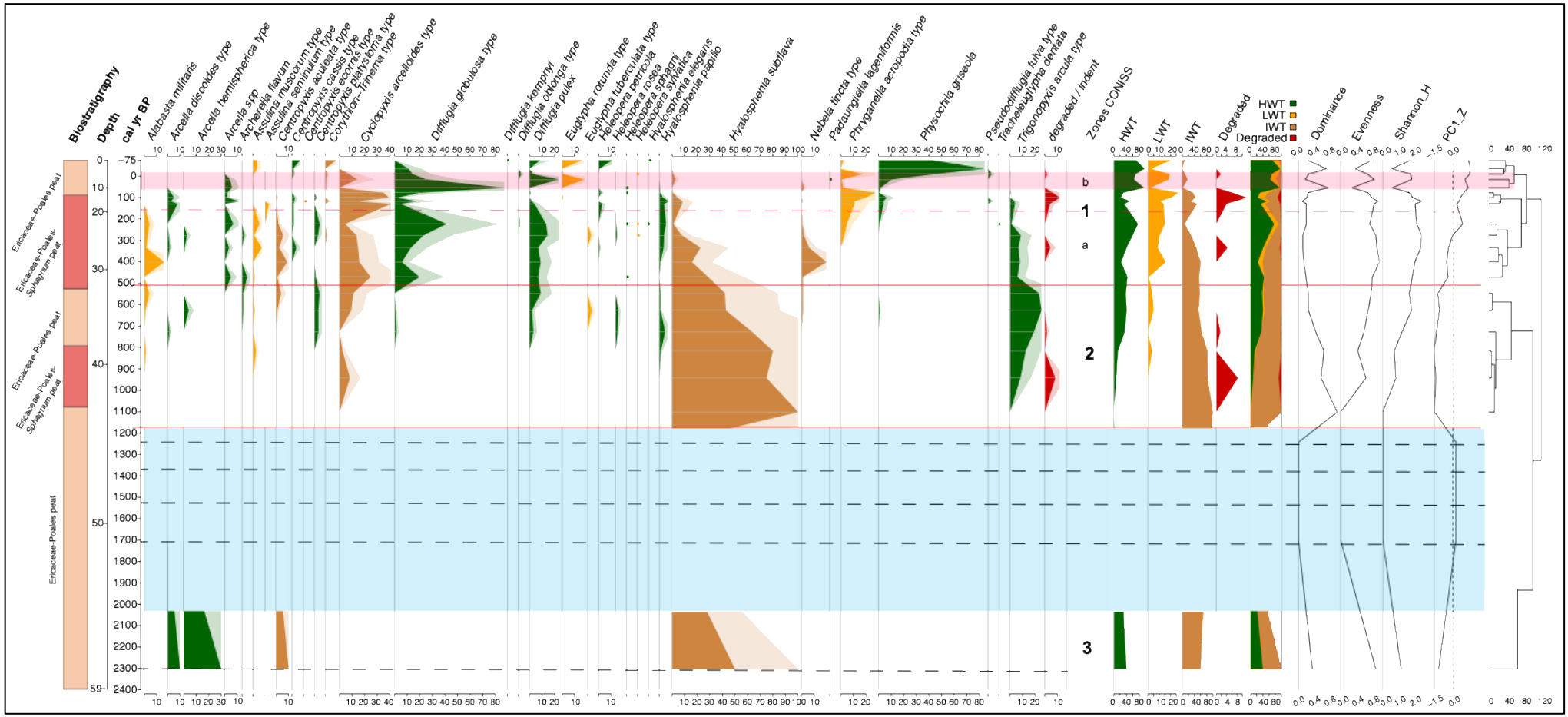

Figure 7 *Stratigraphic diagram of testate amoeba assemblages from the Laurentian core (0–59 cm; ~2300 cal yr BP to present). Relative abundances are expressed as percentages of the total assemblage. Zones (LZ3–LZ1), including subzones LZ1a and LZ1b (separated by dashed red line), were defined using CONISS; significant cluster boundaries are indicated by continuous red line and the dendrogram is shown at right. The industrial isochron interval (4–12 cm) is marked by horizontal red lines. Hydrological affinity groupings (HWT, IWT, LWT, Degraded), diversity indices, and zonation PC1 scores are presented as summary panels. The red shading is the radiocarbon-derived timespan of the Industrial Isochron (1,880-1,975 CE). The blue shading and dashed black line represent samples and depth where microfossil counts were below 50 and thus not significant. Biostratigraphy is presented here for substrate context and described in detail in Chapter 2 (page 34)*

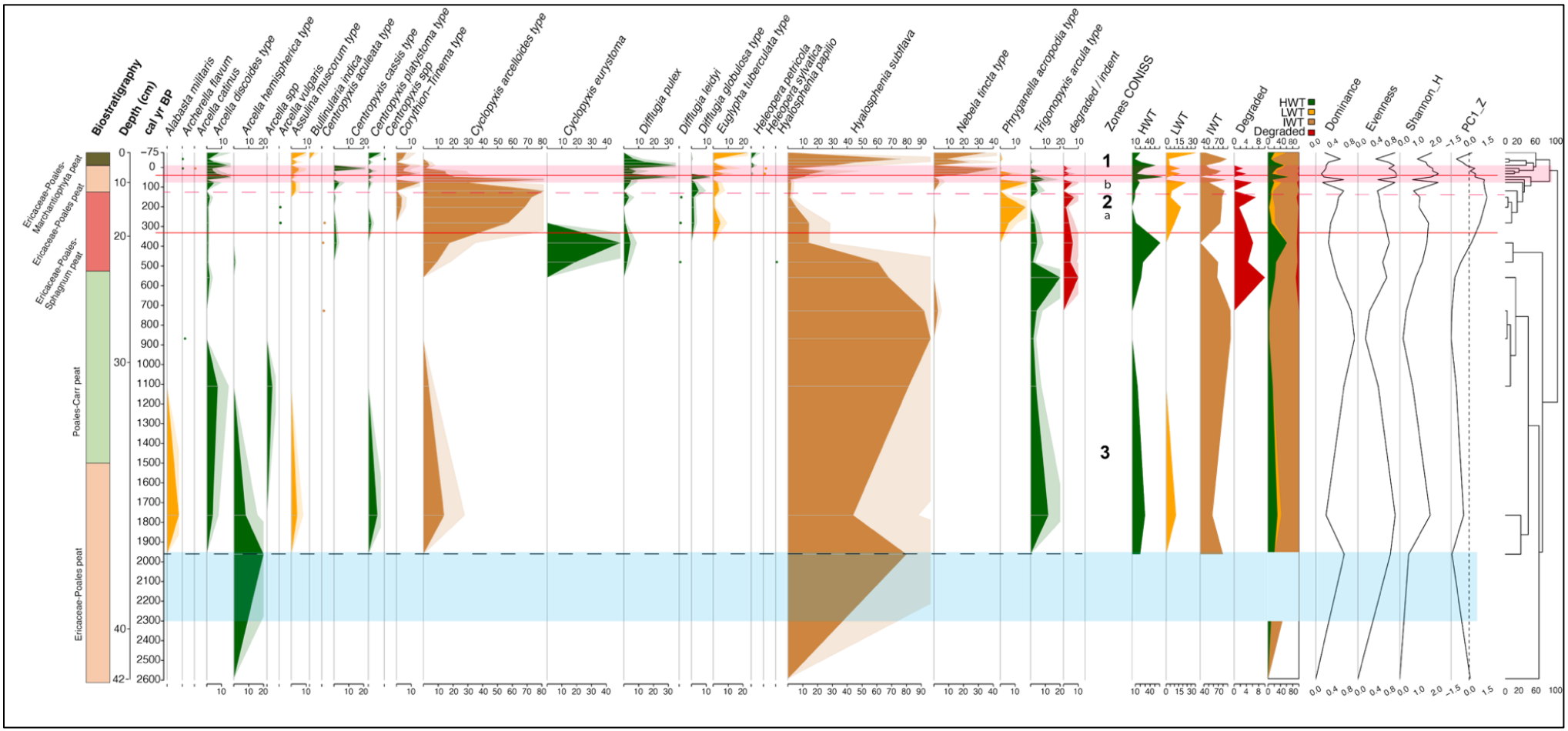

Figure 8 *Stratigraphic diagram of testate amoeba assemblages from the Transplant core (0–42 cm; ~2600 cal yr BP to present). Relative abundances are expressed as percentages of the total assemblage. Zones (TZ3–TZ1), including subzones TZ2a and TZ2b (separated by dashed red line), were defined using CONISS; significant cluster boundaries are indicated by continuous red lines and the dendrogram is shown at right. Hydrological affinity groupings (HWT, IWT, LWT, Degraded), diversity indices, and zonation PC1 scores are presented as summary panels. The red shading is the radiocarbon-derived timespan of the Industrial Isochron (1,880-1,975 CE). The blue shading and dashed black line represent the sample and depth where microfossil counts were below 50 and thus not significant. Biostratigraphy is presented here for substrate context and described in detail in Chapter 2 (page 34)*

3.3.2 Constrained Ordination of Community Composition

Canonical correspondence analysis (CCA) was used to assess the relationship between TA community composition and major geochemical gradients across the three peat cores. The constrained model included five predictors: TMM_PC1, S%, BASE_NUT_PC1, CARBON_PC1, and OTHER_PC1. Total inertia of the species matrix was 5.498, of which 1.100 (20.0%) was explained by the constrained environmental variables, leaving 4.398 (79.9%) as unconstrained variation. Thus, geochemical gradients account for approximately one-fifth of total community variance.

Axis structure. The first constrained axis (CCA1) had an eigenvalue of 0.437 and accounted for 39.8% of constrained variance (7.95% of total inertia). The second axis (CCA2) had an eigenvalue of 0.358 and explained 32.5% of constrained variance (6.51% of total inertia). Together, CCA1 and CCA2 captured 72.3% of the constrained variation and 14.5% of total community variance.

Permutation tests confirmed that the overall model was highly significant ($p < 0.001$). All major predictors were significant when tested individually ($p \leq 0.043$), with TMM_PC1 contributing the largest χ^2 fraction among terms. Variance inflation factors ranged between ~1.5 and ~4.6, indicating moderate but acceptable collinearity among geochemical variables.

Structure of ordination space. Samples from the industrial intervals of Laurentian (LZ1b) and Transplant (TZ2b-TZ1) plot at the extreme positive end of CCA1. Pre-industrial assemblages from all three cores cluster toward negative or intermediate CCA1 scores. Cartier exhibits a more gradual displacement along this axis, without the pronounced extremity observed at the other two sites. CCA1 therefore represents the dominant geochemical turnover axis across sites. CCA2

captures additional variation associated with carbon composition and base/nutrient status but does not align strictly with industrial phase boundaries.

Samples with fewer than 50 tests, including sterile intervals (TA sum = 0), were projected passively into ordination space using their geochemical profiles as predictors. These are displayed as open circles in the CCA biplot and are not included in the constrained model. Their ordination positions provide spatial context for the geochemical conditions at horizons where TA were absent or poorly preserved.

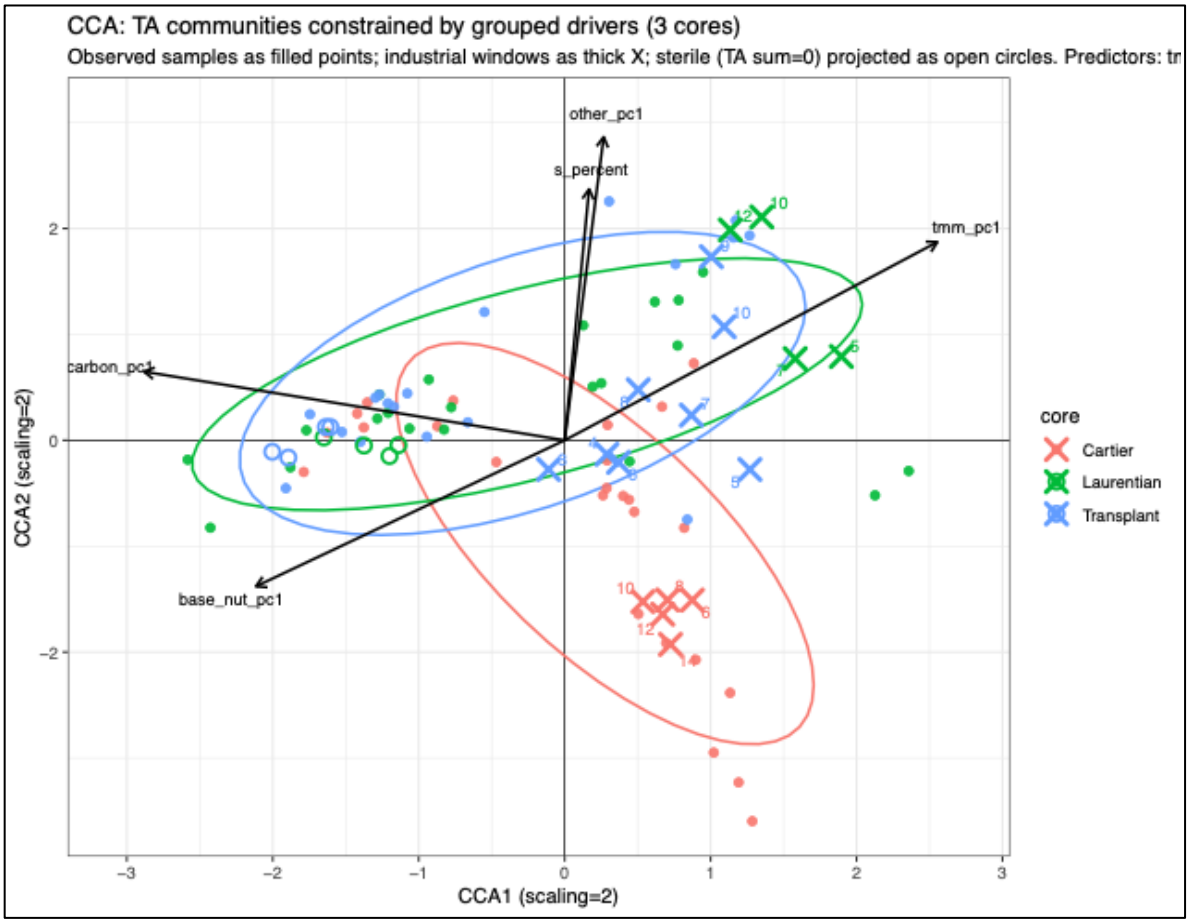

Figure 9 *Canonical correspondence analysis (CCA) of testate amoeba communities constrained by grouped geochemical drivers across the three peatland cores (Cartier, Laurentian, Transplant). Axes represent CCA1 and CCA2 (scaling = 2). Samples are shown as filled points coloured by core; industrial-window samples (defined by depth-based isochron intervals) are marked with thick crosses; sterile levels (TA sum = 0) are projected as open circles. Arrows indicate the direction and relative strength of explanatory gradients: toxic trace metals (tmm_pc1), sulfur (S_percent), base cations–nutrients (Base_nut_pc1), carbon composition (Carbon_pc1), and the residual composite (othwer_PC1). The length and orientation of vectors reflect their correlation with the ordination axes. Ellipses represent 95% confidence envelopes around core centroids.*

3.3.3 Variation Partitioning of Geochemical Predictors

Variation partitioning was conducted to disentangle the independent and shared contributions of four geochemical gradients to community composition: TMM_PC1, S%, BASE_NUT_PC1, and CARBON_PC1. Together, these four predictors explained 20.5% of total community variation (adj. $R^2 = 0.205$), consistent with the magnitude of constrained variance observed in the CCA.

When covariance among predictors was controlled, carbon composition accounted for the largest independent fraction of explained variation (adj. $R^2 = 0.057$; $F = 6.53$; $p = 0.001$). This unique carbon component was approximately three times larger than that of any other predictor, indicating that shifts in peat carbon composition represent the strongest independent chemical correlate of assemblage structure across the three cores.

The toxic trace-metal composite retained a smaller but statistically significant independent effect (adj. $R^2 = 0.019$; $F = 2.87$; $p = 0.019$). Although TMM_PC1 strongly structured the primary constrained axis in the CCA, the variation partitioning results indicate that much of its explanatory power is shared with other altered peat properties, particularly carbon composition. While trace-metal loading clearly contributes to community differentiation, its effect is partly embedded within broader geochemical changes to the peat matrix.

In contrast, sulfur and the base–nutrient composite explained only small independent fractions of variation (adj. $R^2 = 0.009$ and 0.010, respectively). Neither retained strong statistical support once carbon and trace metals were controlled (S: $F = 1.82$, $p = 0.097$; BASE_NUT: $F = 1.95$, $p = 0.057$). These results indicate that the apparent influence of sulfur and base status in the full model largely reflects shared covariance with carbon and metal gradients rather than strong independent control of community composition.

A substantial proportion of the explained variance was shared among predictors, particularly between carbon and TMM. This covariance structure suggests that trace-metal enrichment co-occurs with broader alteration of peat chemical composition. Thus, although trace metals define the dominant constrained gradient in ordination space, carbon-related changes represent the strongest independent geochemical correlate of community restructuring across the study region.

3.3.4 Community Differences Among Disturbance Phases (PERMANOVA)

Permutational multivariate analysis of variance (PERMANOVA), stratified by core, was used to test whether community composition differed significantly among pre-industrial, industrial, and post-industrial phases (see Appendix 8). Phase boundaries were defined using the industrial isochron intervals identified from geochemical profiles (S, TMM enrichment) and age–depth models in Chapter 2. The global PERMANOVA indicated a significant effect of phase on community composition ($p < 0.01$, $F = 5.036$, $Df = 2$, $R^2 = 0.103$), demonstrating that temporal phase classification corresponds to statistically distinguishable assemblage structures. Tests for homogeneity of multivariate dispersion (betadisper) did not indicate significant differences in dispersion among phases, suggesting that the observed PERMANOVA result reflects differences in centroid position rather than unequal within-group variability.

When examined within individual cores, phase effects were strongest at Laurentian and Transplant, where industrial and post-industrial samples were more clearly separated in multivariate space. Cartier exhibited weaker but still detectable phase structuring. These results are consistent with the constrained ordination, in which industrial and post-industrial samples shift along the primary trace-metal gradient.

3.3.5 Species-Level Responses to Disturbance Phase and Geochemical Gradients

Global phase-associated taxa

Multilevel pattern analysis identified 11 taxa significantly associated with disturbance phases (α = 0.05) out of 46 identified species. Three taxa were associated with a single phase, while eight were associated with combined phases, indicating that most significant responses reflected transitional or legacy effects rather than strict confinement to a single interval.

Three taxa were significantly associated with the post-industrial phase alone. *Heleopera petricola* exhibited the strongest association (IndVal = 0.763, $p = 0.001$), followed by *Hyalosphenia elegans* (IndVal = 0.553, $p = 0.038$) and *Centropyxis* spp. (IndVal = 0.535, $p = 0.006$). One taxon, *Cyclopyxis arcelloides* type, was significantly associated with the combined pre-industrial and industrial phases (IndVal = 0.803, $p = 0.016$), indicating persistence through the onset of disturbance but not into the post-industrial interval.

The largest group comprised taxa associated with the combined industrial and post-industrial phases (seven species). These included *Corythion-Trinema* type (IndVal = 0.847, $p = 0.001$), *Assulina muscorum* type (IndVal = 0.826, $p = 0.001$), *Nebela tincta* type (IndVal = 0.815, $p = 0.001$), and *Difflugia pulex* (IndVal = 0.810, $p = 0.006$), all exhibiting high indicator values. Additional taxa within this group were *Physochila griseola* (IndVal = 0.669, $p = 0.023$), *Euglypha tuberculata* type (IndVal = 0.491, $p = 0.047$), and *Euglypha strigosa* type (IndVal = 0.354, $p = 0.040$). Importantly, no taxa were uniquely associated with the industrial phase alone. Instead, species responses either persisted across the industrial-post-industrial boundary or became most pronounced during the post-industrial interval. This pattern suggests that the period

of maximum contamination did not produce a discrete, transient assemblage but rather initiated community restructuring that extended beyond peak pollutant deposition.

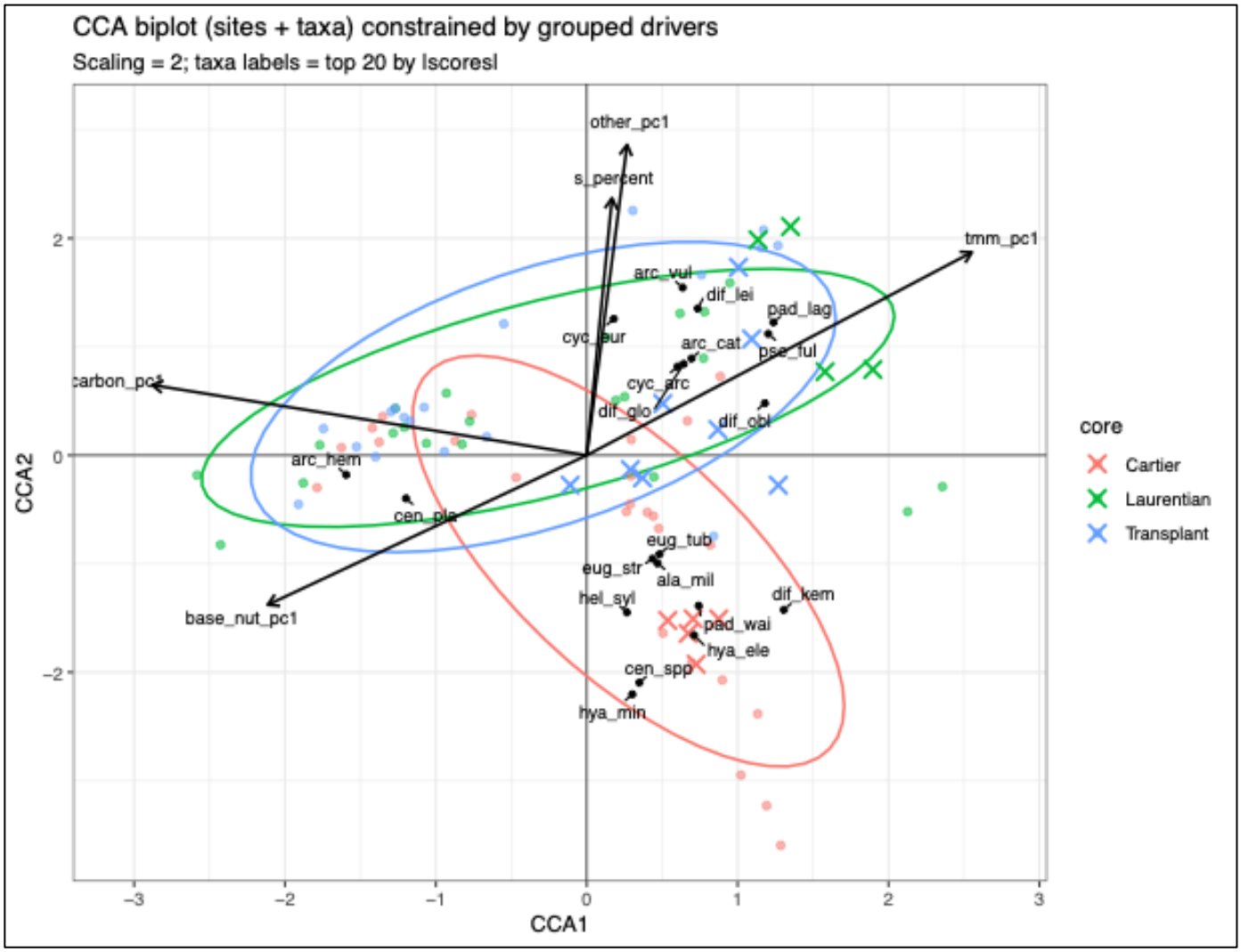

Figure 10 *Canonical correspondence analysis (CCA) biplot of testate amoeba communities constrained by grouped geochemical drivers across the three peatland cores (Cartier, Laurentian, Transplant). Axes represent CCA1 and CCA2 (scaling = 2). Sample scores are shown as coloured points by core, with 95% confidence ellipses around core centroids. Industrial-window samples are marked with crosses. Species scores are plotted as black points with abbreviated labels (first three letters of genus and species); only the top 20 taxa by absolute ordination score are shown to enhance clarity. Arrows indicate the direction and relative strength of explanatory gradients (tmm_pc1, S_percent, base_nut_pc1, carbon_pc1, otherw_PC1). Taxa positioned in the direction of a given vector are positively associated with that gradient, whereas taxa in the opposite direction are negatively associated.*

Phase-associated taxa within individual cores

When IndVal analyses were run separately for each core, the sets of significant phase-associated taxa differed substantially among sites, indicating that the taxonomic expression of phase-related community change was strongly site-contingent rather than uniform across the regional gradient. Only *Corythion-Trinema* type was significant in all three records, suggesting that this group represents the most consistent phase-associated signal detectable across the full disturbance gradient.

At Cartier, nine taxa were significant ($p \leq 0.05$), including *Nebela tincta* type, *Alabasta militaris*, *Euglypha tuberculata* type, *Assulina muscorum* type, *Corythion–Trinema* type, *Centropyxis ecornis* type, *Heleopera sylvatica*, *Euglypha strigosa* type, and *Heleopera petricola*. At Laurentian, eight taxa were significant, led by *Physochila griseola* and *Hyalosphenia subflava*, followed by *Heleopera petricola*, *Centropyxis cassis* type, *Euglypha rotunda* type, *Corythion–Trinema* type, *Trigonopyxis arcula* type, and *Arcella* spp. At Transplant, six taxa were significant, with the strongest associations observed for *Difflugia pulex* and *Arcella discoides* type, followed by *Nebela tincta* type, *Corythion–Trinema* type, *Assulina muscorum* type, and *Euglypha tuberculata* type. The limited overlap between sites is consistent with the idea that phase-associated restructuring is expressed through different taxonomic combinations depending on local conditions, even when the overall community trajectory is driven by the same broad disturbance history.

3.3.6 Species Response Along the Toxic Trace-Metal Gradient

Across the pooled dataset, several taxa exhibited strong monotonic relationships with TMM_PC1. The strongest positive associations were observed for *Cyclopyxis arcelloides* type,

Phryganella acropodia type, *Centropyxis cassis* type, and *Difflugia globulosa* type — taxa that increased in relative abundance as the trace-metal gradient intensified. The strongest negative relationships were expressed by *Trigonopyxis arcula* type, *Arcella hemispherica* type, and *Hyalosphenia subflava*, indicating declining representation toward the more contaminated portion of the gradient. Several taxa identified as significantly phase-associated in the global IndVal analysis also displayed clear alignment with the trace-metal gradient, while others showed weak or near-zero relationships with TMM_PC1, reinforcing the need to treat phase associations as reflecting the combined influence of disturbance-related changes rather than a single chemical control.

3.3.7 Species Response Along Sulfur and Other Geochemical Gradients

Species associations with sulfur differed in both strength and direction relative to the TMM response structure. The strongest positive associations with the sulfur proxy were observed for *Cyclopyxis arcelloides* type and *Difflugia globulosa* type, and to a lesser degree for *Hyalosphenia papilio* and *Phryganella acropodia* type. In contrast, several taxa exhibited pronounced negative relationships with sulfur, including *Assulina muscorum* type, *Corythion–Trinema* type, *Euglypha tuberculata* type, and *Euglypha strigosa* type. These opposing sulfur responses are particularly important because multiple taxa with strong phase associations belong to the group with negative sulfur correlations. This indicates that taxa statistically concentrated in industrial/post-industrial intervals are not necessarily taxa that increase monotonically with sulfur. Instead, the pattern is consistent with assemblage restructuring across disturbance phases that reflects shifting habitat conditions, preservation, and hydrological context in addition to direct chemical forcing. Alternatively, substantial post-depositional downward translocation of sulfur – as documented in Chapter 2 - may account for this apparent poor association between

sulfur, which migrated downward through the peat profile, and the testate amoeba microfossils, which remained in their contemporaneous peat layer.

3.3.8 Placement of Phase-Associated Taxa in Constrained Ordination Space

Species scores from the constrained ordination provide an independent, multivariate view of taxon positioning along the principal constrained gradients. Several phase-associated taxa occupy extreme positions in CCA space, including *Corythion–Trinema* type, *Nebela tincta* type, and *Assulina muscorum* type, whereas *Cyclopyxis arcelloides* type plots toward the opposite end of CCA2. The strong positive TMM association of *Cyclopyxis arcelloides* type, combined with its distinct CCA placement, supports its role as a key taxon structuring the metal-related component of community separation. At the same time, several taxa with significant phase associations plot in positions that are not strongly aligned with simple univariate metal or sulfur responses, highlighting that the constrained ordination reflects the combined effects and covariance structure of the retained predictors rather than a single driver. This reinforces the interpretation that species-level signatures across phases encompass both chemical tolerance signals and additional ecological filtering that is plausibly hydrological in origin, particularly at the more structurally altered sites.

3.3.9 Community Wetness Affinity (WT_index)

Community wetness affinity was examined across depth, phase, and in relation to ordination structure. Across all cores combined (n = 80), WT_index was positively correlated with CCA1 (Spearman $\rho = 0.47$, $p = 1.02 \times 10^{-5}$) and more weakly with CCA2 ($\rho = 0.29$, $p = 0.010$). Note that CCA1 represents the dominant geochemical turnover axis across sites, while CCA2 captures the additional variation associated with carbon composition and base nutrient status. These

relationships indicate that community wetness affinity covaries significantly with the dominant geochemical gradient identified in the CCA.

Patterns differed among cores. At Cartier (n = 29), WT_index was strongly correlated with both CCA1 (ρ = 0.60) and CCA2 (ρ = 0.69). At Transplant (n = 26), a strong positive relationship was observed with CCA1 (ρ = 0.63), whereas the association with CCA2 was weak (ρ = −0.10). Laurentian (n = 25) showed comparatively weaker correlations with CCA1 (ρ = 0.28) and a

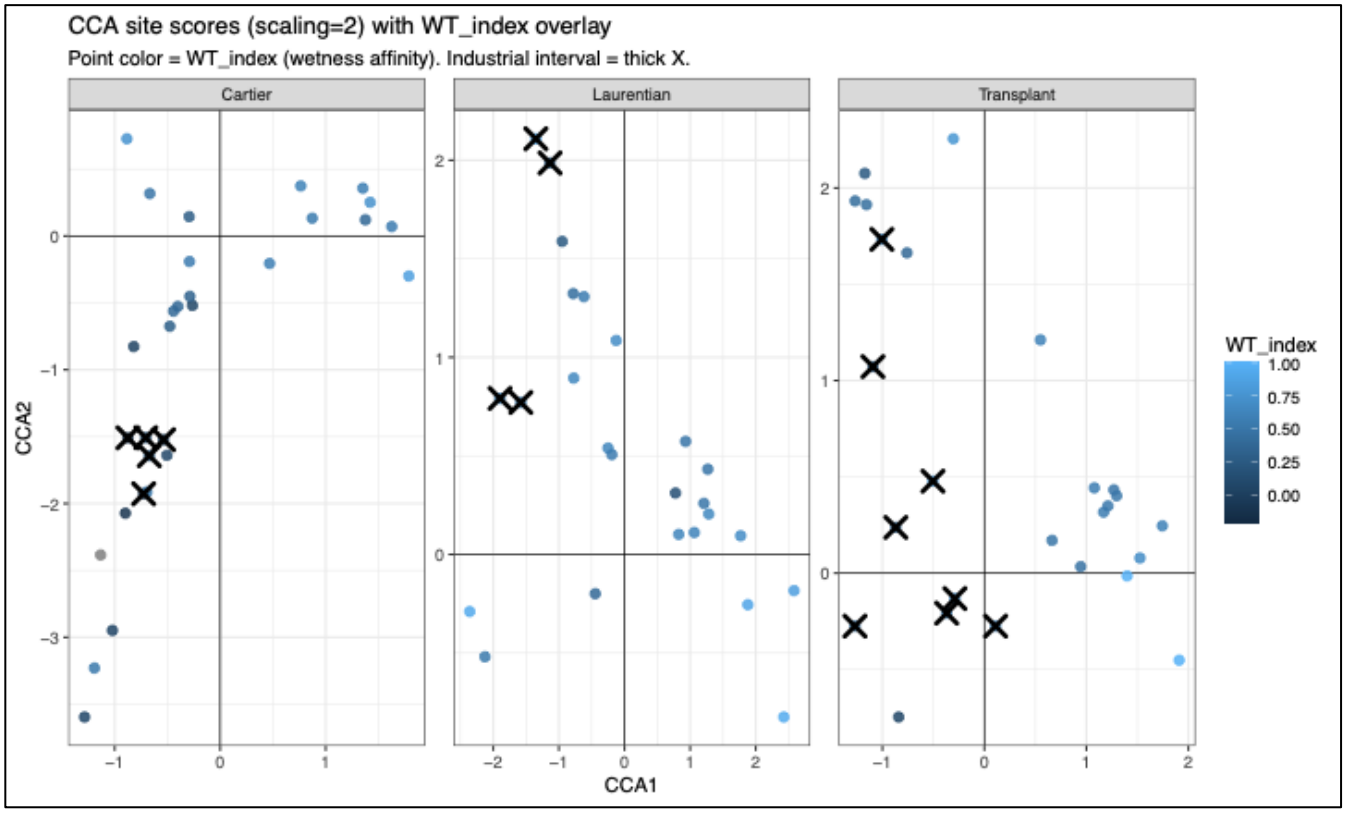

modest negative association with CCA2 (ρ = −0.33). These differences indicate variable alignment between wetness affinity and geochemical gradients among sites.

Figure 11 *CCA site scores with community wetness affinity (WT_index) overlaid. Point colour represents WT_index values. Industrial-window samples are marked with thick crosses. WT_index exhibits a structured gradient along CCA1 across cores, consistent with its significant correlation with the primary constrained axis, while showing site-specific variability.*

Phase-based comparisons revealed site-specific patterns. At Cartier, WT_index differed significantly among phases (ANOVA, $p < 0.05$), with higher affinity values in the post-industrial interval. Laurentian exhibited greater within-phase variability, with phase differences approaching but not consistently exceeding conventional significance thresholds. Transplant showed marked contrasts between the pre-industrial and post-industrial intervals, with lower wetness affinity values characterising the pre-industrial phase and higher values in more recent sediments. Across depth profiles, WT_index exhibited moderate variability within zones rather than abrupt step changes precisely coincident with isochron boundaries.

Table 5 *Dominant testate amoebae taxa by phase (Post-industrial, Industrial, Pre-Industrial) for each core (Cartier, Laurentian, Transplant). Includes taxon name, mean (%), and standard deviation (%).*

Site	Phase	Taxon	Mean (%)	SD (%)
Cartier	Post-industrial	*Alabasta militaris*	28.39	6.7
		Nebela tincta type	15.45	5.43
		Hyalosphenia elegans	13.83	12.41
	Industrial	*Alabasta militaris*	27.13	6.31
		Difflugia pulex	19.67	5.96
		Assulina muscorum type	8.19	4.18
	Pre-industrial	*Hyalosphenia subflava*	23.81	26.34
		Trigonopyxis arcula type	12.22	19.12
		Difflugia pulex	11.32	11.47
Laurentian	Post-industrial	*Physochila griseola*	63.48	29.27
		Euglypha rotunda type	7.86	11.12
		Heleopera petricola	5.71	7.23
	Industrial	*Difflugia globulosa type*	36.76	33.76
		Physochila griseola	14.4	20.81
		Cyclopyxis arcelloides type	14.2	15
	Pre-industrial	*Hyalosphenia subflava*	26.96	29.18
		Cyclopyxis arcelloides type	8.68	12.2
		Trigonopyxis arcula type	7.66	8.38
Transplant	Post-industrial	*Hyalosphenia subflava*	38.73	52.41
		Nebela tincta type	21.58	18.98
		Eugylpha tuberculata type	12.46	15.38
	Industrial	*Cyclopyxis arcelloides type*	21.36	25.99
		Hyalosphenia subflava	16.91	16.28
		Nebela tincta type	15.8	16.35
	Pre-industrial	*Hyalosphenia subflava*	35.99	39.15
		Cyclopyxis arcelloides type	16.21	28.29
		Trigonopyxis arcula type	13.1	26.4

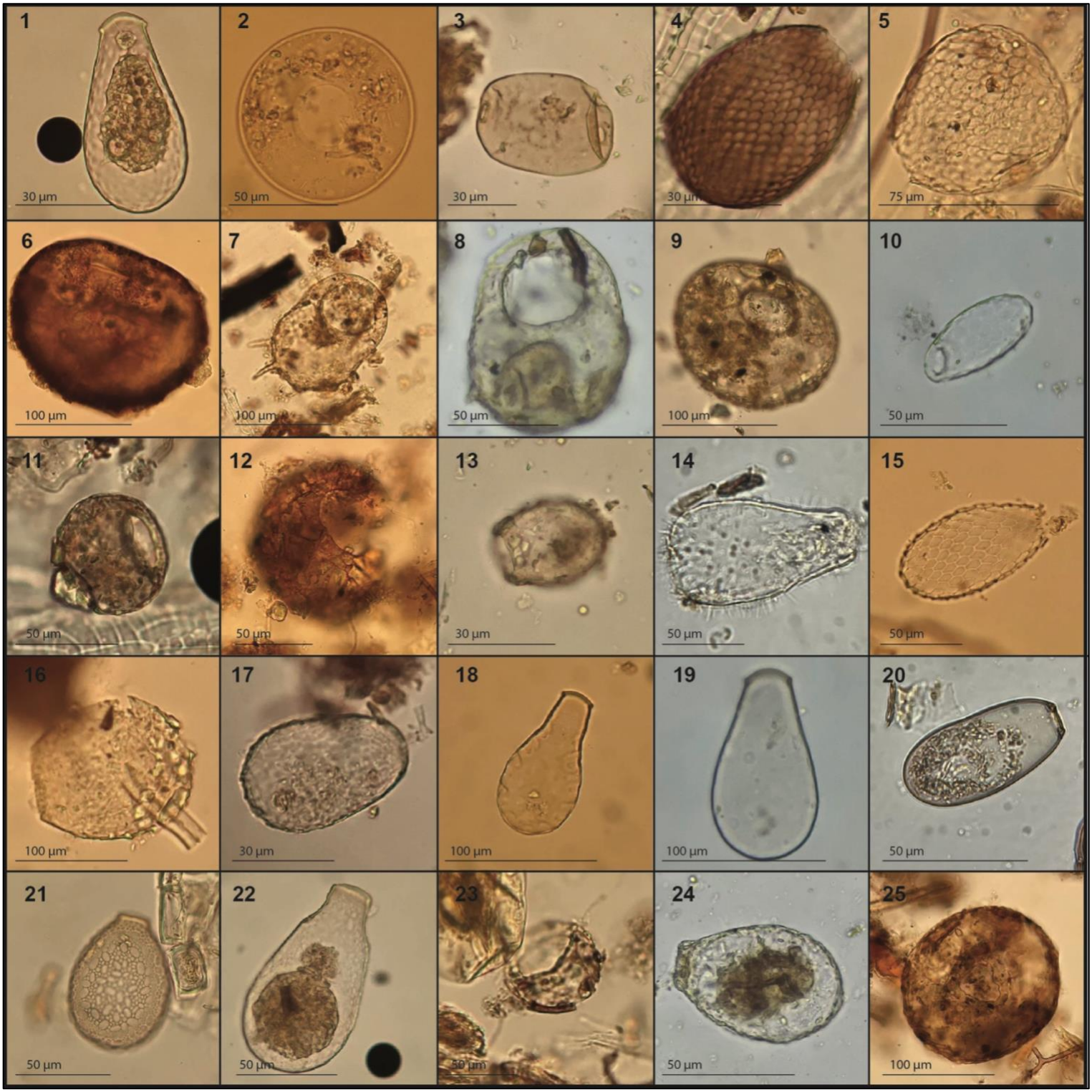

Figure 12 *Plate of selected testate amoebae as observed across all peatland sites. (1) Alabasta militaris (2) Arcella discoides type (3) Archerella flavum (4) Assulina muscorum (5) Assulina seminulum type (6) Bullinularia indica (7) Centropyxis aculeata (8) Centropyxis cassis type (9) Centropyxis ecornis type (10) Corythion-Trinema type (11) Cyclopyxis arcelloides type (12) Difflugia globulosa type (13) Difflugia pulex (14) Euglypha strigosa type (15) Euglypha tuberculata type (16) Heleopera petricola (17) Heleopera sylvatica (18) Hyalosphenia elegans (19) Hyalosphenia papilio (20) Hyalosphenia subflava (21) Nebela tincta type (22) Padaungiella wailesi type (23) Phryganella acropodia type (24) Physochila griseola (25) Trigonopyxis arcula type.*

3.4 Discussion

3.4.1 Baseline Community Structure and Autogenic Controls

Across all three peatlands, pre-industrial testate amoeba assemblages were characterised by sustained dominance of taxa typically associated with wet, ombrotrophic conditions, particularly *Hyalosphenia subflava*, with secondary contributions from *Trigonopyxis arcula* type, *Archerella flavum*, and *Nebela tincta* type. This sphagnophilous baseline is consistent with the modern ecological literature, in which *H. subflava* and *Archerella flavum* are strongly associated with wet *Sphagnum* microhabitats (Booth et al., 2025; Lamentowicz and Mitchell, 2005; Amesbury et al., 2018). The coherence of these pre-industrial assemblages across sites indicates that, prior to industrial deposition, all three peatlands supported broadly similar microbial communities structured by autogenic peat development processes and long-term hydrological stability.

Stratigraphic clustering (CONISS) supports this interpretation: pre-disturbance zones exhibit gradual internal variability but no abrupt transitions comparable to those observed in upper industrial intervals. These patterns resemble the long-term baselines documented in European and North American ombrotrophic peatlands before the onset of industrial-era contamination (Swindles et al., 2016; Lamentowicz et al., 2013; Elliott et al., 2012). In particular, the dominance of *H. subflava* in the pre-disturbance intervals parallels findings from British blanket bogs, where this taxon is a reliable indicator of stable, moist conditions prior to drainage or atmospheric degradation (Creevy et al., 2018; Swindles et al., 2016).Variation partitioning indicates that carbon composition (CARBON_PC1) explains the largest unique fraction of community variance when controlling for trace metals, sulfur, and base–nutrient gradients. In intact peatlands, carbon composition integrates multiple autogenic processes - organic matter

accumulation, humification state, and redox conditions - that evolve gradually as the peat column develops (Charman, 2001; Booth et al., 2025).

Testate amoebae are widely used as proxies for water table depth (WTD) reconstructions within peatlands due to their habitual relations to peat biogeochemistry and surface wetness (Nolan et al., 2019; Booth, 2008). In peatlands, water table fluctuations are naturally driven by seasonal distribution of precipitation, temperature-controlled evapotranspiration, and the seasonal growth cycle of vegetation (Renaud et al., 2025). Changes in water levels are reflected in alterations of test size, aperture size, and fluctuations of mixotrophic forms (Marcisz et al., 2020). Assemblages that indicate high water tables typically contain large-test taxa and mixotrophic species (e.g. *Difflugia globulosa*), while low water tables are marked by small-test taxa (e.g. *Nebela militaris*) (Booth, 2008; Marcisz et al., 2020). Human-induced pollution loading (e.g. toxic metals and metalloids) can also alter TA community structure by lowering overall diversity and abundance, typically favouring more tolerant species (e.g. *Cyclopyxis arcelloides)* (Freitas et al., 2022). TA have also been found to respond to pollution loading through shifts toward taxa with smaller tests (Mitchell et al., 2008). Literature suggests that both water-table decline and pollution stress can generate overlapping signatures within TA community assemblages: shifts toward smaller, dry-adapted tests, loss of mixotrophic taxa, and reduced diversity (Marcisz et al., 2020; Freitas et al., 2022). Therefore a dry water table signal may be mimicked or amplified by a pollution signal and can be difficult to distinguish on the basis of testate amoeba data alone. While disentangling the drivers completely may not be possible, a multi-proxy strategy (e.g. pollen, geochemical tracers) could provide insight into the influences on water table changes (Mitchell et al., 2008; Marcisz et al., 2020).

Although hydrology is widely recognised as the first-order ecological control on TA distributions in undisturbed peatlands (Mitchell et al., 2008; Swindles et al., 2016; Kuuri-Riutta et al., 2022), the WT_index used here represents community wetness affinity rather than a direct measurement of water-table depth. Hydrology is therefore treated as a fundamental ecological backdrop whose influence is partially encoded in the peat substrate properties captured by the carbon variable which is also tightly coupled with the hydrology (Waddington et al., 2015; Furukawa et al., 2025). The concordance between the microbial baselines presented here and the peat stratigraphic evidence from Chapter 2 - which documents intact peat structure, stable organic accumulation, and the absence of pronounced sulfur or metal enrichment in pre-industrial sections — strengthens the interpretation of a stable pre-disturbance ecological regime across the three sites.

3.4.2 Industrial Deposition and Community Restructuring

Pronounced community restructuring coincident with the industrial isochron is evident at Laurentian and Transplant, whereas Cartier exhibits a comparatively muted response. At the two proximal sites, the industrial and post-industrial intervals are marked by a shift from sphagnophilous taxa toward assemblages dominated by *Cyclopyxis arcelloides* type, *Centropyxis cassis* type, *Phryganella acropodia* type, and *Difflugia globulosa* type. These genera are consistently identified in the broader literature as disturbance-tolerant or pollution-associated taxa. *Cyclopyxis* and *Centropyxis* species have been reported as indicators of metal contamination in Canadian lake sediments affected by mine tailings (Patterson et al., 1996; Reinhardt et al., 1998), in cupriferous peatlands in New Brunswick where *C. arcelloides* abundance was high in open areas with elevated copper (Asada and Warner, 2009), and in heavily polluted bogs in the Polish–Czech “Black Triangle” (Fiałkiewicz-Kozieł et al., 2015).

The emergence of *Phryganella acropodia* as a pollution-associated taxon is likewise consistent with findings from the Izery Mountains, where this species was distinguished alongside *Centropyxis aerophila* as a proxy for extreme atmospheric dust deposition from brown coal combustion (Fiałkiewicz-Kozieł et al., 2015).

The concurrent decline of mixotrophic and sphagnophilous taxa at Laurentian and Transplant mirrors a broader pattern documented in European industrial peatlands. Fiałkiewicz-Kozieł et al. (2015) reported the collapse of mixotrophic TA (e.g., *Archerella flavum*, *Hyalosphenia papilio*) and their replacement by agglutinated forms in response to extreme aluminium and copper deposition in the Izery Mountains. A comparable transition has been documented at the Śnieżka peatland, , where fly ash deposition was hypothesised to have physically harmed mixotrophic metabolism and eliminated communities living at the *Sphagnum* capitula (Fiałkiewicz-Kozieł et al., 2023; Marcisz et al., 2020). In the Sudbury context, the elimination of *Sphagnum* at the onset of the Industrial Isochron - documented by Gignac and Beckett (1986) and confirmed stratigraphically in Chapter 2 - would have removed the primary habitat substrate for sphagnophilous TA, compounding any direct toxic effects of metals and sulfur on the organisms.

Phase-based PERMANOVA confirms significant compositional differences among pre-industrial, industrial, and post-industrial intervals. Constrained ordination demonstrates that the toxic trace-metal composite (TMM_PC1) aligns strongly with the primary CCA axis. However, variation partitioning reveals that much of this explanatory power is shared with carbon composition and other geochemical variables. This covariance structure is ecologically informative: it suggests that industrial deposition did not act on TA communities solely through direct metal toxicity but also through cascading modification of peat chemistry and substrate

properties. This interpretation is consistent with the vertical stratification of pollution effects described in Chapter 2, in which industrial contamination simultaneously reduced decomposition in surface peat while promoting chemical degradation in horizons below the identified Industrial Isochron The stronger microbial restructuring observed at Laurentian and Transplant mirrors the greater magnitude of sulfur and metal enrichment documented stratigraphically at those sites, supporting a gradient-based interpretation of industrial impact.

Cartier, by contrast, retained *Sphagnum* dominance throughout the industrial period and shows comparatively limited geochemical alteration. Its TA assemblage exhibits detectable but modest phase structuring, consistent with its position at the outer edge of the atmospheric fallout zone. This gradient response - from persistent restructuring at proximal sites to subtle modulation at the distal reference - is broadly analogous to the spatial patterns observed by Nguyen-Viet et al. (2007) along atmospheric metal deposition gradients in Vietnam, where TA species richness and density declined with increasing lead concentration in moss substrates.

3.4.3 Carbon Composition, Hydrology, and Indirect Mediation

The emergence of carbon composition as the strongest unique explanatory variable warrants careful interpretation. In undisturbed peatland systems, TA communities are widely understood to be structured primarily by hydrological gradients, particularly near-surface water-table position and moisture availability (Mitchell et al., 2008; Swindles et al., 2016; Booth et al., 2025; Kuuri-Riutta et al., 2022). This hydrological sensitivity underpins the widespread use of TA in water-table transfer functions and establishes hydrology as the expected first-order ecological control under intact ombrotrophic conditions (Charman et al., 2006; Amesbury et al., 2018).

However, the assumption that TA assemblage turnover can be straightforwardly attributed to water-table change is increasingly questioned in contaminated or degraded systems. Payne et al. (2012) raised this issue explicitly, noting that atmospheric pollution can bias peatland paleoclimate reconstructions derived from TA because contaminants may restructure communities in ways that mimic or partially obscure hydrological signals. Experimental sulfate addition studies demonstrate that chemical inputs can alter TA assemblage structure even when hydrological variables are partially controlled (Payne et al., 2013). Similarly, Fiałkiewicz-Kozieł et al. (2015) showed that in peatlands subjected to extreme atmospheric dust and metal deposition, community restructuring and functional trait shifts correlated more strongly with geochemical indicators of pollution than with hydrological proxies. These findings caution against interpreting all TA turnover in contaminated systems as evidence of water-table change alone.

Within this context, the strong independent contribution of CARBON_PC1 in the present study likely reflects integrated peat substrate properties - organic matter quality, humification state, and redox conditions - rather than any single chemical parameter. At Laurentian and Transplant, Chapter 2 documents substantial sulfur enrichment, altered peat chemistry, and a shift toward fen-like vegetation with loss of persistent *Sphagnum* dominance. Present-day field observations at these sites indicate diminished hummock–lawn microtopography relative to Cartier, consistent with the structural degradation and peat compaction described by McCarter et al. (2024). These physical changes to the peat matrix modify near-surface moisture regimes and aeration conditions, creating indirect pathways through which pollution-driven substrate alteration could influence microbial community composition.

This interpretation frames the relationship between hydrology and pollution not as mutually exclusive drivers but as interacting forces operating within a shared ecological framework. In relatively intact systems such as Cartier, where peat structure and *Sphagnum* dominance were maintained, TA communities exhibit comparatively limited restructuring and baseline hydrological controls likely remained operative. At Laurentian and Transplant, however, the ecological context within which hydrology operates has itself been modified by industrial contamination - an effect captured, in part, by the carbon composition variable. Similar interactive models have been proposed for peatlands affected by drainage and land-use change, where altered substrate properties mediate biological responses beyond what water-table change alone would predict (Creevy et al., 2018; Daza Secco et al., 2018). The combined ordination and variation partitioning results therefore indicate that chemical alteration of the peat matrix played a central role in mediating microbial community restructuring, while the direct hydrological contribution remains embedded within the shared variance structure.

3.4.4 Absence of Discrete Microbial Recovery

Despite temporal separation from peak industrial deposition, no clear post-industrial recovery assemblage emerges in the stratigraphic clustering. Although PERMANOVA indicates statistically significant differences among phases, CONISS does not resolve a discrete recovery zone distinct from the industrial interval at either Laurentian or Transplant. Industrial-associated taxa persist in the uppermost samples, and community composition does not revert toward the pre-disturbance structure documented in basal zones.

This finding is significant in the context of both the Sudbury restoration narrative and the broader literature on peatland recovery from atmospheric contamination. In the Sudbury region, large-scale regreening of forested uplands has been underway since the late 1970s, with over 10

million trees planted across more than 3,000 hectares of barren and semi-barren land (Watkinson et al., 2022). However, peatlands were not actively targeted by these efforts and have been expected to recover passively in response to declining atmospheric inputs (Gunn et al., 1995; Newman et al., 2023). The TA record indicates that, at least at the microbial level, passive recovery has not occurred at the two proximal sites and that communities remain structured by the legacy of industrial contamination.

This pattern resonates with findings from other industrially impacted peatlands. At Holcroft Moss, a lowland raised bog near Manchester in the heartland of the English Industrial Revolution, paleoecological records spanning several centuries document a steady decline in *Sphagnum* and non-pollen palynomorph richness coincident with industrialisation, with only modest *Sphagnum* recovery in the uppermost peat despite post-industrial declines in atmospheric pollution (Garcés-Pastor et al., 2023). The authors noted that subsurface pollution legacies and ongoing nitrogen deposition may hinder full biological recovery even decades after emissions abatement. In the Polish Sudetes, the Śnieżka peatland - exposed to extreme industrial emissions from the Black Triangle - similarly shows persistent shifts in TA functional traits that have not fully reversed despite significant post-1990 reductions in SO_2 and particulate emissions (Fiałkiewicz-Kozieł et al., 2023). A comparable pattern has been documented in Polish kettle-basin peatlands where anthropogenic acidification produced long-lasting shifts in TA community structure (Lamentowicz et al., 2007).

These patterns align with the emerging understanding that peatland recovery from industrial contamination is not simply the inverse of degradation. Rather, contamination can produce hysteresis effects - persistent changes in substrate chemistry, vegetation composition, peat physical structure, and microbial community organisation that maintain the system in an altered

state long after the original stressor has been reduced (Milner et al., 2021). In the Sudbury peatlands, the loss of *Sphagnum* represents a potential threshold change with cascading consequences for microbial habitat. *Sphagnum* functions as a powerful ecosystem engineer: it acidifies its environment, maintains high water tables through its exceptional water-holding capacity, and creates the fine-scale microtopographic mosaic of hummocks and hollows exploited by diverse TA assemblages (Rydin and Jeglum, 2013). Without *Sphagnum*, the substrate and moisture conditions required by many pre-disturbance TA taxa may no longer exist, even if metal and sulfur inputs have declined. This creates a feedback loop: the microbial community cannot recover to its pre-disturbance composition because the habitat that supported that composition has been structurally and chemically altered.

The microbial patterns are fully consistent with the peat stratigraphic evidence from Chapter 2, which demonstrates that Laurentian and Transplant have not returned to *Sphagnum*-dominated ombrotrophic conditions but instead remain chemically altered fen-like systems. Cartier, by contrast, retained *Sphagnum* dominance throughout and exhibits comparatively limited microbial reorganisation. The convergence of vegetation, peat chemistry, and microbial proxies across independent analytical frameworks strengthens the interpretation that industrial disturbance has produced a persistent ecological state shift at the more heavily impacted sites - one that is unlikely to reverse through passive recovery alone.

3.4.5 Implications for Peatland Disturbance Studies and Restoration

This study demonstrates that testate amoeba communities in industrially contaminated peatlands record pollution gradients in ways that are both complementary to and partially independent of peat stratigraphy and vegetation proxies. The integration of stratigraphic clustering, constrained

ordination, variation partitioning, PERMANOVA, and species-level analyses provides a multi-dimensional view of community response that reveals both abrupt industrial restructuring and longer-term legacy effects not captured by any single technique alone.

Several findings carry broader implications. First, the emergence of carbon composition as the strongest unique explanatory variable - exceeding the independent contribution of the direct toxic metal signal - underscores the importance of considering integrated substrate properties rather than single contaminants when interpreting TA turnover in polluted environments. This echoes the emphasis of Fiałkiewicz-Kozieł et al. (2015) on examining multiple geochemical dimensions of pollution impact simultaneously and suggests that variation partitioning should become a standard analytical step in paleoecological studies of contaminated peatlands.

Second, the imperfect alignment between chronological phases and CONISS zones highlights the value of analysing both classification frameworks independently. Industrial disturbance imposed statistically detectable shifts in community composition (confirmed by PERMANOVA) without necessarily producing discrete stratigraphic clusters corresponding to ecosystem recovery. This decoupling (significant phase effects without a distinct recovery zone) has practical implications for biomonitoring: the absence of a zonation boundary should not be taken as evidence of ecological stasis, nor should it be interpreted as indicating that recovery has occurred.

Third, the site-contingent nature of species-level phase associations (Section 3.3.8) indicates that the taxonomic expression of industrial disturbance varies with local context, even where the regional forcing is shared. Only *Corythion–Trinema* type was consistently phase-associated across all three sites, suggesting that broadly generalizable pollution indicator taxa may be fewer than assumed and that site-specific calibration remains essential. This has important implications

for the development of transfer functions and biomonitoring indices in contaminated peatland landscapes.

Finally, the persistence of industrial-era community structure at Laurentian and Transplant carries direct implications for the Sudbury peatland restoration effort. If microbial communities have not passively recovered despite decades of reduced atmospheric inputs, then restoration strategies focussed solely on upland regreening and watershed-level emission reductions may be insufficient for peatland ecosystems. Active interventions targeting peat hydrological function - such as the *Sphagnum* recovery and hydrophysical restoration approaches currently being explored in the Sudbury region (McCarter et al., 2023, 2024) - may be required to re-establish the substrate conditions necessary for microbial community recovery. The TA record provides a microbial baseline against which future restoration outcomes can be evaluated, and we recommend that TA monitoring be incorporated into the assessment framework for ongoing peatland restoration in the Sudbury region and comparable industrially impacted landscapes.

Chapter 4 – Conclusions

4.1 Chapter 2 Conclusions

Peat stratigraphies from Laurentian, Transplant, and Cartier record a clear geochemical imprint of Sudbury's industrial era, with sharp enrichment of Cu, Ni, Pb, Cd, As, Zn, and S in alignment to the Industrial Isochron at the two proximal poor fens and substantially lower loadings at the distal site. These concentration peaks, together with vertical mobilization of metal and sulfur profiles, indicate that smelter-derived contaminants were not confined to surface peat but underwent meaningful post-depositional redistribution. Evidence for downward migration of sulfate and pH sensitive trace metals, combined with Ca depletion and progressive N-P enrichment at Laurentian and Transplant, demonstrates that atmospheric sulfur loading altered peatland stoichiometry and internal biogeochemical cycling in ways not observed at Cartier.

In the context of carbon dynamics, Cartier exhibits a Holocene trajectory consistent with global peatland syntheses, whereas Laurentian and Transplant display slightly depressed long-term LARCA values and older age-depth relationships for equivalent peat thickness. This pattern indicates a carbon deficit at the proximal sites, attributable not to suppressed recent accumulation alone but to enhanced decomposition and carbon loss from older catotelm strata. The vertical redistribution of sulfate and metals likely generated a migrating reactive front that increased organic matter solubility, stimulated DOC production and export, and promoted chemical degradation of partially humified peat. Physical evidence of peat compression and elevated bulk density at the proximal sites supports this interpretation of long-term mass loss.

Paradoxically, both Laurentian and Transplant exhibit an industrial-era LARCA peak, reflecting reduced decomposition in near-surface horizons under conditions of extreme metal toxicity and

acidity. Suppressed microbial activity, shifts toward more recalcitrant vegetation inputs, and peat consolidation-moisture feedbacks collectively inflated apparent accumulation during peak contamination, even as deeper peat experienced enhanced decomposition. The result is a vertically stratified carbon regime: surface preservation under toxic stress coexisting with sub-surface carbon depletion driven by sulfur-mediated chemical priming.

These findings demonstrate that historical sulfur and TMM deposition in the Sudbury region altered peatland carbon dynamics through both direct and indirect pathways. Rather than simply suppressing productivity or uniformly enhancing decomposition, industrial pollution generated depth-dependent carbon responses, ultimately producing a legacy carbon deficit in polluted fens. These results showcase the vulnerability of deep, millennia-old peat carbon to anthropogenic chemical forcing and highlight the importance of considering vertical geochemical mobility and post-depositional processes when assessing long-term carbon consequences of pollution.

4.2 Chapter 3 Conclusions

Testate amoeba stratigraphies from the three Sudbury peatlands reveal pronounced community restructuring at sites proximal to the smelting centre, a muted response at the distal reference site, and a persistent absence of microbial recovery at the most heavily impacted locations. Pre-industrial assemblages at all three sites were dominated by sphagnophilous taxa, particularly *Hyalosphenia subflava*, indicating long-term hydrological stability. Industrial contamination triggered a shift toward disturbance-tolerant *centropyxid* and agglutinated forms at Laurentian and Transplant, consistent with patterns documented in metal-contaminated peatlands globally.

Constrained ordination and variation partitioning demonstrate that industrial contamination influenced TA communities both directly, through elevated trace-metal concentrations, and

indirectly, through modification of peat carbon composition and substrate properties. Carbon composition emerged as the strongest independent geochemical correlate of community change (adj. $R^2 = 0.057$), exceeding the unique contribution of toxic trace metals (adj. $R^2 = 0.019$). This finding suggests that the cascading effects of pollution on peat chemistry may be more ecologically consequential for microbial community structure than direct metal toxicity alone.

Critically, no discrete recovery assemblage was detected at Laurentian or Transplant despite temporal separation from peak industrial emissions. Industrial-era taxa persist in the surface samples, and CONISS does not resolve a post-disturbance recovery zone. This finding indicates that passive recovery following atmospheric pollution abatement has not reversed the microbial legacy of contamination and that the ecological state shift observed at these sites may require active restoration - particularly *Sphagnum* reintroduction and hydrological rehabilitation - to reverse. These results contribute to a growing body of evidence that peatland recovery trajectories following extreme atmospheric contamination are site-specific, non-linear, and mediated through both direct toxic effects and indirect modification of the peat substrate. Testate amoebae provide a sensitive, stratigraphically preserved record of these processes and should be integrated into monitoring frameworks for peatland restoration in polluted landscapes.

4.3 Thesis Conclusions

This thesis demonstrates that industrial pollution in the Sudbury region reshaped peatland ecosystems through tightly coupled biogeochemical and microbial pathways. Chapter 2 shows that sulfur and TMMs altered peat chemistry, nutrient stoichiometry, and long-term carbon balance, producing a vertically stratified carbon regime characterized by surface preservation and deeper carbon loss. Chapter 3 reveals that these same geochemical characteristics restructured

microbial communities, with testate amoebae responding both directly to trace-metal stress and indirectly to shifts in peat carbon composition and substrate quality. In both cases, indirect, chemically mediated pathways emerge as more ecologically consequential than direct toxicity alone. Crucially, neither peat carbon dynamics nor microbial assemblages show clear evidence of autonomous recovery following emission reductions, indicating persistent legacy effects. Together, these findings position the Sudbury peatlands as a globally relevant example of how extreme smelting pollution can induce long-lasting, depth-integrated state shifts in carbon storage and microbial structure, emphasizing the need for restoration strategies that address both hydrological integrity and the chemically altered peat substrate.

References

Chapter 1 References

Andersen, R., Chapman, S. J., Artz, R. R. E. (2010). Microbial communities in natural and disturbed peatlands: A review. *Journal of Soil Biology and Biochemistry, 57*, 979-994. https://doi.org/10.1016/j.soilbio.2012.10.003

Arsenault, J., Talbot, J., Brown, L. E., Helbig, M., Holden, J., Hoyos-Santillan, J., et al. (2023). Climate-driven spatial and temporal patterns in peatland pool biogeochemistry. *Global Change Biology, 29*(14), 4056-4068. https://doi.org/10.1111/gcb.16748

Asada, T., Warner, B. G. (2009). Plants and testate amoebae as environmental indicators in cupriferous peatlands, New Brunswick, Canada. *Ecological Indicators* 9(1): 129–137. https://doi.org/10.1016/j.ecolind.2008.02.006

Belyea, L. R., Clymo, R. S. (2001). Feedback control of the rate of peat formation. *Proceedings Biological Sciences, 268*(1473), 1315-1321. https://doi.org/10.1098/rspb.2001.1665

Berger, A., Tricot, C. (1992). The greenhouse effect. *Surveys in Geophysics, 13,* 523-549. https://doi.org/10.1007/BF01904998

Bindler, R. (2006). Mire in the past – looking to the future: Geochemistry of peat and the analysis of past environmental changes. *Global and Planetary Change, 53*(4), 209-221. https://doi.org/10.1016/j.gloplacha.2006.03.004

Birks, H. J. B., Lotter, A. F., Juggins, S., Smol, J. P. (eds) (2010). Tracking Environmental Change Using Lake Sediments, Volume 5: Data Handling and Numerical Techniques.

Dordrecht: Springer. Retrieved from https://link.springer.com/content/pdf/10.1007/978-94-007-2745-8.pdf

Boonman, J., Harpenslager, S. F., van Dijk, G., Smolders, A. J. P., Hefting, M. M., van de Riet, B., van der Velde, Y. (2024). Redox potential is a robust indicator for decomposition processes in drained agricultural peat soils: A valuable tool in monitoring peatland wetting efforts. *Geoderma, 441*. https://doi.org/10.1016/j.geoderma.2023.116728

Booth, R. K., Stansfield, A., Cowper, E., Kodero, J. M. (2025). Testate amoebae as paleoenvironmental indicators in peatlands: Calibration-dataset synthesis and assessment of modern analogues using the Neotoma Paleoecology Database. *Quaternary Science Reviews, 366.* https://doi.org/10.1016/j.quascirev.2025.109491

Chambers, F. M., Beilman, D. W., Yu, Z. (2011). Methods for determining peat humification and for quantifying peat bulk density, organic matter and carbon content for paleostudies of climate and peatland carbon dynamics. *Mires and Peat, 7*(7). https://doi.org/10.19189/001c.128415

Chan, W. H. and Lusis, M. A., (1985). Post-superstack Sudbury smelter emissions and their fate in the atmosphere: An overview of the Sudbury environment study results. *Water, Air, and Soil Pollution, 26(1)*: 43-58. https://doi.org/10.1007/BF00299487

Clymo, R. S. (1987). The ecology of peatlands. *Science Progress (1933-), 71*(4), 593-614. https://www.jstor.org/stable/43420701

Dickopp, J., Lengerer, A., Kazda, M. (2018). Relationship between groundwater levels and oxygen availability in fen peat soils. *Ecological Engineering, 120,* 85-93. https://doi.org/10.1016/j.ecoleng.2018.05.033

Dieleman, C. M., Lindo, Z., McLaughlin, J. W., Craig, A. E., Branfireun, B. A. (2016). Climate change effects on peatland decomposition and porewater dissolved organic carbon biogeochemistry. *Biogeochemistry, 128,* 385-396. https://doi.org/10.1007/s10533-016-0214-8

Freedman, B., Hutchinson, T. C. (1980). Pollution inputs from the atmosphere and accumulations in soils and vegetation near a nickel-copper smelter at Sudbury, Ontario, Canada. *Canadian Journal of Botany, 58*(1)*,* 108-132. https://doi.org/10.1139/b89-014

Frolking, S., Roulet, N., Fuglestvedt, J. (2006). How northern peatlands influence the Earth's radiative budget: Sustained methane emission versus sustained carbon sequestration. *Journal of Geophysical Research: Biogeosciences, 111(G1)*. https://doi.org/10.1029/2005JG000091

Frolking, S., Talbot, J., Jones, M. C., Treat, C. C., Kauffman, J. B., Tuittila, E-S., Roulet, N. (2011). Peatlands in the Earth's 21st century climate system. *Environmental Reviews, 19*, 371-396. https://doi.org/10.1139/a11-014

Gignac, L. D., Beckett, P. J. (1986). The effect of smelting operations on peatlands near Sudbury, Ontario, Canada. *Canadian Journal of Botany, 64(6)*, 1138-1147. https://doi.org/10.1139/b86-157

Gorham, E., Janssens, J. A. (1992). Concepts of fen and bog re-examined in relation to bryophyte cover and the acidity of surface waters. *Acta Societatis Botanicorum Poloniae, 61*(1), 7-20. https://doi.org/10.5586/asbp.1992.001

Gorham, E., Lehman, C., Dyke, A., Clymo, D., Janssens, J. (2012). Long-term carbon sequestration in North American peatlands. *Quaternary Science Reviews, 58*, 77-82. https://doi.org/10.1016/j.quascirev.2012.09.018

Gong, Y., Wu, J., Vogt, J., Ma, W. (2020). Greenhouse gas emissions from peatlands under manipulated warming, nitrogen addition, and vegetation composition change; A review and data synthesis. *Environmental Reviews.* https://doi.org/10.1139/er-2019-0064

Gu, X., Tsyganov, A. N., Mazei, N. G., Babeshko, K. V., Chernyshiv, V. A., Novenko, E. Y, Mazei, Y. A. (2025). Testate amoebae as palaeohydrological indicators in the boreal and subarctic permafrost mires in the western part of the central Siberian Plateau. *Quaternary Science Reviews, 349.* https://doi.org/10.1016/j.quascirev.2024.109108

Gunn, J., (1995). Environmental restoration and recovery of an industrially-disturbed landscape. In: Gunn, J. M. (ed.) *Restoration and Recovery of an Industrial Region*. New York: Springer, pp. 1–15. Retrieved from; https://www.greatersudbury.ca/live/environment-and-sustainability1/regreening-program/pdf-documents/restoration-and-recovery-of-an-industrial-region-progress-in-restoring-the-smelter-damaged-landscape-near-sudbury-canada/

Gunn, J., Keller, W., Negusanti, J., Potvin, R., Beckett, P., Winterhalder, K. (1995). Ecosystem recovery after emission reductions: Sudbury, Ontario. *Water, Air, and Soil Pollution, 85(3)*, 1783-1788. https://doi.org/10.1007/BF00477238

Holden, J., Burt, T. P. (2003). Hydrological studies on blanket peat: the significance of the acrotelm-catotelm model. *Journal of Ecology, 91*(1)*,* 86-102. https://www.jstor.org/stable/3599540

Jassey, V. E. J., Chiapusio, G., Binet, P., Buttler, A., Laggoun-Défarge, F., Delarue, F., et al. (2013). Above- and belowground linkages in *Sphagnum* peatland: Climate warming affects plant–microbial interactions. *Global Change Biology*, *19*(3), 811–823. https://doi.org/10.1111/gcb.12075

Koskinen, M., Anttila, J., Vranová, V., Holík, L., Roche, K., Vorenhout, M., et al. (2025). Covariation of redox potential profiles and the water table level at peatland sites representing different drainage regimes: implications for ecological modelling. *Biogeosciences, 22*(15), 3989-4012. https://doi.org/10.5194/bg-22-3989-2025

Kroetsch, D. J., Geng, X., Chang, S. X., Saurrette, D. D. (2011). Organic soils of Canada: Part 1. Wetland organic soils. *Canadian Journal of Soil Science, 91*(5), 807-822. https://doi.org/10.4141/cjss10043

Kuuri-Riutta, O., Väliranta, M., Tuittila, E-S. (2022). Literature review on testate amoebae as environmental indicators as a functional part of the microbial community in northern peatlands. *Mires and Peat, 28(28).* https://doi.org/10.19189/MaP.2022.OMB.StA.2412

Lamentowicz, M., Gałka, M., Milecka, K., Tobolski, K., Lamentowicz, Ł., Fiałkiewicz-Kozieł, B., Blaauw, M. (2013). A 1300-year multi-proxy, high-resolution record from a rich fen in northern Poland: Reconstructing hydrology, land-use and climate change. *Journal of Quaternary Science*, *28*(6), 582–594. https://doi.org/10.1002/jqs.2650

Limpens, J., Berendse, F., Blodau, C., Canadell, J. G., Freeman, C., Holden, J., et al. (2008). Peatlands and the carbon cycle: from local processes to global implications – a synthesis. *Biogeosciences, 5*(5), 1475-1491. https://doi.org/10.5194/bg-5-1475-2008

Lourenco, M., Fitchett, J. M., Woodborne, S. (2022). Peat definitions: A critical review. *Progress in Physical Geography: Earth and Environment, 47*(4). https://doi.org/10.1177/03091333221118353

Luke, S., Preston, M. D., Basiliko, N., Watmough, S. A. (2015). Microbial communities, biomass, and carbon mineralization in acidic, nutrient-poor peatlands impacted by metal and acid deposition. *Water, Air, & Soil Pollution, 226(19)*. https://doi.org/10.1007/s11270-014-2265-6

Martin-Ortega, J., Allott, T. E. H., Glenk, K., Schaafsma, M. (2014). Valuing water quality improvements from peatland restoration: Evidence and challenges. *Ecosystem Services, 9,* 34-43. https://doi.org/10.1016/j.ecoser.2014.06.007

Martínez Cortizas, A., Biester, H., Mighall, T., Bindler, R. (2007). Climate-driven enrichment of pollutants in peatlands. *Biogeosciences, 4(5)*, 905-911. https://doi.org/10.5194/bg-4-905-2007

McCarter, C.P.R., Tutt, E., Moore, P. A., Furukawa, A. K., Verkaik, G. J., Wilkinson, S. L., et al. (2024). Hydrophysical properties of peat in undisturbed and smelter-impacted peatlands: Implications for moss recovery, drought and wildfire. *Journal of Hydrological Processes, 38(12)*. https://doi.org/10.1002.hyp.70034

Mitchell, E. A. D., Charman, D. J., Warner, B. G. (2008). Testate amoebae analysis in ecological and paleoecological studies of wetlands: Past, present and future. *Biodiversity and Conservation, 17*(9), 2115–2137. https://doi.org/10.1007/s10531-007-9221-3

Mitsch, W. J., Bernal, B., Nahlik, A. M., Mander, Ü., Zhang, L., Anderson, C. L., Jørgensen, S. E., Brix, H. (2012). Wetlands, carbon, and climate change. *Landscape Ecology, 28,* 583-597. https://doi.org/10.1007/s10980-012-9758-8

Nasser, N. A., Patterson, R. T., Roe, H. M., Galloway, J. M., Falck, H., Palmer, M. J., et al. (2016). Lacustrine arcellinina (testate amoebae) as bioindicators of arsenic contamination. *Microbial Ecology, 72*(1), 130-149. https://doi.org/10.1007/s00248-016-0752-6

National Wetlands Working Group. (1997). *The Canadian Wetland Classification System 2nd Edition*. Waterloo, ON: University of Waterloo, Wetlands Research Centre. Retrieved from https://nawcc.wetlandnetwork.ca/Wetland%20Classification%201997.pdf

Ndayishimiye, J. C., Nyirabuhoro, P., Xinyun, C., Saldaev, D., Mazei, Y., Gao, X. (2025). Determinants of testate amoeba community dynamics in urban waters: Effects of heatwave, air pollution, and hydrological gradient. *Water Research, 286.* https://doi.org/10.1016/j.watres.2025.124248

Newman, J. E., Levasseur, P. A., Beckett, P., Watmough, S. A. (2023). The impact of severe pollution from smelter emissions of carbon and metal accumulation in peatlands in Ontario, Canada. *Journal of Environmental Pollution, 320*. https://doi.org/10.1016/j.envpol.2023.121102

Osborne, C., Gilbert-Parkes, S., Spiers, G., Lamit, L. J., Lilleskov, E. A., Basiliko, N., et al. (2024). Global patterns of metal and other element enrichment in bog and fen peatlands. *Archives of Environmental Contamination and Toxicology, 86,* 125-139. https://doi.org/10.1007/s00244-024-01051-3

Parmar, T. K., Rawtani, D., Agrawal, Y. K. (2016). Bioindicators: the natural indicator of environmental pollution. *Frontiers in Life Science, 9*(2), 110-118. https://doi.org/10.1080/21553769.2016.1162753

Patterson, R. T., Barker, T., Burbidge, S. M. (1996). Arcellaceans (Thecamoebians) as proxies of arsenic and mercury contamination in northeastern Ontario lakes. *Journal of Foraminiferal Research, 26*(2), 172–183. https://doi.org/10.2113/gsjfr.26.2.172

Payne, R. J., Mitchell, E. A. D., Nguyen-Viet, H., Gilbert, D. (2012). Can pollution bias peatland paleoclimate reconstruction? *Quaternary Research, 78*(2), 170-173. https://doi.org/10.1016/j.yqres.2012.05.004

Piaszczyk, W., Szlachta, A., Łyszczarz, S., Szymański, N., Jasik, M., Żelazny, M., et al. (2025). The effect of soil chemical properties and ecological implications on the distribution of heavy metals in different types of peatland. *Ecological Indicators, 178.* https://10.1016/j.ecolind.2025.113922

Potvin, R. R., Negusanti, J. J., (1995). Declining Industrial Emissions, Improving Air Quality, and Reduced Damage to Vegetation. In: J. M. Gunn (ed), Restoration and Recovery of an Industrial Region: Progress in Restoring the Smelter-Damaged Landscape Near Sudbury, Canada. Springer New York, New York, NY, pp. 51-65.

Potvin, R. (2007). *Air quality trends in the Sudbury Area 1953 – 2002.* Paper presented at Mining and the Environment Conference*,* Sudbury, ON. Retrieved from https://pdf.library.laurentian.ca/medb/conf/Sudbury07/Potvin.pdf

Reinhardt, E. G., Dalby, A. P., Kumar, A., Patterson, R. T. (1998). Arcellaceans as pollution indicators in mine tailing contaminated lakes near Cobalt, Ontario, Canada. *Micropaleontology*, *44*(2), 131–148. https://doi.org/10.2307/1486066

Renou-Wilson, F., Moser, G., Fallon, D., Farrell, C. A. Müller, C., Wilson, D. (2019). Rewetting degraded peatlands for climate and biodiversity benefits: Results from two raised bogs. *Ecological Engineering, 127,* 547-560. https://doi.org/10.1016/j.ecoleng.2018.02.014

Robroek, B. J. M., Albrecht, R. J. H., Hamard, S., Pulgarin, A., Bragazza, L., Buttler, A., Jassey, V. E. J. (2016). Peatland vascular plant functional types affect dissolved organic matter chemistry. *Plant and Soil, 407,* 135-143. https://doi.org/10.1007/s11104-015-2710-3

Rousell, D. H., Long, D. G. F. (1998). Are outliers of the Huronian Supergroup preserved in structures associated with the collapse of the Sudbury Impact Crater? *The Journal of Geology, 106(4)*. https://doi.org/10.1086/516032

Rydin, H., Gunnarsson, U., Sundberg, S. (2006). The role of *Sphagnum* in peatland development and persistence. In: R.K. Wieder and D.H. Vitt (Editors), Ecological Studies, Vol. 188; Boreal Peatland Ecosystems. Springer-Verlag Berlin, Heidelberg. https://doi.org/10.1007/978-3-540-31913-9_4

Saarinen, O. W. (2013). *From meteorite impact to constellation city: A historical geography of Greater Sudbury.* Waterloo, ON: Wilfrid Laurier University Press

Seward, J., Bräuer, S., Beckett, P., Roy-Léveillée, P., Emilson, E., Watmough, S., Basiliko, N. (2023). Recovery of smelter-impacted peat and *Sphagnum* moss: A microbial perspective. *Microbial Ecology, 86*(4), 2894-2903. https://10.1007/s00248-023-02289-5

Shotyk, W. (1996). Natural and anthropogenic enrichments of As, Cu, Pb, Sb, and Zn in ombrotrophic versus minerotrophic peat bog profiles, Jura Mountains, Switzerland. *Water, Air, and Soil Pollution, 90,* 375-405. https://doi.org/10.1007/BF00282657

Sickles II, J. E., Shadwick, D. S., (2015). Air quality and atmospheric deposition in the eastern US: 20 years of change. *Atmospheric Chemistry and Physics, 15*(1): 173-197. https://doi.org/10.5194/acp-15-173-2015

Sitte, J., Akob, D. M., Kaufmann, C., Finster, K., Banerjee, D., Burkhardt, E-M., et al. (2010). Microbial links between sulfate reduction and metal retention in uranium- and heavy metal contaminated soil. *Applied Environmental Microbiology, 76*(10), 3143-3152. https://doi.org/10.1128/AEM.00051-10

Souter, L., Watmough, S. A. (2016). The impact of drought and air pollution on metal profiles in peat cores. *The Science of the Total Environment, 541,* 1031-1040. https://doi.org/10.1016/j.scitotenv.2015.09.137

Steinmann, P., Shotyk, W. (1997). Chemical composition, pH, and redox state of sulfur and iron in complete vertical porewater profiles from two *Sphagnum* peat bogs, Jura Mountains, Switzerland. *Geochimica et Cosmochimica Acta, 61*(6), 1143-1163. https://doi.org/10.1016/S0016-7037(96)00401-2

Swindles, G. T., Green, S. M., Brown, L., Holden, J., Raby, C. L., Turner, T. E., et al. (2016). Evaluating the use of dominant microbial consumers (testate amoebae) as indicators of blanket peatland restoration. *Ecological Indicators, 69,* 318-330. https://doi.org/10.1016/j.ecolind.2016.04.038

Tarnocai, C. (2009). The impact of climate change on Canadian peatlands. *Canadian Water Resources Journal, 34*(4), 453-466. https://doi.org/10.4296/cwrj3404453

Tipping, E., Smith, E. J., Lawlor, A. J., Hughes, S., Stevens, P. A. (2003). Predicting the release of metals from ombrotrophic peat due to drought-induced acidification. *Journal of Environmental Pollution, 123(2)*, 239-253. https://doi.org/10.1016/S0269-7491(02)00375-5

Vodyanitskii, Y. N., Shoba, S. A. (2015). Biogeochemistry of carbon, iron, and heavy metals in wetlands (Analytical review). *Moscow University Soil Science Bulletin, 70,* 89-97. https://doi.org/10.3103/S0147687415030072

Wanner, M., Birkhofer, K., Fischer, T., Shimizu, M., Shimano, S., Puppe, D. (2020). Soil testate amoebae and diatoms as bioindicators of an old heavy metal contaminated floodplain in Japan. *Microbial Ecology*, *79*(1), 123–133. https://doi.org/10.1007/s00248-019-01383-x

Ward, S. E., Ostle, N. J., Oakley, S. Quirk, H., Henrys, P. A., Bardgett, R. D. (2013). Warming effects on greenhouse gas fluxes in peatlands are modulated by vegetation composition. *Ecology Letters, 16*(10), 1285-1293. https://doi.org/10.1111/ele/12167

Wieder, R. K.,. Vitt, D. H., Benscotter, B. W. (2006). Peatlands and the boreal forest. In: Wieder, R. K., Vitt, D. H. (eds). Ecological Studies, Vol. 188. Springer-Verlag, Berlin: Heidelberg. Retrieved from https://link.springer.com/content/pdf/10.1007/978-3-540-31913-9.pdf#page=22

Wilkinson, D. M., Mitchell, E. A. D. (2010). Testate amoebae and nutrient cycling with particular reference to soils. *Geomicrobiology Journal, 27*(6-7), 520-533. https://doi.org/10.1080/01490451003702925

Chapter 2 References

Ames, D. E., Golightly, J. P., Lightfoot, P. C., Gibson, H. L. (2002). Vitric compositions in the Onaping Formation and their relationship to the Sudbury Igneous Complex, Sudbury Structure. *Economic Geology.* https://doi.org/10.2113/gsecongeo.97.7.1541

Andersen, R., Grasset, L., Thormann, M. N., Rochefort, L. Francez, A-J. (2010). Changes in microbial community structure and function following *Sphagnum* peatland restoration. *Soil Biology and Biochemistry, 42*(2), 291-301. https://doi.org/10.1016/j.soilbio.2009.11.006

Baird, A. J., Belyea, L. R., Comas, X., Reeve, A. S. (2009). Understanding carbon cycling in northern peatlands: Recent developments and future prospects. In: Baird, A. J., Belyea, L.R., Comas, X., et al. (eds) *Carbon Cycling in Northern Peatlands*. Geophysical Monograph Series 184. Washington, DC: American Geophysical Union, pp. 1-7. https://doi.org/10.1029/2008GM000875

Barber, K. E. (1981). Peat stratigraphy and climatic change: a palaeoecological test of the theory of cyclic peat bog regeneration. *Rotterdam: Balkema.*

Barrett, S. E., Watmough, S. A. (2015). Factors controlling peat chemistry and vegetation composition in Sudbury peatlands after 30 years of pollution emission reductions. *Environmental Pollution, 206*, 122-132. https://doi.org/10.1016/j.envpol.2015.06.021

Berger, S., Gebauer, G., Blodau, C., Knorr, K-H. (2017). Peatlands in a eutrophic world – assessing the state of a poor fen-bog transition in southern Ontario, Canada, after long term nutrient input and altered hydrological conditions. *Journal of Soil Biology and Biochemistry, 114,* 131-144. https://doi.org/10.1016/j.soilbio.2017.07.011

Blaauw, M., Christen, J. A. (2011). Flexible paleoclimate age-depth models using an autoregressive gamma process. *Bayesian Analysis, 6(3)*, 457-474. https://doi.org/10.1214/11-BA618

Boonman, J., Harpenslager, S.F., van Dijk, G., Smolders, A.J.P., Hefting, M.M., van de Riet, B., van der Velde, Y. (2024). Redox potential is a robust indicator for decomposition processes in drained agricultural peat soils: A valuable tool in monitoring peatland wetting efforts. *Geoderma, 441*. https://doi.org/10.1016/j.geoderma.2023.116728

Bourbonniere, R. A. (2013). Review of water chemistry research in natural and disturbed peatlands. *Canadian Water Resources Journal, 34(4)*, 393-414. https://doi.org/10.4296/cwrj3404393

Bourgeau-Chavez, L. L., Grelik, S. L., Billmire, M., Jenkins, L. K., et al. (2020). Assessing boreal peat fire severity and vulnerability of peatlands to early season wildland fire. *Frontiers for Global Change, 3*. https://doi.org/10.3389/ffgc.2020.00020

Broder, T., Biester, H. (2015). Hydrologic controls on DOC, As and Pb export from a polluted peatland – the importance of heavy rain events, antecedent moisture conditions and hydrological connectivity. *Biogeosciences, 12*(15), 4651-4664. https://doi.org/10.5194/bg-12-4651-2015

Cabała, J., Smieja-Król, B., Jablonska, M., Chrost, L. (2013). Mineral components in a peat deposit: Looking for signs of early mining and smelting activities in Silesia-Cracow region (Southern Poland). *Environmental Earth Sciences, 69*, 2559-2568. https://doi.org/10.1007/s12665-012-2080-6

Charman, D. J., Beilman, D. W., Blaauw, M., Booth, R. K., Brewer, S., Chambers, F. M., et al. (2013). Climate-related changes in peatland carbon accumulation during the last millennium. *Journal of Biogeosciences, 10*, 929-944. https://doi.org/10.5194/bg-10-929-2013

Chan, W. H. and Lusis, M. A., (1985). Post-superstack Sudbury smelter emissions and their fate in the atmosphere: An overview of the Sudbury environment study results. *Water, Air, and Soil Pollution, 26(1)*: 43-58. https://doi.org/10.1007/BF00299487

Chaudhary, N., Miller, P. A., Smith, B. (2017). Modelling Holocene peatland dynamics with an individual-based dynamic vegetation model. *Biogeosciences*, *14,* 2571–2596. https://doi.org/10.5194/bg-14-2571-2017

City of Greater Sudbury (2013). Greater Sudbury Natural Heritage Report. Sudbury, ON: City of Greater Sudbury. Retrieved from: https://www.greatersudbury.ca/linkservid/A90ABF71-0FCF-E9CF-57B73B076A96698C/showMeta/0/

Clark, P. U., Shakun, J. D., Baker, P. A., Bartlein, P. J., Brewer, S., Brook, E., et al. (2012). Global climate evolution during the last deglaciation. *Proceedings of the National Academy of Sciences of the United States of America, 109(19)*, E1134-E1142. https://doi.org/10.1073/pnas.1116619109

Clymo, R. S. (1987). The ecology of peatlands. *Science Progress (1933-), 71*(4), 593-614. https://www.jstor.org/stable/43420701

Clymo, R. S., Pearce, D. M. E. (1995). Methane and carbon dioxide production in, transport through, and efflux from a peatland. *Philosophical Transactions A: Mathematical, Physical and Engineering Sciences, 351 (1696)*, 249-259. https://doi.org/10.1098/rsta.1995.0032

Clymo, R. S., Turunen, J., Tolonen, K. (1998). Carbon accumulation in peatland. *Oikos, 81(2)*, 368-388. https://doi.org/10.2307/3547057

Coggins, A. M., Jennings, S. G., Ebinghaus, R. (2006). Accumulation rates of the heavy metals lead, mercury and cadmium in ombrotrophic peatlands in the west of Ireland. *Journal of Atmospheric Environment, 40(2)*, 260-278. https://doi.org/10.1016/j.atmosenv.2005.09.04

De Vleeschouwer, F., Fagel, N., Cheburkin, A., Pazdur, A., Sikorski, J., Mattielli, N., et al. (2009). Anthropogenic impacts in North Poland over the last 1300 years - A record of Pb, Zn, Cu, Ni, and S in an ombrotrophic bog. *Science of the Total Environment, 407(21)*, 5674-5684. https://doi.org/10.1016/j.scitotenv.2009.07.020

Dentener, F., Drevet, J., Lamarque, J. F., Bey, I., Eickhout, B., Fiore, A. M., et al. (2006). Nitrogen and sulfur deposition on regional and global scales: A multimodel evaluation. *Global Biogeochemical Cycles, 20(4)*. https://doi.org/10.1029/2005GB002672

Environment Canada. (2025). Environment and Climate Change Canada Historical Climate Data. [Sudbury A, Climate ID 6068153] Retrieved from https://climate.weather.gc.ca/index_e.html

Evans, C. D., Jones, T. G., Burden, A., Ostle, N., Zieliński, P., Cooper, M. D. A., et al. (2012). Acidity controls on dissolved organic carbon mobility in organic soils. *Global Change Biology, 18(11)*, 3317-3331. https://doi.org/10.1111/j.1365-2486.2012.02794.x

Frolking, S., Roulet, N., Fuglestvedt, J. (2006). How northern peatlands influence the Earth's radiative budget: Sustained methane emission versus sustained carbon sequestration. *Journal of Geophysical Research: Biogeosciences, 111(G1)*. https://doi.org/10.1029/2005JG000091

Frolking, S., Talbot, J., Jones, M. C., Treat, C. C., Kauffman, J. B., Tuittila, E-S., Roulet, N. (2011). Peatlands in the Earth's 21st century climate system. *Environmental Reviews, 19*, 371-396. https://doi.org/10.1139/a11-014

Furukawa, A. K., Sutton, O. F., Simone, K. L., Verkaik, G. J., Moore, P. A., Clark, A., et al. (2025). Hydrological feedbacks in northern peatlands 2: Peat depth as a control on peatland resilience. *Ecohydrology, 18*(8). https://doi.org/10.1002/eco.70158

Gignac, L. D., Beckett, P. J. (1986). The effect of smelting operations on peatlands near Sudbury, Ontario, Canada. *Canadian Journal of Botany, 64(6)*, 1138-1147. https://doi.org/10.1139/b86-157

Gorham, E., Lehman, C., Dyke, A., Clymo, D., Janssens, J. (2012). Long-term carbon sequestration in North American peatlands. *Quaternary Science Reviews, 58*, 77-82. https://doi.org/10.1016/j.quascirev.2012.09.018

Grieve, R. A. F., Therriault, A. M. (2003). Vredefort, Sudbury, Chicxulub: Three of a kind? *Annual Review of Earth and Planetary Sciences, 28(1)*, 305-338. https://doi.org/10.1146/annurev.earth.28.1.305

Gunn, J., (1995). Environmental restoration and recovery of an industrially-disturbed landscape. In: Gunn, J. M. (ed.) *Restoration and Recovery of an Industrial Region*. New York: Springer, pp. 1–15. Retrieved from; https://www.greatersudbury.ca/live/environment-and-sustainability1/regreening-program/pdf-documents/restoration-and-recovery-of-an-industrial-region-progress-in-restoring-the-smelter-damaged-landscape-near-sudbury-canada/

Gunn, J., Keller, W., Negusanti, J., Potvin, R., Beckett, P., Winterhalder, K. (1995). Ecosystem recovery after emission reductions: Sudbury, Ontario. *Water, Air, and Soil Pollution, 85(3)*, 1783-1788. https://doi.org/10.1007/BF00477238

Gunn, J., Sein, R., Keller, B., Beckett, P. (2001). Liming of acid and metal contaminated catchments for the improvement of drainage water quality. *Water, Air, and Soil Pollution, 130,* 1439-1444. https://doi.org/10.1023/A:1013908913162

Hansson, S.V., Bindler, R., De Vleeschouwer, F. (2015). Ussing peat records as natural archives of past atmospheric metal deposition. In: Blais, J., Rosen, M., Smol, J. (eds) Environmental Contaminants. Developments in Paleoenvironmental Research, vol 18. Springer, Dordrecht. https://doi.org/10.1007/978-94-017-9541-8_12

Heffernan, L., Estop-Aragonés, C., Knorr, K. H., Talbot, J., Olefeldt, D. (2020). Long-term impacts of permafrost thaw on carbon storage in peatlands: Deep losses offset by surficial accumulation. *Journal of Geophysical Research: Biogeosciences, 125(3)*. https://doi.org/10.1029/2019JG005501

Hughes, P. D. M., Mallon, G., Brown, A., Essex, H. J., Stanford, J. D., Hotes, S. (2013). The impact of high tephra loading on late-Holocene carbon accumulation and vegetation succession in peatland communities. *Quaternary Science Reviews, 67*, 160-175. https://doi.org/10.1016/j.quascirev.2013.01.015

Hutchinson, T. C. and Whitby, L. M., (1977). The effects of acid rainfall and heavy metal particulates on a boreal forest ecosystem near the Sudbury smelting region of Canada. *Water, Air, and Soil Pollution, 7*, 421-438. https://doi.org/10.1007/BF00285542

Kaila, A., Asam, Z. Z., Sarkkala, S., Xiao, L., Laurén, A., Vasander, H., Nieminen, M. (2012). Decomposition of harvest residue needles on peatlands drained for forestry – Implications for nutrient and heavy metal dynamics. *Journal of Forest Ecology and Management, 277*. 141-149. https://doi.org/10.1016/j.foreco.2012.03.024

Kalmykova, Y., Rauch, S., Strömvall, A. M., Morrison, G., Stolpe, B., Hasselliöv, M. (2010). Colloid-facilitated metal transport in peat filters. *Water Environment Research, 82(6)*. 506-511. https://doi.org/10.2175/106143009X1259484815430

Keizer, P.S., Gajewski, K., McLeman, R. (2015). Forest dynamics in relation to multi-decadal late-Holocene climatic variability, eastern Ontario, Canada. *Review of Palaeobotany and Palynology, 219,* 106-115. https://doi.org/10.1016/j.revpalbo.2015.04.001 Keller, W., Pitblado, J. R., Carbone, J., (1992). Chemical responses of acidic lakes in the Sudbury, Ontario area to reduced smelter emissions, 1981-89. *Canadian Journal of Fisheries and Aquatic Sciences, 49*(S1), 25-32. https://doi.org/10.1139/f92-297.

Keller, W., Heneberry, J. H., Gunn, J. M., (1998). Effects of emission reductions from the Sudbury smelters on the recovery of acid-and metal-damaged lakes. *Journal of Aquatic Ecosystem Stress and Recovery, 6*, 189-198. https://doi.org/10.1023/A:1009975116685

Kjær, K.H., Bjørk, A.A., Kjeldson, K.K., Hansen, E.S., Andresen, C.S., Siggaard-Andersen, M-L., et al. (2022). Glacier response to the Little Ice Age during the Neoglacial cooling in Greenland. *Earth-Science Reviews, 227.* https://doi.org/10.1016/j.earscirev.2022.103984

Landry, J., and Rochefort, L. (2012). *The drainage of peatlands: Impacts and rewetting techniques,* Québec, QC: Université Laval. Retrieved from https://www.gret-perg.ulaval.ca/fileadmin/Fichiers/centre_recherche/Drainage_guide_Web_02.pdf

Lakehead University Environmental Laboratory, (2025). Lakehead University: Thunder Bay, ON. https://www.lakeheadu.ca/centre/lucas/laboratories/luel

Lautenbach, W. E., Miller, J., Beckett, P. J., Negusanti, J. J., Winterhalder, K. (1995). Municipal land restoration program: The regreening process. In: Gunn, J. M. (ed.) *Restoration and recovery of an industrial region,* 109-122, New York, NY: Springer. https://doi.org/10.1007/978-1-4612-2520-1_8

Levasseur, P. A., Aherne, J., Basiliko, N., Emilson, E. J. S., Preston, M. D., Sager, E. P. S., Watmough, S. A. (2023), Soil carbon pools and fluxes following the regreening of a mining and smelting degraded landscape. *Science of the Total Environment, 904*. https://doi.org/10.1016/j.scitotenv.2023.166734

Lévesque, P. E. M., Dinel, H., Larouche, A. (1988). Guide to identification of plant macrofossils in Canadian peatlands (1817). Ottawa, ON: Agriculture Canada. Retrieved from https://publications.gc.ca/collections/collection_2014/aac-aafc/agrhist/A15-1817-1988-eng.pdf

Likens, G. E., Driscoll, C. T., Buso, D. C. (1996). Long-term effects of acid rain: Response and recovery of a forest ecosystem. *Science, 272(5259)*, 244-246. https://doi.org/10.1126/science.272.5259.244

Loisel, J., Yu, Z., Beilman, D. W., Camill, P., Alm, J., Amesbury, M. J. et al. (2014). A database and synthesis of northern peatland soil properties and Holocene carbon and nitrogen accumulation. *The Holocene, 24(9)*. https://doi.org/10.1177/0959683514538073

Luke, S., Preston, M. D., Basiliko, N., Watmough, S. A. (2015). Microbial communities, biomass, and carbon mineralization in acidic, nutrient-poor peatlands impacted by metal and acid deposition. *Water, Air, & Soil Pollution, 226(19)*. https://doi.org/10.1007/s11270-014-2265-6

Luo, N., Yu, R., Wen, B., Li, X., Liu, X., Li, X. (2023). Identifying anthropogenic sources of heavy metals in alpine peatlands over the past 150 years; Examples from typical peatlands in Altay Mountains, Northwest China. *International Journal of Environmental Research and Public Health, 20(6)*. https://doi.org/10.3390/ijerph20065013

Magnan, G., Garneau, M. (2014). Evaluating long-term regional climate variability in the maritime region of the St. Lawrence North Shore (eastern Canada) using a multi-site comparison of peat-based paleohydrological records. *Journal of Quaternary Science, 29*(3), 209-220. https://doi.org/10.1002/jqs.2694

Martínez Cortizas, A. M., Biester, H., Mighall, T., Bindler, R. (2007). Climate-driven enrichment of pollutants in peatlands. *Biogeosciences, 4(5)*, 905-911. https://doi.org/10.5194/bg-4-905-2007

Mauquoy, P., Hughes, P. D. M., van Geel, B. (2010). A protocol for plant macrofossil analysis of peat deposits. *Mires and Peat, 7(06)*. https://doi.org/10.19189/001c.128413

McCarter, C. P. R., Rezanezhad, F., Quinton, W. L., Gharedaghloo, B., Lennartz, B., Price, J., et al. (2020). Pore-scale controls on hydrological and geochemical processes in peat: Implications

on interacting processes. *Earth-Science Reviews, 207.* https://doi.org/10.1016/j.earscirev.2020.103227

McCarter, C. P. R., Wilkinson, S. L., Moore, P. A., Waddington, J. M. (2021). Ecohydrological trade-offs from multiple peatland disturbances: The interactive effects of drainage, harvesting, restoration and wildfire in a southern Ontario bog. *Journal of Hydrology, 601*. https://doi.org/10.1016/j.hydrol.2021.126793

McCarter, C.P.R., Moore, P.A., Waddington, J.M. (2023). Modelling the potential for peat-block transplants to restore industrially contaminated *Sphagnum* peatlands. *Ecological Engineering, 187.* https://doi.org/10.1016/j.ecoleng.2022.106874

McCarter, C.P.R., Tutt, E., Moore, P. A., Furukawa, A. K., Verkaik, G. J., Wilkinson, S. L., et al. (2024). Hydrophysical properties of peat in undisturbed and smelter-impacted peatlands: Implications for moss recovery, drought and wildfire. *Journal of Hydrological Processes, 38(12)*. https://doi.org/10.1002.hyp.70034

McDonough, A. M., Bird, A., Luciani, M. A., Todd, A. (2022). Establishing trace element concentrations for lichens and bryophytes in the ring of fire region of the Hudson Bay Lowlands, Ontario, Canada. *Journal of Environmental Monitoring and Assessment, 194(3)*. https://doi.org/10.1007/s10661-022-09890-0

Moore, T. R., Bubier, J. L., Bledzki, L. (2007). Litter decomposition in temperate peatland ecosystems: The effect of substrate and site. *Ecosystems, 10(6)*, 949-963. https://doi.org/10.1007/s10021-007-9064-5

Monet, S. (2013). *Greater Sudbury Natural Heritage Report,* Sudbury, ON: City of Greater Sudbury. Retrieved from https://www.greatersudbury.ca/linkservid/A90ABF71-0FCF-E9CF-57B73B076A96698C/showMeta/0/

Morris, P. J., Swindles, G. T., Valdes, P. J., Bacon, K. L. (2018), Global peatland initiation driven by regionally asynchronous warming. *Proceedings of the National Academy of Sciences of the United States of America, 115(19)*, 4851-4856. https://doi.org/10.1073/pnas.1717838115

Müller, J., Joos, F. (2021). Committed and projected future changes in global peatlands - Continued transient model simulations since the Last Glacial Maximum. *Biogeosciences, 18(12)*, 3657-3687. https://doi.org/10.5194/bg-18-3657-2021

Munford, K. E., Gilbert-Parkes, S., Mykytczuk, N. C. S., Basiliko, N., Yakimovich, K. M., Poulain, A., Watmough, S. A. (2023). How arsenic contamination influences downslope wetland plant and microbial community structure and function. *Science of the Total Environment, 876*. https://doi.org/10.1016/j.scitotenv.2023.162839

National Wetlands Working Group. (1997). *The Canadian Wetland Classification System 2nd Edition*. Waterloo, ON: University of Waterloo, Wetlands Research Centre. Retrieved from https://nawcc.wetlandnetwork.ca/Wetland%20Classification%201997.pdf

Nedwell, D. B., Watson, A. (1995). CH_4 production, oxidation and emission in a U.K. ombrotrophic peat bog: Influence of SO_4^{2-} from acid rain. *Soil Biology and Biochemistry, 27(7)*, 893-903. https://doi.org/10.1016/0038-0717(95)00018-A

Newman, J. E., Levasseur, P. A., Beckett, P., Watmough, S. A. (2023). The impact of severe pollution from smelter emissions of carbon and metal accumulation in peatlands in Ontario, Canada. *Journal of Environmental Pollution, 320*. https://doi.org/10.1016/j.envpol.2023.121102

Nieminen, T. M., Ukonmaanaho, L., Shotyk, W. (2002). Enrichment of Cu, Ni, Zn, Pb and As in an ombrotrophic peat bog near a Cu-Ni smelter in Southwest Finland. *Science of the Total Environment, 292(1-2)*, 81-89. https://doi.org/10.1016/S0048-9697(02)00028-1

Novák, M., Pacherova, P. (2008). Mobility of trace metals in pore waters of two Central European peat bogs. *Science of The Total Environment, 294(2-3)*, 331-337. https://doi.org/10.1016/j.scitotenv.2008.01.036

Novák, M., Adamová, M., Wieder, R. K., Bottrell, S. H. (2005). Sulfur mobility in peat. *Journal of Applied Geochemistry, 20(4)*, 673-681. https://doi.org/10.1016/j.apgeochem.2004.11.009

Novák, M., Zemanova, L., Voldrichova, P., Stepanova, M., Adamova, M., Pacherova, P., et al. (2011). Experimental evidence for mobility/immobility of metals in peat. *Environmental Science and Technology, 45,* 7180-7187. https://doi.org/10.1021/es201086v

Nwaishi, F., Petrone, R. M., Price, J., Andersen, R. (2015). Towards developing a functional-based approach for constructed peatlands evaluation in the Alberta Oil Sands Region, Canada. *Wetlands, 35(2)*. https://doi.org/10.1007/s13157-014-0623-

Ontario Ministry of Natural Resources. (2021). Forest Regions of Ontario. Toronto: Queen's Printer for Ontario. Retrieved from https://www.ontario.ca/page/forest-regions

Ontario Ministry of Natural Resources and Forestry. (2025). Ontario Geohub – Wetland. Toronto: Queen's Printer for Ontario. Retrieved from https://geohub.lio.gov.on.ca/datasets/5216a770ef684d2fae8bcc13ee9c4357_15/about

Pamer, L. J. (2008). Characterization of anthropogenic pollution in *Sphagnum* peat from the Sudbury region: Sudbury region peatlands as archives of atmospheric base metal deposition. (Master's Thesis) Sudbury, ON: Laurentian University. Retrieved from https://central.bac-lac.gc.ca/.item?id=MR44859&op=pdf&app=Library&is_thesis=1&oclc_number=694268382

Pearce, A. J. (1976). Contemporary rates of bedrock weathering, Sudbury, Ontario. *Canadian Journal of Earth Sciences*, *13(1),* 188-193. https://doi.org/10.1139/e76-020

Pearson, D. A. B., Gunn, J. M., Keller, W. (2001 Chapter 9: The Past, Present and Future of Sudbury's Lakes. In: Rousell, D. H., Jansons, K. J. (eds), The Physical Environment of the City of Greater Sudbury, Ontario Geological Survey Special Volume 6, Ontario Geological Survey, 195-215.

Pennington, P.R., Watmough, S. (2015). The biogeochemistry of metal-contaminated peatlands in Sudbury, Ontario, Canada. *Water, Air, and Soil Pollution, 226*(326). https://doi.org/10.1007/s11270-015-2572-6

Porter, T.J., Schoenemann, S.W., Davies, L.J., Steig, E.J., Bandara, S., Froese, D.G. (2019). Recent summer warming in the northwestern Canada exceeds the Holocene thermal maximum. *Nature Communications.* https://doi.org/10.1038/s41467-019-09622-y

Potvin, R. R., Negusanti, J. J., (1995). Declining Industrial Emissions, Improving Air Quality, and Reduced Damage to Vegetation. In: J. M. Gunn (ed), Restoration and Recovery of an

Industrial Region: Progress in Restoring the Smelter-Damaged Landscape Near Sudbury, Canada. Springer New York, New York, NY, pp. 51-65.

Potvin, R. (2007). *Air quality trends in the Sudbury Area 1953 – 2002.* Paper presented at Mining and the Environment Conference, Sudbury, ON. Retrieved from https://pdf.library.laurentian.ca/medb/conf/Sudbury07/Potvin.pdf

Price, J. S., Schlotzhauer, S. M. (1999). Importance of shrinkage and compression in determining water shortage changes in peat: The case of a mined peatland. *Hydrological Processes, 13(16)*, 2591-2601. https://doi.org/10.1002/(SICI)1099-1085(199911)13:16<2591::AID-HYP933>3.0.CO;2-E

Qiu, C., Zhu, D., Ciais, P., Guenet, B., Peng, S. (2020). The role of northern peatlands in the global carbon cycle for the 21st century. *Global Ecology and Biogeography, 29(5)*, 956-973. https://doi.org/10.1111/geb.13081

Rausch, T., Wachter, A. (2005), Sulfur metabolism: A versatile platform for launching defence operations. *Trends in Plant Science, 10(10)*, 503-509. https://doi.org/10.1016/j.tplants.2005.08.006

Reeve, A. S., Siegel, D. I., Glaser, P. H. (2001). Simulating dispersive mixing in large peatlands. *Journal of Hydrology, 242*(1-2), 103-114. https://doi.org/10.1016/S0022-1694(00)00386-3

Reimer, P. J., Austin, W. E. N., Bard, E., Bayliss, A., Blackwell, P. G., Ramsey, C. B., et al. (2020). The IntCal20 northern hemisphere radiocarbon age calibration curve (0 – 55 cal kBP). *Radiocarbon, 62(4)*, 725-757. https://doi.org/10.1017/RDC.2020.41

Rensson, H., Seppä, Crosta, X., Goosse, H., Roche, D.M. (2012). Global characterization of the Holocene Thermal Maximum. *Quaternary Science Reviews, 48,* 7-19. https://doi.org/10.1016/j.quascirev.2012.05.022

Rochefort, L., Vitt, D. H., Bayley, S. E. (1990). Growth, production, and decomposition dynamics of *Sphagnum* under natural and experimentally acidified conditions. *Ecology, 71(5)*, 1986-2000. https://doi.org/10.2307/1937607

Rooney, R. C., Bayley, S. E., Schindler, D. W. (2011). Oil sands mining and reclamation cause massive loss of peatland and stored carbon. *Proceedings of the National Academy of Sciences of the United States of America, 109(13)*, 4933-4937. https://doi.org/10.1073/pnas.1117693108

Rousell, D. H., Long, D. G. F. (1998). Are outliers of the Huronian Supergroup preserved in structures associated with the collapse of the Sudbury Impact Crater? *The Journal of Geology, 106(4)*. https://doi.org/10.1086/516032

Rowe, J. S. (1972). *Forest regions of Canada.* Canadian Forestry Service Publication No. 1300. Ottawa, ON: Department of the Environment, Canadian Forestry Service. Retrieved from https://publications.gc.ca/collections/collection_2019/eccc/Fo47-1300-eng.pd

Saarinen, O. W. (2013). *From meteorite impact to constellation city: A historical geography of Greater Sudbury.* Waterloo, ON: Wilfrid Laurier University Press

Schillereff, D. N., Chiverrell, R. C., Sjöström, J. K., Kylander, M. E., Boyle, J. F., Davies, J. A. C. et al. (2021). Phosphorus supply affects long-term carbon accumulation in mid-latitude ombrotrophic peatlands. *Communications Earth & Environment, 2*. https://doi.org/10.1038/s43247-021-00316-2

Schweingruber, F. H., Kučerová, A., Adamec, L., and Doležal, J. (2020). *Anatomic atlas of aquatic and wetland plant stems.* Springer Nature. https://doi.org/10.1007/978-3-030-33420-8

Seward, J., Bräuer, S., Beckett, P., Roy-Léveillée, P., Emilson, E., Watmough, S., Basiliko, N. (2023). Recovery of smelter-impacted peat and *Sphagnum* moss: A microbial perspective. *Microbial Ecology, 86*(4), 2894-2903. https://10.1007/s00248-023-02289-5

Shaw, A.J., Piatkowski, B., Duffy, A.M., Aguero, B., Imwattana, K., Nieto-Lugilde, M., et al. (2022). Phylogenomic structure and speciation in an emerging model: the *Sphagnum magellanicum* complex (Bryophyta). *New Phytologist, 236*(4), 1497-1511. https://doi.org/10.1111/nph.18429

Sherman, G., Beckett, P. (2003). *Carbon sequestration patterns in the replanted areas of the Sudbury barrens.* Paper presented at Sudbury Mining and the Environment International Conference, Sudbury, ON. Retrieved from https://pdf.library.laurentian.ca/medb/conf/Sudbury03/SmelterLandscape/139.pdf

Shotyk, W., Norton, S. A., Farmer, J. G. (1996). Peat bogs reveal history of atmospheric deposition of lead and other metals. *Eos, Transactions American Geophysical Union, 77(50)*, 507. https://doi.org/10.1029/96EO00338

Shotyk, W. (1988). Review of the inorganic geochemistry of peats and peatland waters. *Earth-Science Reviews, 25(2)*, 95-176. https://doi.org/10.1016/0012-8252(88)90067-0

Sickles II, J. E., Shadwick, D. S., (2015). Air quality and atmospheric deposition in the eastern US: 20 years of change. *Atmospheric Chemistry and Physics, 15*(1): 173-197. https://doi.org/10.5194/acp-15-173-2015

Smieja-Król, B., Fiałkiewicz-Kozieł, B., Sikorski, J., Palowski, B. (2010). Heavy metal behaviour in peat – A mineralogical perspective. *Journal of Science of the Total Environment, 408(23)*, 5924-5931. https://doi.org/10.1016/j.scitotenv.2010.08.032

Souter, L., Watmough, S. A. (2016). The impact of drought and air pollution on metal profiles in peat cores. *The Science of the Total Environment, 541,* 1031-1040. https://doi.org/10.1016/j.scitotenv.2015.09.137

Strack, M. (ed.) (2008). Peatlands and climate change. *IPS, International Peat Society.* Saarijärvi: Finland. Retrieved from https://www.researchgate.net/profile/James-Waddington/publication/37792364_Restoration_of_peatlands_and_greenhouse_gas_balances/links/0fcfd507d79f198155000000/Restoration-of-peatlands-and-greenhouse-gas-balances.pdf

Szkokan-Emilson, E. J., Kielstra, B., Watmough, S., Gunn, J. (2013). Drought-induced release of metals from peatlands in watersheds recovering from historical metal and sulphur deposition. *Biogeochemistry, 116*, 131-145. https://doi.org/10.1007/s10533-013-9919-0

Tipping, E., Smith, E. J., Lawlor, A. J., Hughes, S., Stevens, P. A. (2003). Predicting the release of metals from ombrotrophic peat due to drought-induced acidification. *Journal of Environmental Pollution, 123(2)*, 239-253. https://doi.org/10.1016/S0269-7491(02)00375-5

Tipping, E., Benham, S., Boyle, J. F., Crow, P., Davies, J., Fischer, U., et al. (2014). Atmospheric deposition of phosphorus to land and freshwater. *Environmental Science: Processes Impacts, 16*, 1608-1617. https://doi.org/10.1039/C3EM00641G

Treat, C. C., Jones, M. C., Camill, P., Gallego-Sala, A., Garneau, M., Harden, J. W., et al. (2015). Effects of permafrost aggradation on peat properties as determined from a pan-Arctic

synthesis of plant macrofossils. *Journal of Geophysical Research: Biogeosciences, 121(1)*, 78-94. https://doi.org/10.1002/2015JG003061

Turetsky, M. R., St. Louis, V. (2006). Disturbance in boreal peatlands. In: Wieder RK and Vitt DH (eds) *Boreal Peatland Ecosystems*. Ecological Studies 188. Berlin: Springer, pp. 359–379. https://doi.org/10.1007/978-3-540-31913-9_16

Urban, N. R., Bayley, S. E., Eisenriech, S. J. (1989). Export of dissolved organic carbon and acidity from peatlands. *Water Resources Research, 25(7)*, 1619-1628. https://doi.org/10.1029/WR025i007p01619

Vet, R., Artz, R., Carou, S., Shaw, M. (2013). A global assessment of precipitation chemistry and deposition of sulfur, nitrogen, sea salt, base cations, organic acids, acidity and pH, and phosphorus. *Atmospheric Environment, 93*, 3-100. https://doi.org/10.1016/j.atmosenv.2013.10.06

VETAC, (2024). *2024 Annual Report Regreening Program*. Sudbury, ON: The City of Greater Sudbury. Retrieved from https://www.greatersudbury.ca/live/environment-and-sustainability1/regreening-program/pdf-documents/2024-regreening-annual-report/

Vile, M. A., Bridgham, S. D., Wieder, R. K. (2003a). Response of anaerobic carbon mineralization rates to sulfate amendments in a boreal peatland. *Ecological Applications, 13*(3), 720-734. https://doi.org/10.1890/1051-0761(2003)013[0720:ROACMR]2.0.CO;2

Vile, M. A., Bridgham, S. D., Wieder, R. K., Novák, M. (2003b). Atmospheric sulfur deposition alters pathways of gaseous carbon production in peatlands. *Global Biogeochemical Cycles, 17*(2). https://doi.org/10.1029/2002GB001966

Vitt, D. H., Wieder, R. K., Scott, K. D., Faller, S. (2009). Decomposition and peat accumulation in rich fens of boreal Alberta, Canada. *Ecosystems, 12*, 360-373. https://doi.org/10.1007/s10021-009-9228-6

Volik, O., Elmes, M., Petrone, R. M., Kessel, E. (2020). Wetlands in the Athabasca Oil Sands Region: The nexus between wetland hydrological function and resource extraction. *Environmental Reviews, 28(3)*, 246-261. https://doi.org/10.1139/er-2019-0040

Waddington, J. M., Morris, P. J., Kettridge, N., Granath, G., Thompson, D. K., Moore, P. A. (2014). Hydrological feedbacks in northern peatlands. *Ecohydrology, 8*(1), 113-127. https://doi.org/10.1002/eco.1493

Walker, D., Walker, P. M. (1961). Stratigraphic evidence of regeneration in some Irish bogs. *Journal of Ecology, 49(1)*, 169-185. https://doi.org/10.2307/2257432

Watkinson, A., Juckers, M., D'Andrea, L., Beckett, P., Spiers, G. (2022). Ecosystem recovery of the Sudbury Technogenic Barrens 30 years post-restoration. *Eurasian Soil Science, 55*(5), 663-672. https://doi.org/10.1134/s106422932205012X

Watmough, S. A. (2023). Soil carbon pools and fluxes following the regreening of a mining and smelting degraded landscape. *Science of the Total Environment, 904*. https://doi.org/10.1016/j.scitotenv.2023.166734

Yu, Z., Loisel, J., Brosseau, D. P., Beilman, D. W., Hunt, S. J. (2010). Global peatland dynamics since the Last Glacial Maximum. *Geophysical Research Letters, 37(13)*. https://doi.org/10.1029/2010GL043584

Yu, Z., Beilman, D. W., Frolking, S., MacDonald, G. M., Roulet, N. T., Camill, P., Charman, D. J. (2011). Peatlands and their role in the global carbon cycle. *Eos, Transactions American Geophysical Union, 92(12)*, 97-98. https://doi.org/10.1029/2011EO120001

Zhao, B., Zhuang, Q. (2023). Peatlands and their carbon dynamics in northern high latitudes from 1990 to 2300: A process-based biogeochemistry model analysis. *Biogeosciences, 20(1)*, 251-270. https://doi.org/10.5194/bg-20-251-2023

Chapter 3 References

Amesbury, M. J., Booth, R. K., Roland, T. P., Bunbury, J., Clifford, M. J., Charman, D. J., et al. (2018). Towards a Holarctic synthesis of peatland testate amoeba ecology: Development of a new continental-scale palaeohydrological transfer function for North America and comparison to European data. *Quaternary Science Reviews, 201,* 483-500. https://doi.org/10.1016/j.quascirev.2018.10.034

Andersen, R., Grasset, L., Thormann, M. N., Rochefort, L., Francez, A-J. (2010). Changes in microbial community structure and function following *Sphagnum* peatland restoration. *Soil Biology and Biochemistry*, *42*(2), 291-301. https://doi.org/10.1016/j.soilbio.2009.11.006

Asada, T., Warner, B. G. (2009). Plants and testate amoebae as environmental indicators in cupriferous peatlands, New Brunswick, Canada. *Ecological Indicators* 9(1): 129–137. https://doi.org/10.1016/j.ecolind.2008.02.006

Baird, A. J., Belyea, L. R., Morris, P. J. (2009). Upscaling of peatland–atmosphere fluxes of methane: Small-scale heterogeneity in process rates and the pitfalls of "bucket-and-slab" models. In: Baird, A. J., Belyea, L. R., Comas, X., et al. (eds) *Carbon Cycling in Northern Peatlands*.

Geophysical Monograph Series 184. Washington, DC: American Geophysical Union, pp. 37–53. https://doi.org/10.1029/2008GM000826

Barber, K. E. (1981). Peat stratigraphy and climatic change: a palaeoecological test of the theory of cyclic peat bog regeneration. *Rotterdam: Balkema.*

Barrett, S. E., Watmough, S. A. (2015). Factors controlling peat chemistry and vegetation composition in Sudbury peatlands after 30 years of pollution emission reductions. *Environmental Pollution, 206*, 122-132. https://doi.org/10.1016/j.envpol.2015.06.021

Bennett, K. D. (1996). Determination of the number of zones in a biostratigraphical sequence. *New Phytologist*, *132*(1), 155–170. https://doi.org/10.1111/j.1469-8137.1996.tb04521.x

Birks, H. J. B., Lotter, A. F., Juggins, S., Smol, J. P. (eds) (2010). Tracking Environmental Change Using Lake Sediments, Volume 5: Data Handling and Numerical Techniques. Dordrecht: Springer. Retrieved from https://link.springer.com/content/pdf/10.1007/978-94-007-2745-8.pdf

Blaauw, M., Christen, J. A. (2011). Flexible paleoclimate age-depth models using an autoregressive gamma process. *Bayesian Analysis, 6(3)*, 457-474. https://doi.org/10.1214/11-BA618

Booth, R. K., Sullivan, M. E. (2007). Testate amoebae as paleohydrological proxies in peatlands; A workshop focused on testate amoeba identification, ecology, and their use in paleoenvironmental reconstruction. Unpublished laboratory manual, Lehigh University.

Booth, R.K. (2008). Testate amoebae as proxies for mean annual water-table depth in *Sphagnum*-dominated peatlands of North America. *Journal of Quaternary Science, 23*(1), 43-57. https://doi.org/10.1002/jqs.1114

Booth, R. K., Lamentowicz, M., Charman, D. J. (2010). Preparation and analysis of testate amoebae in peatland palaeoenvironmental studies. *Mires and Peat*, *7*(2010/11)(2), 1–7. https://doi.org/10.19189/001c.128409

Booth, R. K., Stansfield, A., Cowper, E., Kodero, J. M. (2025). Testate amoebae as paleoenvironmental indicators in peatlands: Calibration-dataset synthesis and assessment of modern analogues using the Neotoma Paleoecology Database. *Quaternary Science Reviews, 366.* https://doi.org/10.1016/j.quascirev.2025.109491

Chan, W. H. and Lusis, M. A., (1985). Post-superstack Sudbury smelter emissions and their fate in the atmosphere: An overview of the Sudbury environment study results. *Water, Air, and Soil Pollution, 26(1)*: 43-58. https://doi.org/10.1007/BF00299487

Charman, D. J. (2001). Biostratigraphic and palaeoenvironmental applications of testate amoebae. *Quaternary Science Reviews, 20*(16–17), 1753–1764. https://doi.org/10.1016/S0277-3791(01)00036-1

Charman, D. J., Blundell, A., Chiverrell, R. C., Hendon, D., Langdon, P. G. (2006). Compilation of non-annually resolved Holocene proxy climate records: Stacked Holocene peatland palaeo-water table reconstructions from northern Britain. *Quaternary Science Reviews*, *25(3-4),* 336-350. https://doi.org/10.1016/j.quascirev.2005.05.005

Creevy, A. L., Andersen, R., Rowson, J. G., Payne, R. J. (2018). Testate amoebae as functionally significant bioindicators in forest-to-bog restoration. *Ecological Indicators, 84,* 274-282. https://doi.org/10.1016/j.ecolind.2017.08.062

Daza Secco, E., Haimi, J., Högmander, H., Taskinen, S., Niku, J., Meissner, K. (2018). Testate amoebae community analysis as a tool to assess biological impacts of peatland use. *Wetlands Ecology and Management, 26,* 597-611. https://doi.org/10.1007/s11273-018-9594-y

De Cáceres, M., Legendre, P. (2009). Associations between species and groups of sites: Indices and statistical inference. *Ecology, 90*(12), 3566–3574. https://doi.org/10.1890/08-1823.1

Dirszowsky, R.W. (2020). Natural and human impacted landscapes of the Sudbury mining region. In: Slaymaker, O., Natto, N. (eds) Landscapes and Landforms of Eastern Canada, World Geomorphological Landscapes. Springer, Cham. https://doi.org/10.1007/978-3-030-35137-3_23

Dufrêne, M., Legendre, P. (1997). Species assemblages and indicator species: The need for a flexible asymmetrical approach. *Ecological Monographs, 67*(3), 345–366. https://doi.org/10.1890/0012-9615(1997)067[0345:SAAISTJ2.0.CO;2

Elliott, S. M., Roe, H. M., Patterson, R. T. (2012). Testate amoebae as indicators of hydroseral change: An 8500-year record from Mer Bleue Bog, eastern Ontario, Canada. *Quaternary International*, *268*, 128–144. https://doi.org/10.1016/j.quaint.2011.08.020

Environment Canada. (2025). Environment and Climate Change Canada Historical Climate Data. [Sudbury A, Climate ID 6068153] Retrieved from https://climate.weather.gc.ca/index_e.html

Fiałkiewicz-Kozieł, B., Smieja-Król, B., Ostrovnaya, T. M., Frontasyeva, M., Siemińska, A., Lamentowicz, M. (2015). Peatland microbial communities as indicators of the extreme atmospheric dust deposition. *Water, Air, and Soil Pollution, 226*(4), 97. https://doi.org/10.1007/s11270-015-2338-1

Fiałkiewicz-Kozieł, B., Łokas, E., Smieja-Król, B., Turner, S., De Vleeschouwer, F., Woszcyk, M., et al. (2023). The Śnieżka peatland as a candidate global boundary stratotype section and point for the Anthropocene series. *The Anthropocene Review*, *10*(1), 24–66. https://doi.org/10.1177/20530196221136425

Frietas, Y., Ramos, B., Silva, Y., Sampaio, G., Nascimento, L., Branco, C., Miranda, V. (2022). Testate amoebae: a review on their multiple uses as bioindicators. *Acta Protozoologica, 61,* 1-21. https://doi.org/10.4467/16890027AP.22.001.15671

Frolking, S., Roulet, N., Fuglestvedt, J. (2006). How northern peatlands influence the Earth's radiative budget: Sustained methane emission versus sustained carbon sequestration. *Journal of Geophysical Research: Biogeosciences, 111(G1)*. https://doi.org/10.1029/2005JG000091

Furukawa, A. K., Sutton, O. F., Simone, K. L., Verkaik, G. J., Moore, P. A., Clark, A., et al. (2025). Hydrological feedbacks in northern peatlands 2: Peat depth as a control on peatland resilience. *Ecohydrology, 18*(8). https://doi.org/10.1002/eco.70158

Garcés-Pastor, S., Fletcher, W., Ryan, P. (2023). Ecological impacts of the industrial revolution in a lowland raised peat bog near Manchester, NW England. *Ecology and Evolution*, *13*(2), e9807. https://doi.org/10.1002/ece3.9807

Gignac, L. D., Beckett, P. J. (1986). The effect of smelting operations on peatlands near Sudbury, Ontario, Canada. *Canadian Journal of Botany, 64(6)*, 1138-1147. https://doi.org/10.1139/b86-157

Gorham, E. (1991). Northern peatlands: Role in the carbon cycle and probable responses to climatic warming. *Ecological Applications, 1*(2), 182-195. https://doi.org/10.2307/1941811

Grimm, E. C. (1987). CONISS: A FORTRAN 77 program for stratigraphically constrained cluster analysis by the method of incremental sum of squares. *Computers and Geosciences, 13*(1), 13–35. https://doi.org/10.1016/0098-3004(87)90022-7

Gu, X., Tsyganov, A. N., Mazei, N. G., Babeshko, K. V., Chernyshiv, V. A., Novenko, E. Y, Mazei, Y. A. (2025). Testate amoebae as palaeohydrological indicators in the boreal and subarctic permafrost mires in the western part of the central Siberian Plateau. *Quaternary Science Reviews, 349.* https://doi.org/10.1016/j.quascirev.2024.109108

Gunn, J., (1995). Environmental restoration and recovery of an industrially-disturbed landscape. In: Gunn, J. M. (ed.) *Restoration and Recovery of an Industrial Region*. New York: Springer, pp. 1–15. Retrieved from; https://www.greatersudbury.ca/live/environment-and-sustainability1/regreening-program/pdf-documents/restoration-and-recovery-of-an-industrial-region-progress-in-restoring-the-smelter-damaged-landscape-near-sudbury-canada/

Gunn, J., Keller, W., Negusanti, J., Potvin, R., Beckett, P., Winterhalder, K. (1995). Ecosystem recovery after emission reductions: Sudbury, Ontario. *Water, Air, and Soil Pollution, 85(3)*, 1783-1788. https://doi.org/10.1007/BF00477238

Harris, L. I., Richardson, K., Bona, K. A., Davidson, S. J., Finkelstein, S. A., Garneau, M., et al. (2021). The essential carbon service provided by northern peatlands. *Frontiers in Ecology and the Environment, 20*(4), 222–230. https://doi.org/10.1002/fee.2437

Hutchinson, T. C. and Whitby, L. M., (1977). The effects of acid rainfall and heavy metal particulates on a boreal forest ecosystem near the Sudbury smelting region of Canada. *Water, Air, and Soil Pollution, 7(4)*: 421-438. https://doi.org/10.1007/BF00285542

Jassey, V. E. J., Chiapusio, G., Binet, P., Buttler, A., Laggoun-Défarge, F., Delarue, F., et al. (2013b). Above- and belowground linkages in *Sphagnum* peatland: Climate warming affects plant–microbial interactions. *Global Change Biology*, *19*(3), 811–823. https://doi.org/10.1111/gcb.12075

Juggins, S. (2019). *rioja: Analysis of Quaternary Science Data.* R package version 0.9-21. Available at: https://cran.r-project.org/package=rioja

Juggins, S. (2025). *riojaPlot: Stratigraphic diagrams in R.* R package version 0.1-24. Available at https://github.com/nsj3/riojaPlot

Keller, W., Heneberry, J. H., Gunn, J. M., (1998). Effects of emission reductions from the Sudbury smelters on the recovery of acid-and metal-damaged lakes. *Journal of Aquatic Ecosystem Stress and Recovery, 6*, 189-198. https://doi.org/10.1023/A:1009975116685

Kuuri-Riutta, O., Väliranta, M., Tuittila, E-S. (2022). Literature review on testate amoebae as environmental indicators as a functional part of the microbial community in northern peatlands. *Mires and Peat, 28(28).* https://doi.org/10.19189/MaP.2022.OMB.StA.2412

Lamentowicz, M., Mitchell, E. A. D. (2005). The ecology of testate amoebae (Protists) in *Sphagnum* in north-western Poland in relation to peatland ecology. *Microbial Ecology, 50*(1), 48–63. https://doi.org/10.1007/s00248-004-0105-8

Lamentowicz, M., Tobolski, K., Mitchell, E. A. D. (2007). Palaeoecological evidence for anthropogenic acidification of a kettle-hole peatland in northern Poland. *The Holocene*, *17*(8), 1185–1196. https://doi.org/10.1177/0959683607085123

Lamentowicz, M., Gałka, M., Milecka, K., Tobolski, K., Lamentowicz, Ł., Fiałkiewicz-Kozieł, B., Blaauw, M. (2013). A 1300-year multi-proxy, high-resolution record from a rich fen in northern Poland: Reconstructing hydrology, land-use and climate change. *Journal of Quaternary Science*, *28*(6), 582–594. https://doi.org/10.1002/jqs.2650

Lautenbach, W. E., Miller, J., Beckett, P. J., Negusanti, J. J., Winterhalder, K. (1995). Municipal land restoration program: The regreening process. In: Gunn, J. M. (ed.) *Restoration and recovery of an industrial region,* 109-122, New York, NY: Springer. https://doi.org/10.1007/978-1-4612-2520-1_8

Lazorek, M., Eyles, N., Eyles, C., Doughty, M., L'Heureux, E., Milkereit, B. (2006). Late Quaternary seismo-stratigraphy of Lake Wanapitei, Sudbury, Ontario, Canada: Arguments for a possible meteorite impact origin. *Sedimentary Geology, 192*(3-4), 231-242. https://doi.org/10.1016/j.sedgeo.2006.04.010

Levasseur, P. A., Aherne, J., Basiliko, N., Emilson, E. J. S., Preston, M. D., Sager, E. P. S., Watmough, S. A. (2023), Soil carbon pools and fluxes following the regreening of a mining and smelting degraded landscape. *Science of the Total Environment, 904*. https://doi.org/10.1016/j.scitotenv.2023.166734

Lund, M., Christensen, T. R., Lindroth, A., Schubert, P. (2012). Effects of drought conditions on the carbon dioxide dynamics in a temperate peatland. *Environmental Research Letters, 7.* https://doi.org/10.1088/1748-9326/7/4/045704

Marcisz, K., Jassey, V. E. J., Kosakyan, A., Krashevska, V., Lahr, D. J. G., Lara, E., et al. (2020). Testate amoeba functional traits and their use in paleoecology. *Frontiers in Ecology and Evolution*, *8,* 540. https://doi.org/10.3389/fevo.2020.57966

Mauquoy, P., Hughes, P. D. M., van Geel, B. (2010). A protocol for plant macrofossil analysis of peat deposits. *Mires and Peat, 7(06)*. https://doi.org/10.19189/001c.128413

McCarter, C.P.R., Tutt, E., Moore, P. A., Furukawa, A. K., Verkaik, G. J., Wilkinson, S. L., et al. (2024). Hydrophysical properties of peat in undisturbed and smelter-impacted peatlands: Implications for moss recovery, drought and wildfire. *Journal of Hydrological Processes, 38(12)*. https://doi.org/10.1002.hyp.70034

Milner, A. M., Baird, A. J., Green, S. M., Swindles, G. T., Young, D. M., Sanderson, N. K. et al. (2021). A regime shift from erosion to carbon accumulation in a temperate northern peatland. *Journal of Ecology, 109*(1), 125-138. https://doi.org/10.1111/1365-2745.13453

Mitchell, E. A. D., Charman, D. J., Warner, B. G. (2008). Testate amoebae analysis in ecological and paleoecological studies of wetlands: Past, present and future. *Biodiversity and Conservation, 17*(9), 2115–2137. https://doi.org/10.1007/s10531-007-9221-3

Nasser, N. A., Patterson, R. T., Roe, H. M., Galloway, J. M., Falck, H., Palmer, M. J., et al. (2016). Lacustrine arcellinina (testate amoebae) as bioindicators of arsenic contamination. *Microbial Ecology, 72*(1), 130-149. https://doi.org/10.1007/s00248-016-0752-6

Ndayishimiye, J. C., Nyirabuhoro, P., Xinyun, C., Saldaev, D., Mazei, Y., Gao, X. (2025). Determinants of testate amoeba community dynamics in urban waters: Effects of heatwave, air pollution, and hydrological gradient. *Water Research, 286.* https://doi.org/10.1016/j.watres.2025.124248

Newman, J. E., Levasseur, P. A., Beckett, P., Watmough, S. A. (2023). The impact of severe pollution from smelter emissions of carbon and metal accumulation in peatlands in Ontario, Canada. *Journal of Environmental Pollution, 320*. https://doi.org/10.1016/j.envpol.2023.121102

Nguyen-Viet, H., Bernard, N., Mitchell, E. A. D., Cortet, J., Badot, P-M., Gilbert, D. (2007). Relationship between testate amoeba (Protist) communities and atmospheric heavy metals accumulated in *Barbula indica* (Bryophyta) in Vietnam. *Microbial Ecology*, *53*(1), 53–65. https://doi.org/10.1007/s00248-006-9108-y

Nguyen-Viet, H., Bernard, N., Mitchell, E. A. D., Badot, P-M., Gilbert, D. (2008). Effect of lead pollution on testate amoebae communities living in *Sphagnum fallax*: An experimental study. *Ecotoxicology and Environmental Safet, 69*(1), 130–138. https://doi.org/10.1016/j.ecoenv.2007.02.007

Nolan, C., Tipton, J., Booth, R.K., Hooten, M.B., Jackson, S.T. (2019). Comparing and improving methods of reconstructing peatland water-table depth from testate amoebae. *The Holocene, 29*(8), 1350-1361. https://doi.org/10.1177/0959683619846969

Oksanen, J., Simpson, G. L., Blanchet, F. G., et al. (2022). *vegan: Community Ecology Package*. R package version 2.6-4. Available at: https://CRAN.R-project.org/package=vegan

Ontario Ministry of Natural Resources. (2021). Forest Regions of Ontario. Toronto: Queen's Printer for Ontario. Retrieved from https://www.ontario.ca/page/forest-regions

Ontario Ministry of Natural Resources and Forestry. (2025). Ontario Geohub – Wetland. Toronto: Queen's Printer for Ontario. Retrieved from https://geohub.lio.gov.on.ca/datasets/5216a770ef684d2fae8bcc13ee9c4357_15/about \

Pamer, L. J. (2008). Characterization of anthropogenic pollution in *Sphagnum* peat from the Sudbury region: Sudbury region peatlands as archives of atmospheric base metal deposition. (Master's Thesis) Sudbury, ON: Laurentian University. Retrieved from https://central.bac-lac.gc.ca/.item?id=MR44859&op=pdf&app=Library&is_thesis=1&oclc_number=694268382

Parmar, T. K., Rawtani, D., Agrawal, Y. K. (2016). Bioindicators: the natural indicator of environmental pollution. *Frontiers in Life Science, 9*(2), 110-118. https://doi.org/10.1080/21553769.2016.1162753

Patterson, R. T., Barker, T., Burbidge, S. M. (1996). Arcellaceans (Thecamoebians) as proxies of arsenic and mercury contamination in northeastern Ontario lakes. *Journal of Foraminiferal Research, 26*(2), 172–183. https://doi.org/10.2113/gsjfr.26.2.172

Payne, R. J., Mitchell, E. A. D. (2009). How many is enough? Determining optimal count totals for ecological and palaeoecological studies of testate amoebae. *Journal of Paleolimnology* 42(4): 483–495. https://doi.org/10.1007/s10933-008-9299-y

Payne, R., Gauci, V., Charman, D. J. (2010). The impact of simulated sulfate deposition on peatland Testate Amoebae. *Microbial Ecology, 59*(1). 76-83. https://doi.org/10.1007/s00248-009-9552-6

Payne, R. J., Mitchell, E. A. D., Nguyen-Viet, H., Gilbert, D. (2012). Can pollution bias peatland paleoclimate reconstruction? *Quaternary Research, 78*(2), 170-173. https://doi.org/10.1016/j.yqres.2012.05.004

Potvin, R. R., Negusanti, J. J., (1995). Declining Industrial Emissions, Improving Air Quality, and Reduced Damage to Vegetation. In: J. M. Gunn (Editor), Restoration and Recovery of an Industrial Region: Progress in Restoring the Smelter-Damaged Landscape Near Sudbury, Canada. Springer New York, New York, NY, pp. 51-65.

Potvin, R. (2007). *Air quality trends in the Sudbury Area 1953 – 2002.* Paper presented at Mining and the Environment Conference*,* Sudbury, ON. Retrieved from https://pdf.library.laurentian.ca/medb/conf/Sudbury07/Potvin.pdf

Qiu, C., Zhu, D., Ciais, P., Guenet, B., Peng, S. (2020). The role of northern peatlands in the global carbon cycle for the 21st century. *Global Ecology and Biogeography, 29(5)*, 956-973. https://doi.org/10.1111/geb.13081

R Core Team (2024). *R: A Language and Environment for Statistical Computing.* Vienna: R Foundation for Statistical Computing. Available at: https://www.R-project.org/

Reinhardt, E. G., Dalby, A. P., Kumar, A., Patterson, R. T. (1998). Arcellaceans as pollution indicators in mine tailing contaminated lakes near Cobalt, Ontario, Canada. *Micropaleontology*, *44*(2), 131–148. https://doi.org/10.2307/1486066

Renaud, A., Mügler, C., Durand, V., Pessel, M. (2025). Natural and anthropogenic drivers of the water table dynamics in a riparian fen peatland. *Journal of Hydrology, 652.* https://doi.org/10.1016/j.hydrol.2024.132655

Rowe, J. S. (1972). *Forest regions of Canada.* Canadian Forestry Service Publication No. 1300. Ottawa, ON: Department of the Environment, Canadian Forestry Service. Retrieved from https://publications.gc.ca/collections/collection_2019/eccc/Fo47-1300-eng.pd

Rydin, H., Jeglum, J. (2013). The Biology of Peatlands, 2nd edn. Oxford: Oxford University Press. Retrieved from; https://www.researchgate.net/publication/264545254_The_biology_of_peatlands_second_edition

Saarinen, O. W. (2013). *From meteorite impact to constellation city: A historical geography of Greater Sudbury.* Waterloo, ON: Wilfrid Laurier University Press

Schweingruber, F. H., Kučerová, A., Adamec, L., and Doležal, J. (2020). *Anatomic atlas of aquatic and wetland plant stems.* Springer Nature. https://doi.org/10.1007/978-3-030-33420-8

Seward, J., Bräuer, S., Beckett, P., Roy-Léveillée, P., Emilson, E., Watmough, S., Basiliko, N. (2023). Recovery of smelter-impacted peat and *Sphagnum* moss: A microbial perspective. *Microbial Ecology, 86*(4), 2894-2903. https://10.1007/s00248-023-02289-5

Seward, J. D. (2023). Recovery of smelter-impacted peatlands (Sudbury, Ontario): Botanical and microbial community perspectives. (Doctoral Thesis) Sudbury, ON: Laurentian University. Retrieved from https://laurentian.scholaris.ca/server/api/core/bitstreams/b9ab4fd4-b9a4-4922-9fd4-4a1f1ea4987a/content

Sherman, G., Beckett, P. (2003). *Carbon sequestration patterns in the replanted areas of the Sudbury barrens.* Paper presented at Sudbury Mining and the Environment International Conference, Sudbury, ON. Retrieved from https://pdf.library.laurentian.ca/medb/conf/Sudbury03/SmelterLandscape/139.pdf

Sickles II, J. E., Shadwick, D. S., (2015). Air quality and atmospheric deposition in the eastern US: 20 years of change. *Atmospheric Chemistry and Physics, 15*(1): 173-197. https://doi.org/10.5194/acp-15-173-2015

Swindles, G. T., Green, S. M., Brown, L., Holden, J., Raby, C. L., Turner, T. E., et al. (2016). Evaluating the use of dominant microbial consumers (testate amoebae) as indicators of blanket peatland restoration. *Ecological Indicators, 69,* 318-330. https://doi.org/10.1016/j.ecolind.2016.04.038

Szkokan-Emilson, E. J., Kielstra, B., Watmough, S., Gunn, J. (2013). Drought-induced release of metals from peatlands in watersheds recovering from historical metal and sulphur deposition. *Biogeochemistry, 116*, 131-145. https://doi.org/10.1007/210533-013-9919-0

Turetsky, M. R., St. Louis, V. (2006). Disturbance in boreal peatlands. In: Wieder RK and Vitt DH (eds) *Boreal Peatland Ecosystems*. Ecological Studies 188. Berlin: Springer, pp. 359–379. https://doi.org/10.1007/978-3-540-31913-9_16

Turetsky, M. R., Benscoter, B. W., Page, S., Rein, G. (2014). Global vulnerability of peatlands to fire and carbon loss. *Nature Geoscience, 8*, 11–14. https://doi.org/10.1038/ngeo2325

Vitt, D. H., Wieder, R. K., Scott, K. D., Faller, S. (2009). Decomposition and peat accumulation in rich fens of boreal Alberta, Canada. *Ecosystems, 12*, 360-373. https://doi.org/10.1007/s10021-009-9228-6

Waddington, J. M., Morris, P. J., Kettridge, N., Granath, G., Thompson, D. K., Moore, P. A. (2014). Hydrological feedbacks in northern peatlands. *Ecohydrology, 8*(1), 113-127. https://doi.org/10.1002/eco.1493

Walker, D., Walker, P. M. (1961). Stratigraphic evidence of regeneration in some Irish bogs. *Journal of Ecology, 49(1)*, 169-185. https://doi.org/10.2307/2257432

Wanner, M., Birkhofer, K., Fischer, T., Shimizu, M., Shimano, S., Puppe, D. (2020). Soil testate amoebae and diatoms as bioindicators of an old heavy metal contaminated floodplain in Japan. *Microbial Ecology*, *79*(1), 123–133. https://doi.org/10.1007/s00248-019-01383-x

Watkinson, A., Juckers, M., D'Andrea, L., Beckett, P., Spiers, G. (2022). Ecosystem recovery of the Sudbury Technogenic Barrens 30 years post-restoration. *Eurasian Soil Science, 55*(5), 663-672. https://doi.org/10.1134/s106422932205012X

Weltzin, J. F., Bridgham, S. D., Pastor, J., Chen, J., Harth, C. (2003). Potential effects of warming and drying on peatland plant community. *Global Change Biology, 9*(2), 141-151. https://doi.org/10.1046/j.1365-2486.2003.00571.x

Wilkinson, D. M., Mitchell, E. A. D. (2010). Testate amoebae and nutrient cycling with particular reference to soils. *Geomicrobiology Journal, 27*(6-7), 520-533. https://doi.org/10.1080/01490451003702925

Xu, J., Morris, P. J., Liu, J., Holden, J. (2018). PEATMAP: Refining estimates of global peatland distribution based on a meta-analysis. *CATENA, 160,* 134-140. https://doi.org/10.1016/j.catena.2017.09.010

Yu, Z., Loisel, J., Brosseau, D. P., Beilman, D. W., Hunt, S. J. (2010). Global peatland dynamics since the Last Glacial Maximum. *Geophysical Research Letters, 37(13)*. https://doi.org/10.1029/2010GL043584

Yu, Z., Beilman, D. W., Frolking, S., MacDonald, G. M., Roulet, N. T., Camill, P., Charman, D. J. (2011). Peatlands and their role in the global carbon cycle. *Eos, Transactions American Geophysical Union, 92(12)*, 97-98. https://doi.org/10.1029/2011EO120001

Zhao, B., Zhuang, Q. (2023). Peatlands and their carbon dynamics in northern high latitudes from 1990 to 2300: A process-based biogeochemistry model analysis. *Biogeosciences, 20(1)*, 251-270. https://doi.org/10.5194/bg-20-251-2023

Appendices

Appendix 1 Chrono-Biostratigraphy Supplementary Table

Core	Depth Interval (cm)	Age Interval (cal yr BP)	Peat Composition
Laurentian	0 - 13	(-75) - 90	Ericaceae-Poales peat
	13 - 33	90 - 550	Ericaceae-Poales-*Sphagnum* peat
	33 - 39	550 - 890	Ericaceae-Poales peat
	39 - 43	890 - 1100	Ericaceae-Poales-*Sphagnum* peat
	43 - 60	1100 - 2360	Ericaceae-Poales peat
	60 - 100	2360 - 7500	Poales-Carr peat
	100 - 121	7500 - 8520	Herbaceous peat
	121 - 131	8520 - 8660	Poales-Carr peat
	131 - 151	8660 - 9000	Ligneous peat
	151 - 162	9000 - 9270	*Sphagnum*-Poales-Carr peat
	162 - 171	9270 - 9560	*Sphagnum* peat
	171 - 184	9560 - 9940	*Sphagnum*-Poales peat
	184 - 223	9940 - 11104	Poales-Bryidae peat
	223 - 304	11104 - >11240	Gyttja
Transplant	0 - 5	(-76) – 5	Ericaceae-Poales-Marchantiophyta peat
	5 - 12	5 - 120	Ericaceae-Poales peat
	12 - 24	120 - 520	Ericaceae-Poales-*Sphagnum* peat
	24 - 34	520 - 1600	Poales-Carr peat
	34 - 50	1600 - 3700	Ericaceae-Poales peat
	50 - 63	3700 - 5390	Herbaceous-Ligneous peat
	63 - 73	5390 - 6120	Poales-Bryidae peat
	73 - 96	6120 - 7590	Herbaceous-Ligneous peat
	96 - 105	7590 - 8260	Ericaceae-Poales-*Sphagnum* peat
	105 - 155	8260 - 9110	*Sphagnum*-Poales peat
	155 - 165	9110 - 9250	*Sphagnum*-Poales-Carr peat
	165 - 176	9250 - 9390	Poales-Bryidae-*Sphagnum* peat
	176 - 187	9390 - 9520	Poales-Bryidae peat
	187 – 196	9520 – 9720	Poales-Bryidae-*Sphagnum* peat
	196 – 215	9720 – 11150	Bryidae-Ligneous-*Sphagnum* peat
	215 - 246	>11150	Gyttja
Cartier	0 - 26	(-77) – 160	*Sphagnum* peat
	26 - 36	160 - 230	*Sphagnum*-Poales peat
	36 -61	230 - 1710	Herbaceous peat
	61 – 116	1710 - 4900	Herbaceous-Bryidae peat
	116 – 146	4900 - 5770	Ericaceae-Poales-*Sphagnum* peat
	146 – 172	5770 - 6370	Poales-Bryidae peat
	172 – 226	6370 - 7170	Poales-Bryidae-*Sphagnum* peat
	226 – 246	7170 - 7420	Poales-Bryidae peat
	246 – 255	7420 - 7520	Poales-Carr peat
	255 – 276	7520 - 8140	Poales-Bryidae-*Sphagnum* peat
	276 – 288	8140 - 8500	Gyttja
	288 – 295	8500 - 8720	*Sphagnum*-Poales peat
	295 – 318	8720 - 9425	Poales-Bryidae-*Sphagnum* peat
	318 – 439	9425 - >10830	Gyttja

Appendix Table 1 *Chrono-biostratigraphy supplementary data for the total cores of each site (Laurentian, Transplant, Cartier N) including depth intervals (cm), age intervals (cal yr BP), and peat composition.*

Appendix 2 AMS Radiocarbon Age Data

Cartier AMS Radiocarbon Age Data

Depth (cm)	Min Age (cal yr BP)	Max Age (cal yr BP)	Median Age (cal yr BP)	Mean Age (cal yr BP)	Depth (cm)	Min Age (cal yr BP)	Max Age (cal yr BP)	Median Age (cal yr BP)	Mean Age (cal yr BP)
0	-108	-49	-77	-78	**50**	359	1788	850	927
1	-99	-20	-68	-66	**51**	461	1855	928	1007
2	-95	18	-59	-54	**52**	528	1915	1013	1087
3	-92	61	-50	-42	**53**	594	1979	1113	1167
4	-89	103	-43	-30	**54**	648	2069	1205	1248
5	-87	148	-35	-17	**55**	698	2170	1289	1328
6	-80	154	-24	-7	**56**	795	2211	1365	1398
7	-75	173	-15	3	**57**	870	2235	1438	1467
8	-71	195	-5	13	**58**	924	2268	1499	1537
9	-69	225	6	23	**59**	971	2311	1573	1607
10	-66	258	15	33	**60**	1006	2373	1639	1676
11	-56	301	25	46	**61**	1158	2398	1714	1755
12	-49	350	35	60	**62**	1280	2430	1803	1833
13	-45	411	44	73	**63**	1373	2469	1892	1912
14	-42	473	53	86	**64**	1416	2513	1985	1991
15	-38	524	61	99	**65**	1467	2583	2087	2069
16	-29	552	71	112	**66**	1592	2606	2149	2130
17	-20	585	80	124	**67**	1703	2634	2204	2191
18	-16	624	89	136	**68**	1783	2672	2265	2252
19	-12	667	99	148	**69**	1845	2721	2331	2312
20	-7	709	109	160	**70**	1887	2789	2385	2373
21	1	730	118	173	**71**	2049	2807	2451	2447
22	8	747	127	185	**72**	2208	2821	2516	2522
23	16	764	137	197	**73**	2358	2840	2590	2596
24	21	782	148	209	**74**	2464	2864	2673	2670
25	25	809	158	221	**75**	2522	2916	2753	2744
26	34	827	163	232	**76**	2635	2931	2800	2796
27	44	841	171	243	**77**	2736	2950	2849	2848
28	48	856	177	254	**78**	2801	2991	2900	2900
29	53	881	184	265	**79**	2842	3067	2950	2952
30	59	906	191	276	**80**	2864	3177	2998	3004
31	71	925	199	289	**81**	2907	3213	3048	3052
32	82	945	205	302	**82**	2936	3289	3098	3101
33	93	974	212	315	**83**	2956	3381	3145	3149
34	97	1003	218	328	**84**	2974	3496	3188	3198
35	105	1042	227	341	**85**	2988	3616	3231	3246
36	116	1072	232	353	**86**	3026	3673	3275	3294
37	125	1092	237	365	**87**	3049	3755	3322	3342
38	133	1117	242	377	**88**	3070	3835	3368	3390
39	141	1152	248	389	**89**	3084	3929	3407	3438
40	146	1187	254	400	**90**	3098	4027	3449	3486
41	177	1210	261	417	**91**	3151	4066	3504	3539
42	203	1259	268	434	**92**	3183	4110	3569	3591
43	220	1282	279	451	**93**	3204	4180	3629	3644
44	228	1344	296	468	**94**	3222	4262	3678	3696
45	233	1388	318	485	**95**	3244	4335	3726	3749
46	280	1433	453	573	**96**	3299	4366	3770	3794
47	300	1499	551	662	**97**	3339	4414	3820	3839
48	321	1579	647	750	**98**	3377	4457	3864	3883

49	339	1666	749	838	**99**	3406	4511	3915	3928
					100	3434	4564	3965	3973

Appendix Table 2 *AMS radiocarbon age data for Cartier, including depth (cm), minimum age (cal yr BP), maximum age (cal yr BP), median age (cal yr BP), and mean age (cal yr BP).*

Laurentian AMS Radiocarbon Age Data

Depth (cm)	Min Age (cal yr BP)	Max Age (cal yr BP)	Median Age (cal yr BP)	Mean Age (cal yr BP)	Depth (cm)	Min Age (cal yr BP)	Max Age (cal yr BP)	Median Age (cal yr BP)	Mean Age (cal yr BP)
0	-104	-49	-75	-76	**50**	791	2854	1626	1679
1	-94	-26	-61	-60	**51**	813	2975	1699	1759
2	-88	9	-48	-45	**52**	833	3125	1777	1838
3	-84	47	-35	-29	**53**	845	3279	1857	1918
4	-80	87	-23	-14	**54**	858	3432	1940	1997
5	-77	128	-10	2	**55**	872	3619	2026	2077
6	-67	134	2	13	**56**	904	3703	2098	2142
7	-59	144	15	25	**57**	930	3785	2168	2207
8	-54	157	29	36	**58**	950	3868	2231	2271
9	-49	171	42	48	**59**	965	3965	2303	2336
10	-45	189	54	59	**60**	981	4072	2363	2401
11	-32	195	65	72	**61**	1044	4168	2519	2530
12	-19	205	77	85	**62**	1100	4310	2657	2660
13	-13	212	89	97	**63**	1144	4466	2791	2789
14	-6	225	100	110	**64**	1191	4677	2933	2918
15	-1	243	110	122	**65**	1239	4983	3060	3047
16	19	247	117	133	**66**	1465	5034	3206	3207
17	32	251	123	145	**67**	1664	5095	3356	3367
18	41	255	129	156	**68**	1817	5201	3500	3526
19	49	262	138	167	**69**	1958	5313	3656	3686
20	57	275	151	178	**70**	2033	5444	3820	3846
21	93	279	175	195	**71**	2316	5522	3978	3990
22	125	286	203	212	**72**	2530	5625	4141	4134
23	144	295	223	228	**73**	2755	5707	4324	4278
24	152	323	257	245	**74**	2898	5828	4497	4422
25	160	367	276	262	**75**	3017	5947	4671	4566
26	194	392	305	296	**76**	3304	5982	4843	4729
27	210	431	334	329	**77**	3480	6028	5008	4892
28	223	476	368	363	**78**	3612	6088	5177	5055
29	233	527	401	397	**79**	3746	6167	5365	5218
30	241	586	435	431	**80**	3889	6299	5541	5381
31	325	595	471	469	**81**	4391	6338	5704	5581
32	397	606	508	508	**82**	4881	6374	5862	5781
33	463	620	547	546	**83**	5350	6414	6022	5981
34	506	646	592	584	**84**	5823	6466	6195	6181
35	530	715	627	623	**85**	6082	6585	6403	6381
36	571	865	683	691	**86**	6315	6620	6481	6478
37	589	1071	727	758	**87**	6405	6782	6565	6575
38	600	1281	770	826	**88**	6431	7050	6639	6672
39	609	1494	816	894	**89**	6455	7338	6699	6769
40	619	1710	864	961	**90**	6473	7623	6765	6866
41	647	1776	943	1033	**91**	6532	7659	6849	6930
42	669	1873	1024	1106	**92**	6557	7707	6935	6994
43	689	2030	1102	1178	**93**	6578	7759	7018	7057
44	705	2210	1173	1250	**94**	6599	7816	7099	7121

45	719	2423	1243	1323	**95**	6621	7906	7174	7185
46	744	2498	1315	1394	**96**	6685	7932	7231	7244
47	762	2547	1397	1465	**97**	6730	7957	7293	7303
48	771	2613	1472	1536	**98**	6772	7980	7360	7362
49	784	2724	1545	1608	**99**	6810	8017	7430	7421
					100	6835	8055	7496	7480

Appendix Table 3 *AMS radiocarbon age data for Laurentian, including depth (cm), minimum age (cal yr BP), maximum age (cal yr BP), median age (cal yr BP), and mean age (cal yr BP).*

Transplant AMS Radiocarbon Age Data

Depth (cm)	Min Age (cal yr BP)	Max Age (cal yr BP)	Median Age (cal yr BP)	Mean Age (cal yr BP)	Depth (cm)	Min Age (cal yr BP)	Max Age (cal yr BP)	Median Age (cal yr BP)	Mean Age (cal yr BP)
0	-105	-49	-76	-76	**50**	2912	4428	3702	3691
1	-89	-28	-59	-59	**51**	2983	4490	3830	3804
2	-83	-1	-43	-42	**52**	3051	4633	3962	3918
3	-76	29	-27	-26	**53**	3117	4816	4091	4032
4	-71	62	-11	-9	**54**	3178	5056	4206	4145
5	-68	96	5	8	**55**	3221	5266	4301	4259
6	-43	109	18	23	**56**	3563	5291	4426	4408
7	-23	129	32	38	**57**	3768	5314	4560	4558
8	-6	162	48	54	**58**	3957	5361	4719	4707
9	8	196	62	69	**59**	4083	5435	4922	4857
10	18	230	76	84	**60**	4158	5549	5099	5006
11	37	235	97	103	**61**	4434	5572	5195	5123
12	47	240	119	121	**62**	4704	5594	5290	5240
13	53	245	151	140	**63**	4972	5632	5387	5357
14	58	251	178	158	**64**	5215	5690	5485	5474
15	63	265	202	177	**65**	5409	5770	5598	5591
16	100	292	230	208	**66**	5563	5833	5670	5669
17	115	330	252	239	**67**	5624	5923	5739	5747
18	127	371	281	270	**68**	5645	6081	5806	5825
19	135	419	311	301	**69**	5662	6265	5870	5903
20	145	476	338	332	**70**	5675	6438	5940	5981
21	251	482	382	378	**71**	5720	6488	6001	6037
22	328	492	430	425	**72**	5748	6561	6065	6094
23	350	511	480	471	**73**	5769	6678	6121	6151
24	380	601	519	517	**74**	5787	6779	6185	6208
25	406	709	558	563	**75**	5797	6906	6240	6264
26	506	774	645	643	**76**	5848	6942	6302	6320
27	534	911	727	724	**77**	5891	6980	6362	6376
28	551	1065	795	804	**78**	5914	7061	6410	6432
29	577	1225	868	884	**79**	5940	7166	6468	6488
30	595	1386	944	965	**80**	5961	7310	6521	6543
31	865	1417	1110	1122	**81**	6012	7341	6578	6601
32	1124	1448	1279	1280	**82**	6044	7381	6642	6659
33	1303	1522	1439	1437	**83**	6076	7441	6703	6716
34	1399	1755	1600	1595	**84**	6114	7507	6763	6774
35	1449	2017	1764	1752	**85**	6137	7572	6817	6832
36	1576	2092	1861	1855	**86**	6171	7625	6877	6889
37	1683	2189	1962	1958	**87**	6219	7677	6951	6946
38	1772	2304	2062	2061	**88**	6247	7744	7015	7004
39	1866	2446	2171	2164	**89**	6274	7806	7083	7061
40	1956	2588	2270	2266	**90**	6309	7889	7142	7118

41	2225	2663	2419	2435	**91**	6481	7914	7207	7196
42	2388	2895	2593	2605	**92**	6585	7950	7277	7273
43	2445	3162	2763	2774	**93**	6657	7997	7356	7350
44	2485	3461	2933	2943	**94**	6714	8064	7440	7428
45	2509	3777	3105	3112	**95**	6772	8164	7511	7505
46	2632	3821	3234	3228	**96**	6885	8187	7590	7577
47	2709	3900	3370	3343	**97**	6958	8224	7673	7648
48	2780	4042	3493	3459	**98**	7004	8255	7763	7720
49	2849	4218	3594	3575	**99**	7053	8303	7838	7791
					100	7088	8381	7922	7863

Appendix Table 4 *AMS radiocarbon age data for Transplant, including depth (cm), minimum age (cal yr BP), maximum age (cal yr BP), median age (cal yr BP), and mean age (cal yr BP).*

Appendix 3 Systematic Taxonomy of all Identified Testate Amoebae Taxa

Acronym	Taxa / Complex Name	Species Included in Complex	Wetness Affinity
ALA MIL	*Alabasta militaris* (Penard, 1890)	Synonym: *Nebela militaris*	Dry (Marcisz et al., 2020; Duckert et al., 2018)
ARC CAT	*Arcella catinus* (Penard, 1890)	Synonym: *Galeripora catinus* *Arcella arenaria* type	Intermediate (Charman et al., 2000)
ARC DIS	*Arcella discoides* type (Ehrenberg, 1843)	Synonym: *Galeripora discoides* *Arcella megastoma* *Arcella polypora*	Wet (Swindles et al., 2016; Smith et al., 2007; Lamentowicz et al., 2009)
ARC HEM	*Arcella hemispherica* type (Perty, 1852)	Synonym; *Arcella hemisphaerica* *Arcella rotundata*	Wet (Charman et al., 2000)
ARC SPP	*Arcella spp.*		Wet (Charman et al., 2000)
ARC VUL	*Arcella vulgaris* (Ehrenberg, 1830)	*Arcella crenulata*	Wet (Charman et al., 2000)
ARC FLA	*Archerella flavum (*Archer, 1877)	Synonym: *Amphitrema flavum*	Wet (Marcisz et al., 2020; Swindles et al., 2016; Diaconu et al., 2017; Amesbury et al., 2013)
ASS MUS	*Assulina muscorum* (Greeff, 1888)		Dry (Marcisz et al., 2020; Booth et al., 2025; Gu et al., 2025; Lamentowicz & Mitchell, 2005).
ASS SEM	*Assulina seminulum* type (Ehrenberg, 1848)	*Assulina scandinavica*	Dry (Marcisz et al., 2020)
BUL IND	*Bullinularia indica* (Penard, 1907)		Dry (Booth et al., 2025; Gu et al., 2025)
CEN ACU	*Centropyxis aculeata* type (Ehrenberg, 1838)	*Centropyxis spinosa*	Intermediate (Evans et al., 2025)
CEN CAS	*Centropyxis cassis* type (Wallich, 1864)	*Centropyxis aerophila* type *Centropyxis constricta* type	Wet (Charman et al., 2000)
CEN ECO	*Centropyxis ecornis* type (Ehrenberg, 1841)	*Centropyxis cordobensis* *Centropyxis delicatula* type *Centropyxis laevigata* type	Intermediate (Charman et al., 2000)
CEN PLA	*Centropyxis platystoma* type (Penard, 1890)		Wet (Charman et al., 2000)
CEN SPP	*Centropyxis spp.*		Wet (Charman et al., 2000)
COR TRI	*Corythion-Trinema* type (Hoogenraad & De Groot, 1940)	*Trinema complanatum* *Trinema enchelys* *Trinema grandis* *Trinema lineare* *Trinema penardi* *Corythion asperulum* *Corythion constricta* *Corythion dubium* *Corythion delamerei*	Intermediate (Booth et al., 2025; Gu et al., 2025; Charman et al., 2000))

CYC ARC	*Cyclopyxis arcelloides* type (Penard, 1902)	*Cyclopyxis kahli*	Intermediate (Kuuri-Riutta et al., 2022; Charman et al., 2000)
CYC EUR	*Cyclopyxis eurystoma* (Deflandre, 1929)		Wet (Kuuri-Riutta et al., 2022; Charman et al., 2000)
DIF GLO	*Difflugia globulosa* type (Dujardin, 1837)		Wet (Kuuri-Riutta et al., 2022; Booth et al., 2025; Gu et al., 2025)
DIF KEM	*Difflugia kempnyi* (Stepanek, 1953)		Wet (Booth et al., 2025; Gu et al., 2025)
DIF LEI	*Difflugia leidyi* (Wailes, 1913)		Wet (Booth et al., 2025; Gu et al., 2025; Lamentowicz & Mitchell, 2005).
DIF OBL	*Difflugia oblonga* type (Ehrenberg, 1838)	*Difflugia lanceolata* *Difflugia yorkui* *Difflugia bacillifera* *Difflugia bryophila* *Difflugia lascustris*	Wet (Booth et al., 2025; Gu et al., 2025)
DIF PUL	*Difflugia pulex* (Penard, 1890)		Wet (Booth et al., 2025; Gu et al., 2025; Amesbury et al., 2013)
DIF SPP	*Difflugia spp.*		Wet (Booth et al., 2025; Gu et al., 2025)
EUG ROT	*Euglypha rotunda* (Ehrenberg, 1845)	*Euglypha rontunda* *Euglypha laevis*	Dry (Kuuri-Riutta et al., 2022; Lamentowicz & Mitchell, 2005)
EUG STR	*Euglypha strigosa* type (Ehrenberg, 1848)		Dry (Kuuri-Riutta et al., 2022)
EUG TUB	*Euglypha tuberculata* type (Dujardin, 1841)		Dry (Kuuri-Riutta et al., 2022; Liu et al., 2024)
HEL PET	*Heleopera petricola* (Leidy, 1879)		Wet (Charman et al., 2000)
HEL ROS	*Heleopera rosea* (Penard, 1890)		Wet (Charman et al., 2000)
HEL SPH	*Heleopera sphagni* (Leidy, 1874)	Synonym: *Heleopera picta*	Wet (Charman et al., 2000)
HEL SYL	*Heleopera sylvatica* (Penard, 1890)		Dry (Lamentowicz & Mitchell, 2005)
HYA ELE	*Hyalosphenia elegans* (Leidy, 1874)		Wet (Booth et al., 2025; Marcisz et al., 2020)
HYA MIN	*Hyalosphenia minuta* (Cash, 1892)		Dry (Charman et al., 2000; Beaulne et al., 2018)
HYA PAP	*Hyalosphenia papilio* (Leidy, 1874)		Wet (Marcisz et al., 2020; Diaconu et al., 2017)
HYA SUB	*Hyalosphenia subflava* (Cash & Hopkinson, 1909)		Intermediate (Swindles et al., 2018)
NEB TIN	*Nebela tincta* type (Leidy, 1879)	*Nebela collaris* *Nebela bohemica* *Hyalosphenia ovalis* *Nebela parvula*	Intermediate (Marcisz et al., 2020; Booth et al., 2025; Gu et al., 2025; Lamentowicz & Mitchell, 2005)
PAD LAG	*Padaungiella lageniformis* (Penard, 1890)	Synonym: *Nebela lageniformis*	Wet (Charman et al., 2000)
PAD WAI	*Padaungiella wailesi* type (Deflandre, 1936)	Synonym: *Nebela wailesi*	Wet (Charman et al., 2000)
PHR ACR	*Phryganella acropodia* type (Hertwig & Lesser, 1874)		Dry (Kuuri-Riutta et al., 2022; Diaconu et al., 2017)
PHY GRI	*Physochila griseola* (Wailes & Penard, 1911)		Wet (Koenig et al., 2018)
PSE FUL	*Pseudodifflugia fulva* type (Archer, 1870)		Wet (Booth et al., 2025; Gu et al., 2025)
TRA DEN	*Tracheleuglypha dentata* (Deflandre, 1928)		Wet (Kroupalova et al., 2013)
TRI ARC	*Trigonopyxis arcula* type (Penard, 1912)	*Trigonopyxis minuta* type	Dry (Booth et al., 2025; Gu et al., 2025)

Appendix Table 5 *Systematic taxonomy of all identified testate amoebae tax, including acronym, taxa/complex name, all species included in the complex and/or taxa synonyms, and wetness affinities.*

Appendix 4 ICP-OES Geochemical Assays

Cartier ICP-OES Geochemical Assay

Sample	Depth	Al	As	Ba	Be	B	Cd	Ca	Cr	Co	Cu	Fe	Pb	Mg	Mn	Mo	Ni	P	K	Se	Si	Na	Sr	S	Tl	Ti	V	Zn
	cm	*µg/g*	*µg/g*	*µg/g*	*µg/g*	*µg/g*	*µg/g*	*µg/g*	*µg/g*	*µg/g*	*µg/g*	*µg/g*	*µg/g*	*µg/g*	*µg/g*	*µg/g*	*µg/g*	*µg/g*	*µg/g*	*µg/g*	*µg/g*	*µg/g*	*µg/g*	*µg/g*	*µg/g*	*µg/g*	*µg/g*	*µg/g*
CART-C-2	2	226.0	< 1.5	23.8	< 0.2	< 0.5	0.5	2766.2	0.9	< 0.50	7.2	416.6	2.9	736.2	162.6	< 5.0	4.7	410.0	3534.3	2.7	59.0	369.9	5.9	666.3	< 5.0	6.3	< 0.8	29.7
CART-C-3	3	311.4	1.6	26.7	< 0.2	< 0.5	1.3	3166.3	1.8	< 0.50	7.2	464.8	2.4	787.8	197.4	< 5.0	5.6	397.5	2784.0	2.6	112.0	293.3	6.4	620.6	< 5.0	8.4	< 0.8	45.1
CART-C-4	4	670.6	< 1.5	16.7	< 0.2	< 0.5	3.3	3505.0	2.6	0.9	9.5	803.0	3.5	847.7	54.6	< 5.0	7.3	338.4	1413.6	< 2.0	28.8	169.8	7.0	568.9	< 5.0	13.4	1.2	59.2
CART-C-6	6	5138.6	2.4	15.9	< 0.2	< 0.5	1.6	1246.5	48.3	4.6	34.4	10621.7	4.8	2455.7	79.8	< 5.0	20.8	407.8	427.0	< 2.0	236.0	149.2	6.3	678.0	< 5.0	348.7	22.1	17.3
CART-C-7	7	2074.9	2.1	16.0	< 0.2	< 0.5	8.6	4647.8	8.6	2.1	23.1	3335.8	3.5	1134.8	48.9	< 5.0	11.9	397.2	869.0	< 2.0	238.2	142.6	6.4	851.9	< 5.0	71.2	5.2	25.1
CART-C-8	8	758.5	1.9	27.0	< 0.2	< 0.5	9.4	3174.2	1.4	1.8	20.5	1410.5	2.5	1020.7	72.6	< 5.0	12.5	333.8	790.9	2.0	165.1	170.5	8.6	872.4	< 5.0	18.7	1.8	31.1
CART-C-10	10	322.7	< 1.5	18.0	< 0.2	< 0.5	4.8	1507.3	1.7	1.0	13.9	902.9	2.0	668.0	32.8	< 5.0	9.1	306.2	776.0	2.5	161.5	136.8	6.3	880.3	< 5.0	9.6	0.9	24.6
CART-C-11	11	389.8	1.6	18.7	< 0.2	< 0.5	4.6	4237.0	1.2	1.4	26.4	1362.0	3.0	1056.2	25.4	< 5.0	13.2	299.8	655.9	2.1	108.6	187.2	11.0	826.5	< 5.0	8.8	< 0.8	31.3
CART-C-12	12	330.1	2.2	15.2	< 0.2	< 0.5	7.2	4112.9	1.1	1.4	29.5	1508.0	4.2	1077.6	29.0	< 5.0	11.7	310.5	829.4	2.4	88.6	210.5	10.3	782.6	< 5.0	7.3	< 0.8	28.4
CART-C-13	13	320.2	2.2	18.0	< 0.2	< 0.5	6.5	3474.1	0.9	1.7	14.7	1697.2	6.2	718.4	28.1	< 5.0	13.0	348.6	687.8	3.0	92.7	148.9	10.0	830.3	< 5.0	6.8	< 0.8	27.1
CART-C-14	14	390.5	2.5	23.5	< 0.2	< 0.5	9.7	2630.5	0.8	1.9	18.0	1747.7	7.5	723.2	37.6	< 5.0	14.9	352.3	717.8	2.2	61.4	172.0	11.0	828.7	< 5.0	8.4	< 0.8	33.6
CART-C-15	15	362.3	2.2	23.1	< 0.2	< 0.5	8.6	2122.3	0.8	1.7	12.5	1509.8	10.7	581.0	24.8	< 5.0	13.4	311.8	731.1	2.0	111.6	157.3	9.2	807.1	< 5.0	7.2	< 0.8	28.8
CART-C-16	16	429.4	2.5	21.1	< 0.2	< 0.5	9.2	2819.9	1.6	2.0	11.0	1703.0	17.8	680.1	28.7	< 5.0	14.8	337.1	834.9	2.4	62.7	174.7	10.6	841.3	< 5.0	9.0	< 0.8	36.5
CART-C-17	17	318.3	1.7	23.0	< 0.2	< 0.5	4.8	2815.6	2.0	1.3	14.2	1121.9	10.7	577.7	29.1	< 5.0	10.7	316.9	713.7	< 2.0	76.9	140.5	7.5	853.8	< 5.0	9.1	< 0.8	73.5
CART-SM-19	19	1079.6	5.1	46.5	< 0.2	< 0.5	1.7	5670.0	2.1	2.4	27.0	2393.3	61.2	869.7	29.4	< 5.0	32.2	495.0	401.5	3.6	26.5	145.1	19.5	1687.0	< 5.0	30.1	2.4	34.8
CART-SM-21	21	1226.2	5.5	45.8	< 0.2	< 0.5	1.1	4428.3	2.9	2.1	36.1	2058.8	56.7	807.2	24.5	< 5.0	39.2	560.1	325.8	3.3	51.1	154.3	19.1	2604.5	< 5.0	36.9	2.7	31.7
CART-SM-23	23	1372.3	7.6	44.4	< 0.2	< 0.5	1.1	3623.3	2.8	2.2	58.9	1957.7	68.1	760.1	22.0	< 5.0	39.1	679.3	316.7	4.2	47.9	126.7	18.1	3268.7	< 5.0	47.9	3.6	29.8
CART-SM-25	25	1427.1	9.1	51.2	< 0.2	< 0.5	1.5	3493.2	3.3	2.2	78.5	1803.0	76.2	723.4	23.3	< 5.0	49.6	693.1	309.8	4.7	48.0	114.0	18.1	4061.0	< 5.0	51.9	4.0	32.4
CART-SM-27	27	1467.6	10.6	49.6	< 0.2	< 0.5	2.3	3894.3	3.5	2.6	103.7	1866.1	83.3	797.4	23.6	< 5.0	50.1	659.0	268.9	5.3	90.5	113.1	19.7	5144.4	< 5.0	55.0	4.1	39.3
CART-SM-29	29	1289.6	8.7	43.7	< 0.2	< 0.5	2.6	5660.6	3.3	2.3	90.8	1641.4	77.9	982.3	26.0	< 5.0	44.2	480.5	199.1	4.8	95.5	135.4	19.6	4722.5	< 5.0	45.7	3.5	34.7
CART-SM-31	31	1685.2	9.3	43.7	< 0.2	< 0.5	2.3	4260.8	3.7	1.9	104.4	1597.9	65.7	777.3	20.8	< 5.0	39.3	415.8	193.0	4.5	42.4	106.2	20.6	5257.9	< 5.0	56.9	4.7	30.5
CART-SM-33	33	2345.7	10.1	57.7	< 0.2	< 0.5	1.6	3145.8	3.8	1.8	87.2	1649.6	61.9	681.2	18.9	< 5.0	40.4	460.3	196.9	4.4	91.6	116.6	22.7	6842.0	< 5.0	70.0	5.6	30.9
CART-SM-35	35	2121.6	9.2	56.0	< 0.2	< 0.5	1.2	3341.7	3.0	1.3	52.6	1468.6	46.6	675.4	18.7	< 5.0	37.4	415.4	162.6	3.4	74.3	99.4	22.2	6536.2	< 5.0	56.3	4.9	32.6
CART-SM-37	37	1276.5	7.1	41.9	< 0.2	< 0.5	1.1	3942.9	1.7	1.1	28.6	1265.4	23.2	723.4	19.8	< 5.0	19.4	350.1	155.6	3.5	54.7	157.8	20.3	5091.7	< 5.0	30.5	2.7	31.7
CART-SM-39	39	1216.3	5.9	43.3	< 0.2	< 0.5	0.9	3100.6	2.0	1.2	28.8	1300.4	18.6	737.0	17.7	< 5.0	18.2	353.5	135.9	3.6	23.0	104.7	21.7	5212.8	< 5.0	25.0	2.0	28.5
CART-SM-41	41	1629.5	4.6	49.5	< 0.2	< 0.5	0.7	3311.1	1.4	1.2	24.7	1133.8	16.9	672.0	14.5	< 5.0	15.2	437.3	89.4	3.4	14.1	109.9	23.9	5762.7	< 5.0	32.3	2.6	27.2
CART-SM-43	43	1559.0	3.7	43.2	< 0.2	< 0.5	0.5	2475.9	1.0	1.0	8.8	894.9	9.3	545.2	11.2	< 5.0	10.8	473.1	88.5	2.6	53.5	87.2	19.8	5335.8	< 5.0	30.5	2.2	22.2
CART-SM-45	45	1980.0	2.8	48.1	< 0.2	< 0.5	0.6	2719.1	1.5	1.0	6.3	1010.6	7.3	573.0	11.3	< 5.0	12.2	423.4	94.3	3.0	81.4	99.1	23.0	4919.0	< 5.0	36.5	2.8	24.6
CART-SM-47	47	2185.8	2.7	56.6	< 0.2	< 0.5	0.4	3077.6	1.8	1.1	6.7	1073.8	5.6	620.0	11.7	< 5.0	11.4	416.7	111.8	2.9	70.7	127.1	25.2	4092.2	< 5.0	37.5	2.9	23.5
CART-SM-49	49	1806.8	2.8	52.9	< 0.2	< 0.5	0.5	2800.5	1.6	1.0	6.3	1040.8	7.1	643.1	13.7	< 5.0	10.0	372.4	116.8	2.8	56.8	113.0	24.0	3871.6	< 5.0	31.7	2.3	21.7
CART-SM-51	51	2596.7	1.7	63.1	< 0.2	< 0.5	< 0.2	3138.1	2.6	0.9	8.4	1069.2	< 1.5	623.2	7.9	< 5.0	2.5	357.1	75.9	2.0	57.7	114.0	28.2	2347.3	< 5.0	52.6	3.3	5.2
CART-SM-53	53	2878.5	1.6	66.2	< 0.2	< 0.5	< 0.2	3319.6	3.2	0.8	9.9	1111.4	< 1.5	629.7	11.2	< 5.0	2.5	366.7	76.1	2.7	71.3	116.3	29.7	2226.8	< 5.0	65.5	4.0	4.3
CART-SM-55	55	3041.5	1.9	67.4	< 0.2	< 0.5	< 0.2	3168.0	3.0	0.8	10.1	1100.3	< 1.5	580.0	6.5	< 5.0	2.4	279.9	59.7	2.8	60.8	86.5	28.8	2046.4	< 5.0	67.1	4.9	2.8
CART-SM-57	57	2932.5	1.8	65.3	< 0.2	< 0.5	< 0.2	3066.6	2.8	0.7	9.8	1085.8	1.7	576.3	7.3	< 5.0	2.3	287.9	64.9	3.0	65.0	91.4	27.8	2128.8	< 5.0	58.9	5.1	2.5
CART-SM-59	59	3055.9	1.8	59.3	< 0.2	< 0.5	< 0.2	3164.9	2.7	0.9	10.6	1144.2	< 1.5	587.6	6.2	< 5.0	2.4	294.5	69.5	2.9	48.3	100.2	28.6	2261.9	< 5.0	51.0	5.0	2.3

CART-SM-69	69	2315.8	1.6	45.5	< 0.2	< 0.5	< 0.2	2485.2	2.0	0.9	8.7	967.7	2.2	457.2	6.6	< 5.0	3.3	255.3	67.8	2.4	56.3	103.7	21.1	1983.2	< 5.0	37.6	4.2	1.9
CART-SM-79	79	2432.1	1.8	35.5	< 0.2	< 0.5	< 0.2	2361.0	2.6	0.9	10.5	1073.5	< 1.5	402.9	6.4	< 5.0	3.6	223.4	43.9	2.8	15.8	76.9	18.5	1626.6	< 5.0	35.2	5.1	1.4
CART-SM-89	89	3237.1	1.7	40.1	< 0.2	< 0.5	< 0.2	2124.2	4.2	1.0	8.6	1307.9	< 1.5	352.0	7.3	< 5.0	3.6	313.5	44.7	3.0	91.3	77.7	16.9	1713.3	< 5.0	51.4	9.0	< 0.6
CART-SM-99	99	3846.7	1.9	61.3	< 0.2	< 0.5	< 0.2	3064.6	3.6	1.3	13.5	2125.5	2.9	476.9	11.8	< 5.0	4.8	269.6	69.6	2.9	5.9	66.6	24.0	1932.1	< 5.0	61.6	11.1	1.3
CART-SM-109	109	2833.3	1.9	50.0	< 0.2	< 0.5	< 0.2	2661.4	3.0	1.1	12.8	2086.4	< 1.5	443.8	11.1	< 5.0	2.8	257.8	41.4	2.7	64.9	78.7	19.9	1824.1	< 5.0	41.4	7.4	< 0.6
CART-SM-119	119	2422.0	1.7	54.9	< 0.2	< 0.5	< 0.2	3071.2	2.3	1.3	6.6	2379.8	< 1.5	503.0	13.6	< 5.0	2.9	216.7	21.3	2.9	34.8	39.0	21.4	1458.1	< 5.0	25.9	5.3	< 0.6
CART-SM-129	129	2793.0	1.6	55.8	< 0.2	< 0.5	< 0.2	3061.1	3.9	1.5	13.3	2599.5	< 1.5	482.8	14.6	< 5.0	6.5	266.5	18.0	2.9	105.4	46.3	20.5	1960.1	< 5.0	44.9	7.6	0.9
CART-SM-139	139	2439.8	1.9	57.6	< 0.2	< 0.5	< 0.2	2832.1	3.8	1.3	7.8	2486.1	< 1.5	448.6	14.1	< 5.0	5.0	252.9	39.8	2.8	132.7	84.6	19.7	1742.0	< 5.0	32.7	6.1	2.0
CART-SM-149	149	2623.5	2.0	57.1	< 0.2	< 0.5	< 0.2	3104.4	3.0	1.3	9.6	2386.0	1.8	507.8	14.0	< 5.0	4.5	250.3	147.0	2.8	62.5	55.6	21.7	1770.3	< 5.0	38.2	6.4	4.9
CART-SM-159	159	2922.9	1.7	73.0	< 0.2	< 0.5	< 0.2	4002.5	4.3	1.6	8.8	4518.1	1.6	632.6	26.5	< 5.0	4.9	234.1	28.6	2.6	106.5	52.8	24.1	1848.7	< 5.0	47.0	8.3	1.8
CART-SM-169	169	2316.1	2.0	80.4	< 0.2	< 0.5	< 0.2	4896.6	2.1	1.7	4.4	5385.7	1.5	769.7	32.2	< 5.0	2.7	166.7	35.3	2.4	15.0	30.6	27.8	1227.6	< 5.0	23.3	4.8	< 0.6
CART-SM-179	179	2370.6	1.8	79.7	< 0.2	< 0.5	< 0.2	5011.5	2.5	1.8	8.5	6063.1	< 1.5	810.6	36.3	< 5.0	3.5	218.6	23.7	2.7	96.4	41.2	27.2	1616.0	< 5.0	34.8	6.4	0.9
CART-SM-189	189	2329.5	2.1	87.1	< 0.2	< 0.5	< 0.2	5856.7	2.2	1.9	4.0	7571.8	< 1.5	904.7	43.9	< 5.0	3.3	224.5	23.3	2.4	98.8	73.3	29.5	1434.2	< 5.0	26.1	6.1	1.7
CART-SM-199	199	1769.9	1.8	76.4	< 0.2	< 0.5	< 0.2	5667.9	2.3	1.7	6.8	5765.8	3.2	919.3	37.4	< 5.0	4.5	209.2	43.4	2.3	94.9	81.0	28.0	1557.9	< 5.0	28.7	4.1	4.1
CART-SM-209	209	2453.1	2.0	80.6	< 0.2	< 0.5	< 0.2	6156.7	2.8	1.7	6.7	8327.2	< 1.5	968.1	49.8	< 5.0	2.9	226.8	20.7	3.0	85.7	48.2	28.1	1249.1	< 5.0	33.5	8.0	1.8
CART-SM-219	219	1800.0	2.0	58.3	< 0.2	< 0.5	0.2	4897.1	3.1	2.0	6.3	6671.4	< 1.5	829.6	42.3	< 5.0	3.3	163.4	24.2	3.1	74.7	45.3	21.0	1439.5	< 5.0	27.5	5.6	1.5
CART-SM-229	229	1887.9	1.9	50.7	< 0.2	< 0.5	< 0.2	4068.7	4.5	2.0	11.5	5861.2	< 1.5	675.7	36.8	< 5.0	6.0	185.3	34.5	3.5	106.8	74.1	16.8	1815.2	< 5.0	32.2	6.4	2.7
CART-SM-239	239	2496.6	2.0	52.2	< 0.2	< 0.5	< 0.2	4533.2	8.1	2.1	20.3	6536.0	< 1.5	773.2	41.5	< 5.0	11.2	273.1	77.0	2.6	281.8	81.6	16.8	2254.3	< 5.0	60.6	9.3	3.6
CART-SM-249	249	2308.7	1.7	50.3	< 0.2	< 0.5	< 0.2	3988.9	4.9	1.7	17.1	5583.8	1.7	710.3	35.6	< 5.0	6.1	231.1	49.9	2.7	118.9	67.5	17.9	2031.7	< 5.0	45.4	8.8	3.3
CART-SM-259	259	3060.5	2.0	50.2	< 0.2	< 0.5	< 0.2	4708.0	8.7	2.1	25.1	7587.6	< 1.5	794.4	47.3	< 5.0	6.6	278.1	43.1	2.1	133.7	76.7	16.9	2495.1	< 5.0	49.0	15.3	2.5
CART-SM-269	269	5270.6	2.1	55.3	< 0.2	< 0.5	0.5	4739.3	27.2	3.9	30.7	8376.1	2.7	1458.5	62.8	< 5.0	13.5	551.1	139.8	2.7	479.5	113.4	17.5	3310.4	< 5.0	292.0	14.9	21.3
CART-SM-279	279	5925.6	1.7	47.5	< 0.2	< 0.5	0.3	4847.3	28.8	4.5	30.8	8253.7	2.8	1984.8	69.8	< 5.0	15.5	633.2	180.8	2.2	656.1	104.0	15.7	2768.7	< 5.0	362.0	17.4	33.1
CART-SM-289	289	6111.9	1.9	41.5	< 0.2	< 0.5	0.3	8175.7	26.9	5.3	28.6	8210.4	3.0	2310.1	77.2	< 5.0	15.2	708.3	200.9	< 2.0	670.9	170.6	17.0	2486.1	< 5.0	398.5	18.2	25.0
CART-SM-299	299	4364.7	2.2	50.7	< 0.2	< 0.5	0.3	4269.1	19.3	3.9	26.8	5700.9	5.9	1503.0	48.3	< 5.0	15.0	499.0	155.8	2.0	447.8	95.0	21.3	2830.5	< 5.0	214.7	13.0	18.0
CART-SM-309	309	6015.3	1.9	47.1	0.3	< 0.5	0.4	4809.9	34.4	8.4	39.0	9939.7	3.7	2465.1	78.8	< 5.0	24.9	652.0	238.0	< 2.0	984.5	132.0	16.5	2817.3	< 5.0	379.7	24.6	35.9
CART-SM-319	319	5955.5	2.7	40.0	< 0.2	< 0.5	0.5	4652.9	35.2	9.9	60.4	12317.2	4.8	3158.6	92.9	< 5.0	36.5	602.1	294.9	< 2.0	901.6	155.7	17.6	5084.6	< 5.0	386.8	24.5	58.3
CART-SM-329	329	6073.1	2.8	41.5	0.2	< 0.5	0.4	4417.8	36.7	9.1	66.4	11697.1	4.5	3117.4	90.2	< 5.0	35.7	563.1	318.9	< 2.0	912.6	189.3	17.8	4241.6	< 5.0	415.6	29.4	54.9
CART-SM-339	339	6255.6	2.3	33.8	< 0.2	< 0.5	0.2	3707.2	31.1	8.4	43.8	10932.8	4.5	3510.2	102.0	< 5.0	27.9	635.5	348.7	< 2.0	968.8	196.8	14.4	2737.6	< 5.0	559.7	24.4	44.0
CART-SM-349	349	5565.5	3.0	31.5	< 0.2	< 0.5	0.4	4408.3	34.0	8.7	72.1	10512.1	3.9	3137.6	91.4	< 5.0	33.7	566.1	283.0	< 2.0	934.4	181.0	16.8	3212.1	< 5.0	399.1	34.0	44.2
CART-SM-359	359	5894.2	2.3	33.1	< 0.2	< 0.5	0.3	3644.8	29.6	8.7	46.2	10351.7	4.0	3295.3	97.1	< 5.0	26.1	679.4	353.5	< 2.0	1118.6	211.2	13.7	2366.8	< 5.0	468.6	27.0	40.5
CART-SM-369	369	6194.8	2.4	41.4	0.2	< 0.5	0.3	3824.6	32.0	9.4	66.4	11382.8	5.2	3355.3	102.6	< 5.0	31.6	659.9	391.0	< 2.0	1102.3	233.9	14.9	3613.4	< 5.0	470.7	33.3	44.8
CART-SM-379	379	6723.5	2.3	40.9	0.2	< 0.5	0.2	3973.6	30.7	9.9	52.7	11751.4	4.8	3565.1	109.0	< 5.0	32.5	716.8	464.1	< 2.0	903.1	258.1	15.6	3081.3	< 5.0	666.4	32.3	43.6
CART-SM-389	389	6324.1	3.5	42.0	0.4	< 0.5	0.3	4060.1	36.8	10.5	94.7	11037.6	7.5	3382.0	102.6	< 5.0	29.7	737.9	434.1	< 2.0	1059.8	256.4	16.4	2740.9	< 5.0	519.4	44.3	51.6
CART-SM-399	399	7202.4	3.0	45.0	0.3	< 0.5	0.3	3567.4	32.4	9.3	78.8	10670.7	5.8	3601.6	109.2	< 5.0	24.5	697.2	525.2	< 2.0	1190.5	236.7	13.9	1931.4	< 5.0	587.8	31.7	45.4
CART-SM-409	409	6163.9	2.1	31.6	0.2	< 0.5	< 0.2	3314.0	32.1	8.4	64.9	10070.6	4.8	3555.5	107.6	< 5.0	23.7	585.5	426.8	< 2.0	1156.2	215.4	12.6	1664.5	< 5.0	564.5	31.1	37.6
CART-SM-419	419	5412.6	1.5	22.1	< 0.2	< 0.5	< 0.2	2740.4	26.7	6.8	36.1	9299.0	3.6	3659.8	112.0	< 5.0	19.4	539.6	457.6	< 2.0	1290.8	167.0	9.8	638.2	< 5.0	600.7	26.2	31.2
CART-SM-429	429	5320.8	< 1.5	21.3	< 0.2	< 0.5	< 0.2	2754.2	28.5	5.7	36.6	9043.9	4.2	3642.3	109.3	< 5.0	15.6	579.1	489.5	< 2.0	1383.0	162.6	9.6	708.1	< 5.0	604.9	31.3	28.8
CART-SM-439	439	5604.1	2.2	25.1	0.2	< 0.5	< 0.2	2527.7	27.0	6.4	38.5	10030.8	5.5	3726.9	114.9	< 5.0	16.1	513.2	632.3	< 2.0	1472.5	172.9	9.9	806.2	< 5.0	596.2	32.8	38.1

Appendix Table 6 *ICP-OES geochemical assay for Cartier, which includes the following elements; Aluminum (Al), Arsenic (As), Barium (Ba), Beryllium (Be), Boron (B), Cadmium (Cd), Calcium (Ca), Chromium (Cr), Cobalt (Co), Copper (Cu), Iron (Fe), Lead (Pb), Magnesium (Mg), Manganese (Mn), Molybdenum (Mo), Nickel (Ni), Phosphorus (P), Potassium (K), Selenium (Se), Silicon (Si), Sodium (Na), Strontium (Sr), Sulfur (S), Thallium (Tl), Titanium (Ti), Vanadium (V), Zinc (Zn).*

Laurentian ICP-OES Geochemical Assay

Sample	Depth	Al	As	Ba	Be	B	Cd	Ca	Cr	Co	Cu	Fe	Pb	Mg	Mn	Mo	Ni	P	K	Se	Si	Na	Sr	S	Tl	Ti	V	Zn
	cm	*µg/g*	*µg/g*	*µg/g*	*µg/g*	*µg/g*	*µg/g*	*µg/g*	*µg/g*	*µg/g*	*µg/g*	*µg/g*	*µg/g*	*µg/g*	*µg/g*	*µg/g*	*µg/g*	*µg/g*	*µg/g*	*µg/g*	*µg/g*	*µg/g*	*µg/g*	*µg/g*	*µg/g*	*µg/g*	*µg/g*	*µg/g*
LAU-C-1	1	760.8	7.0	54.5	< 0.2	< 0.5	0.8	4849.3	2.7	6.7	104.3	2768.2	13.2	923.4	62.0	< 5.0	221.9	583.1	3173.6	< 2.0	84.9	345.6	14.9	1273.5	< 5.0	13.7	1.1	33.0
LAU-C-2	2	1230.5	12.5	66.3	< 0.2	< 0.5	1.6	4762.8	6.0	17.0	190.1	5468.1	31.4	929.4	67.9	< 5.0	427.7	493.0	827.6	3.5	54.7	157.4	19.3	1439.1	< 5.0	21.1	1.7	36.6
LAU-C-3	3	1764.7	15.7	62.6	< 0.2	< 0.5	1.6	3856.9	20.0	17.0	306.0	6444.1	51.5	831.3	62.4	< 5.0	546.2	673.1	745.3	6.2	118.7	135.2	16.7	1873.5	< 5.0	25.1	2.5	31.0
LAU-C-4	4	2069.4	16.6	64.7	< 0.2	< 0.5	1.6	3906.0	12.5	18.9	371.2	6896.0	65.6	784.3	43.7	< 5.0	740.7	753.0	672.4	6.4	103.7	128.9	17.8	1998.5	< 5.0	36.4	3.5	31.8
LAU-C-5	5	2527.9	19.7	52.2	< 0.2	< 0.5	1.5	3002.5	27.7	19.2	463.9	7683.8	80.2	670.5	43.5	< 5.0	857.9	942.4	808.1	11.2	99.9	123.6	14.0	2355.4	< 5.0	44.6	4.2	28.6
LAU-C-6	6	3161.9	20.9	56.6	< 0.2	< 0.5	1.2	2669.8	16.4	21.8	594.4	8222.5	107.7	648.7	40.7	< 5.0	1107.1	1198.7	704.7	9.9	88.5	119.3	13.1	2777.4	< 5.0	56.0	5.5	25.7
LAU-C-7	7	3839.2	25.6	50.8	< 0.2	< 0.5	1.3	2305.4	19.6	26.5	657.8	7150.9	105.4	651.2	35.2	< 5.0	1463.5	1387.6	759.9	11.9	144.5	118.3	11.3	3305.3	< 5.0	68.1	6.6	25.0
LAU-C-8	8	4230.1	34.0	56.5	< 0.2	< 0.5	1.6	2258.9	21.4	26.4	689.7	7630.1	109.5	578.6	30.1	< 5.0	1564.6	1328.9	725.5	12.0	167.9	101.3	11.3	3667.5	< 5.0	71.2	7.5	24.8
LAU-C-9	9	4145.3	31.6	71.0	< 0.2	< 0.5	1.6	2085.6	19.7	25.7	553.0	6470.9	105.6	522.0	25.8	< 5.0	1558.9	1307.5	688.6	12.1	148.3	108.4	11.8	3915.5	< 5.0	71.9	8.3	26.4
LAU-C-10	10	4300.4	32.0	68.0	< 0.2	< 0.5	2.0	2802.5	20.3	26.3	634.7	5799.4	99.8	549.3	27.1	< 5.0	1471.0	1245.0	695.6	12.2	155.6	108.9	13.3	4510.3	< 5.0	73.4	7.7	27.4
LAU-C-11	11	4483.1	31.8	59.1	< 0.2	< 0.5	1.8	2544.8	18.8	27.1	770.2	7439.8	107.6	589.7	29.1	< 5.0	1569.6	1358.7	758.0	12.8	120.3	123.5	12.4	4235.1	< 5.0	73.6	7.1	27.0
LAU-C-12	12	3902.3	29.1	73.7	< 0.2	< 0.5	2.0	3617.5	15.2	21.3	804.1	6697.6	100.0	548.2	30.2	< 5.0	1210.0	1032.9	627.1	10.6	202.0	123.4	14.9	4757.1	< 5.0	74.6	7.2	28.6
LAU-C-13	13	4641.5	31.2	97.2	< 0.2	< 0.5	2.2	3866.6	15.2	18.8	1138.9	4613.8	112.1	456.7	24.9	< 5.0	1200.6	1004.3	412.5	11.5	117.8	129.0	17.0	6356.5	< 5.0	105.6	9.6	30.6
LAU-C-14	14	4514.7	48.0	177.5	0.3	< 0.5	3.5	4658.7	7.9	15.3	1550.5	5006.3	128.0	348.9	26.5	< 5.0	993.1	728.1	232.6	8.4	163.6	96.0	22.0	7744.3	< 5.0	66.8	8.1	35.7
LAU-C-24	24	2732.8	13.8	106.3	< 0.2	< 0.5	3.0	8967.7	3.5	19.3	449.7	5199.4	25.8	570.4	68.3	< 5.0	903.9	528.8	72.8	4.3	129.4	69.1	39.3	7051.2	< 5.0	32.4	3.2	64.2
LAU-C-26	26	2499.4	9.6	88.0	< 0.2	< 0.5	2.2	9840.2	3.6	18.5	173.2	4819.2	11.9	612.8	70.8	< 5.0	778.6	448.8	49.3	2.0	80.3	61.2	40.6	5897.5	< 5.0	29.5	2.5	67.3
LAU-C-28	28	2429.8	9.1	76.1	< 0.2	< 0.5	1.5	9716.3	3.5	15.8	59.4	3930.8	5.6	611.1	67.2	< 5.0	571.6	389.9	39.6	< 2.0	155.4	60.6	39.2	5273.0	< 5.0	28.3	2.5	59.8
LAU-C-30	30	2794.0	9.6	82.8	< 0.2	< 0.5	0.8	10306.5	3.5	15.6	88.1	3802.6	6.9	676.2	69.3	< 5.0	533.9	407.3	45.6	< 2.0	73.4	71.3	41.7	5574.9	< 5.0	29.9	2.7	53.6
LAU-C-32	32	2808.0	9.7	82.7	< 0.2	< 0.5	0.6	9767.4	3.8	12.3	60.5	2998.5	5.4	659.2	61.7	< 5.0	364.8	368.8	44.2	< 2.0	122.9	78.5	39.0	5156.9	< 5.0	28.8	2.5	40.7
LAU-C-36	36	3757.0	10.2	71.6	< 0.2	< 0.5	0.3	10949.6	6.1	8.3	36.3	2157.9	2.7	794.4	57.8	< 5.0	145.4	430.8	44.4	< 2.0	143.6	75.7	40.6	4345.8	< 5.0	35.0	3.0	23.8
LAU-C-38	38	3635.4	7.8	64.5	< 0.2	< 0.5	0.2	10542.5	7.3	6.6	30.4	1901.8	2.3	782.9	51.8	< 5.0	96.9	400.6	36.9	< 2.0	96.1	70.4	38.4	3797.7	< 5.0	33.2	2.8	16.8
LAU-C-40	40	3907.3	7.3	73.1	< 0.2	< 0.5	0.3	10867.9	7.5	5.9	36.8	1877.3	2.6	812.4	50.6	< 5.0	80.2	440.3	47.6	3.1	165.6	80.2	40.1	3701.5	< 5.0	36.3	3.2	15.9
LAU-C-42	42	3966.1	6.1	71.9	< 0.2	< 0.5	0.2	11093.9	8.5	4.3	33.0	1671.6	2.0	842.2	44.8	< 5.0	47.3	415.9	41.2	< 2.0	123.1	62.9	40.0	3366.2	< 5.0	36.9	3.3	9.7
LAU-C-44	44	3941.6	6.6	61.8	< 0.2	< 0.5	0.2	12205.3	7.6	3.3	33.3	1589.6	1.8	957.1	41.9	< 5.0	29.5	366.1	31.7	< 2.0	183.4	46.3	41.0	3670.6	< 5.0	35.5	2.8	6.2
LAU-C-46	46	4798.5	6.1	88.5	< 0.2	< 0.5	0.3	13515.5	6.2	3.3	38.9	1881.2	3.7	1056.9	41.7	< 5.0	41.9	330.9	36.4	< 2.0	125.9	99.2	47.8	3710.6	< 5.0	38.5	3.2	12.0
LAU-C-48	48	5100.9	4.1	70.9	< 0.2	< 0.5	0.2	12402.5	7.0	2.2	29.0	1592.0	2.6	991.5	32.3	< 5.0	18.8	354.5	43.3	2.7	165.6	72.0	42.8	2959.3	< 5.0	47.7	4.1	4.2
LAU-C-50	50	5881.6	2.9	72.7	< 0.2	< 0.5	0.3	12996.6	8.1	1.9	30.8	1652.3	3.0	1030.4	28.9	< 5.0	14.4	336.1	41.4	2.9	169.4	63.4	44.5	2646.0	< 5.0	67.1	5.2	3.0
LAU-C-52	52	5574.7	2.3	71.4	0.2	< 0.5	0.2	12479.8	7.7	1.7	25.1	1668.9	3.6	959.1	25.4	< 5.0	9.8	280.1	42.6	< 2.0	183.0	54.3	43.6	2160.9	< 5.0	64.6	4.8	2.0
LAU-C-54	54	4341.6	7.7	79.6	< 0.2	< 0.5	0.7	11022.1	6.6	6.8	216.4	2628.8	14.8	827.3	38.6	< 5.0	246.5	337.5	55.3	4.6	179.3	59.6	40.5	3835.8	< 5.0	50.0	4.1	18.8
LAU-C-56	56	4784.8	4.6	75.6	< 0.2	< 0.5	0.4	11188.9	6.6	3.6	90.6	1898.4	7.1	878.3	28.5	< 5.0	96.1	321.2	72.0	2.6	255.1	76.5	39.1	2683.4	< 5.0	53.8	4.4	8.8
LAU-C-58	58	4201.3	2.4	62.6	< 0.2	< 0.5	0.2	11270.7	5.1	2.5	45.4	1627.7	4.1	915.3	23.3	< 5.0	50.2	285.2	49.5	< 2.0	225.1	71.7	36.6	2531.3	< 5.0	56.7	4.4	5.0
LAU-C-60	60	4064.5	4.2	62.9	< 0.2	< 0.5	0.3	11563.7	5.2	3.4	74.8	1886.2	6.3	933.7	28.0	< 5.0	86.9	297.2	44.6	< 2.0	168.4	56.3	38.0	2847.1	< 5.0	51.3	4.0	6.7
LAU-C-70	70	3371.8	2.7	79.9	< 0.2	< 0.5	0.3	16430.1	3.2	2.2	16.0	2486.1	1.8	1244.6	28.2	< 5.0	11.8	202.4	30.7	< 2.0	126.4	82.4	48.5	2010.3	< 5.0	45.9	4.2	3.6
LAU-C-80	80	2937.0	2.2	85.6	< 0.2	< 0.5	< 0.2	17803.5	2.9	2.0	13.0	3105.8	1.7	1254.5	32.8	< 5.0	10.4	186.5	32.4	< 2.0	133.9	69.9	50.4	1797.2	< 5.0	43.0	4.0	1.5
LAU-C-90	90	2908.1	1.9	96.1	< 0.2	< 0.5	0.2	18648.6	3.9	2.1	15.2	3449.4	< 1.50	1264.9	37.6	< 5.0	8.1	218.9	38.6	< 2.0	180.1	78.7	52.2	1883.2	< 5.0	42.1	4.3	1.3
LAU-C-100	100	2882.0	2.3	98.3	< 0.2	< 0.5	< 0.2	18925.9	4.4	1.8	13.5	3631.3	< 1.50	1246.7	41.1	< 5.0	7.3	229.5	44.0	< 2.0	234.7	66.1	51.2	1945.8	< 5.0	48.8	4.2	1.0
LAU-C-110	110	2689.5	3.4	95.2	< 0.2	< 0.5	0.3	17667.9	4.1	2.8	56.8	3761.8	3.4	1157.5	43.0	< 5.0	56.3	232.0	33.4	< 2.0	135.3	53.3	49.0	2178.7	< 5.0	29.5	3.8	3.9
LAU-C-120	120	2122.6	2.9	95.2	< 0.2	< 0.5	< 0.2	16227.2	4.0	1.5	14.1	3382.7	< 1.50	1056.2	41.8	< 5.0	11.7	168.5	27.9	< 2.0	62.0	67.6	43.8	1760.9	< 5.0	20.7	3.5	1.5

LAU-C-130	130	1894.3	3.1	78.1	< 0.2	< 0.5	< 0.2	15277.8	4.6	1.7	12.9	3464.8	< 1.50	1062.1	44.9	< 5.0	13.8	222.8	48.6	< 2.0	132.1	90.5	39.1	2109.4	< 5.0	32.1	3.4	6.6
LAU-C-140	140	1702.0	3.0	63.6	< 0.2	< 0.5	< 0.2	13538.7	3.6	1.4	9.0	3245.8	< 1.50	961.6	43.2	< 5.0	7.2	197.8	31.5	< 2.0	90.3	57.0	34.4	2151.2	< 5.0	28.7	3.6	3.0
LAU-C-150	150	1945.2	3.7	78.3	< 0.2	< 0.5	< 0.2	14321.8	4.4	1.7	17.8	3280.2	< 1.50	1019.6	46.6	< 5.0	18.4	252.7	44.7	< 2.0	198.1	122.2	35.8	2337.4	< 5.0	24.5	4.5	4.5
LAU-C-160	160	3013.0	5.1	70.0	< 0.2	< 0.5	0.5	9886.5	8.9	4.5	95.3	2855.5	6.1	862.3	41.0	< 5.0	103.9	278.1	73.9	< 2.0	90.5	66.1	33.6	2910.6	< 5.0	51.3	6.3	12.0
LAU-C-170	170	3894.5	6.0	77.9	< 0.2	< 0.5	0.7	11331.9	13.2	5.0	66.2	3734.7	4.2	1166.2	52.5	< 5.0	80.5	341.8	138.0	2.1	62.7	68.3	32.4	3310.3	< 5.0	69.6	8.8	13.4
LAU-C-180	180	4190.9	5.9	79.6	< 0.2	< 0.5	0.7	10286.3	17.3	5.8	54.7	4009.0	2.9	1262.2	54.2	< 5.0	54.0	423.7	145.6	< 2.0	14.1	95.8	28.6	3351.0	< 5.0	86.3	13.6	18.6
LAU-C-190	190	4440.6	6.1	68.8	< 0.2	< 0.5	0.7	9691.8	20.5	6.1	46.2	4541.9	2.5	1583.6	59.7	< 5.0	40.3	420.9	165.9	< 2.0	< 5.0	103.6	25.3	3142.0	< 5.0	119.6	16.5	23.9
LAU-C-200	200	4932.5	5.8	65.2	< 0.2	< 0.5	0.7	8027.3	25.4	7.6	60.8	5015.7	2.8	1796.3	58.8	< 5.0	49.5	497.7	225.4	< 2.0	178.1	119.6	21.9	3370.8	< 5.0	135.2	15.7	42.7
LAU-C-210	210	5748.7	7.0	77.1	0.2	< 0.5	0.8	8477.5	29.8	8.9	61.5	5518.7	3.3	2133.0	68.4	< 5.0	48.2	513.5	275.8	< 2.0	199.5	139.7	22.8	2975.1	< 5.0	171.5	24.0	60.1
LAU-C-220	220	6374.9	6.7	69.7	0.3	< 0.5	0.7	6743.7	34.6	11.5	67.1	6611.2	2.7	2533.0	78.3	< 5.0	37.7	518.9	377.0	< 2.0	220.7	192.4	20.3	2810.3	< 5.0	266.4	32.1	55.8
LAU-C-230	230	5408.5	3.5	45.0	< 0.2	< 0.5	< 0.2	3182.4	27.6	6.9	36.6	8359.7	2.6	3353.6	101.1	< 5.0	19.5	432.1	440.8	< 2.0	245.1	170.7	11.7	1658.6	< 5.0	446.1	22.1	26.9
LAU-C-240	240	8120.9	3.1	65.0	0.2	< 0.5	< 0.2	7198.7	35.9	8.7	24.7	12527.3	3.7	7568.7	171.1	< 5.0	24.1	465.6	950.4	< 2.0	442.6	179.6	13.7	800.3	< 5.0	561.7	27.3	26.0
LAU-C-250	250	6148.4	2.0	50.6	< 0.2	< 0.5	< 0.2	6344.1	28.0	8.0	19.4	9881.4	3.0	6385.6	147.5	< 5.0	21.8	397.1	662.5	< 2.0	488.7	123.4	11.1	209.1	< 5.0	406.1	22.6	20.7
LAU-C-260	260	18606.0	3.4	175.6	0.7	< 0.5	< 0.2	12309.0	80.6	15.8	43.2	28369.6	9.8	16024.0	507.2	< 5.0	51.0	471.3	2462.5	< 2.0	1069.8	281.9	22.8	88.1	< 5.0	652.2	48.6	58.5
LAU-C-270	270	16477.3	2.7	135.8	0.5	< 0.5	< 0.2	12400.6	67.3	13.7	34.2	25611.0	7.9	14590.1	433.3	< 5.0	42.7	476.0	2127.8	< 2.0	863.7	269.4	25.2	115.3	< 5.0	778.9	42.5	49.8
LAU-C-280	280	16405.8	2.5	151.2	0.6	< 0.5	< 0.2	11815.1	63.2	14.0	36.4	27995.8	7.6	13863.4	534.1	< 5.0	42.0	466.8	2288.1	< 2.0	858.4	333.7	24.1	126.9	< 5.0	666.6	41.7	51.9
LAU-C-290	290	17369.3	2.7	156.8	0.6	< 0.5	< 0.2	12291.8	69.9	15.0	40.5	27102.4	11.1	14850.2	484.0	< 5.0	46.2	484.5	2435.8	< 2.0	903.0	292.6	24.8	108.1	< 5.0	709.6	44.7	54.3
LAU-C-300	300	17753.5	3.0	155.8	0.6	< 0.5	< 0.2	13247.4	72.7	14.9	38.5	27581.5	8.5	15217.7	507.3	< 5.0	47.6	480.8	2478.3	< 2.0	842.4	322.9	26.5	130.6	< 5.0	763.7	45.4	52.9

Appendix Table 7 *ICP-OES geochemical assay for Laurentian, which includes the following elements; Aluminum (Al), Arsenic (As), Barium (Ba), Beryllium (Be), Boron (B), Cadmium (Cd), Calcium (Ca), Chromium (Cr), Cobalt (Co), Copper (Cu), Iron (Fe), Lead (Pb), Magnesium (Mg), Manganese (Mn), Molybdenum (Mo), Nickel (Ni), Phosphorus (P), Potassium (K), Selenium (Se), Silicon (Si), Sodium (Na), Strontium (Sr), Sulfur (S), Thallium (Tl), Titanium (Ti), Vanadium (V), Zinc (Zn).*

Transplant ICP-OES Geochemical Assay

Sample	Depth	Al	As	Ba	Be	B	Cd	Ca	Cr	Co	Cu	Fe	Pb	Mg	Mn	Mo	Ni	P	K	Se	Si	Na	Sr	S	Tl	Ti	V	Zn
	cm	*µg/g*	*µg/g*	*µg/g*	*µg/g*	*µg/g*	*µg/g*	*µg/g*	*µg/g*	*µg/g*	*µg/g*	*µg/g*	*µg/g*	*µg/g*	*µg/g*	*µg/g*	*µg/g*	*µg/g*	*µg/g*	*µg/g*	*µg/g*	*µg/g*	*µg/g*	*µg/g*	*µg/g*	*µg/g*	*µg/g*	*µg/g*
TR-SM-2	0	960.2	8.1	56.5	< 0.2	< 0.5	1.5	4133.9	3.7	11.1	268.6	3958.9	58.7	647.4	57.6	< 5.0	306.9	729.5	791.6	3.3	139.6	137.0	13.3	1671.8	< 5.0	26.4	2.0	32.2
TR-SM-3	3	1234.2	9.8	49.7	< 0.2	< 0.5	1.7	4634.4	6.1	15.6	283.5	4550.2	53.4	790.8	67.0	< 5.0	410.8	771.5	959.1	2.9	89.0	173.2	14.9	1827.2	< 5.0	30.8	2.2	38.4
TR-SM-5	5	4779.8	28.1	58.0	0.2	< 0.5	1.8	2875.3	17.2	22.2	920.9	7162.1	135.5	521.2	29.7	< 5.0	1296.7	1193.7	528.7	11.6	142.1	104.3	12.2	3996.7	< 5.0	68.9	8.7	27.9
TR-SM-6	6	1083.6	10.6	35.0	< 0.2	< 0.5	2.4	3815.3	4.0	17.3	408.1	4892.0	77.2	616.4	27.1	< 5.0	566.1	782.1	501.6	4.9	77.7	115.1	15.5	1876.4	< 5.0	21.9	2.3	33.3
TR-SM-7	7	1337.7	9.7	37.7	< 0.2	< 0.5	2.1	3353.1	4.4	15.9	389.0	4994.8	70.9	662.8	46.6	< 5.0	511.6	590.2	537.0	4.9	123.2	108.3	13.4	1569.4	< 5.0	26.7	2.2	31.7
TR-SM-9	9	2729.5	19.8	45.0	< 0.2	< 0.5	1.6	2219.3	25.7	19.9	495.9	9126.5	134.1	587.7	42.5	< 5.0	975.6	977.0	588.9	9.2	121.2	124.0	9.7	2386.7	< 5.0	55.6	4.9	24.0
TR-SM-10	10	2902.4	20.8	33.0	< 0.2	< 0.5	1.5	2052.6	23.0	20.0	540.8	9331.4	152.0	503.7	26.2	< 5.0	901.8	1086.7	506.9	10.1	146.5	110.6	9.8	2668.5	< 5.0	47.1	5.4	25.4
TR-SM-12	12	3802.3	39.5	49.1	< 0.2	< 0.5	1.5	2650.1	15.8	23.0	507.8	13340.4	163.4	566.9	37.4	< 5.0	1221.0	1129.8	553.8	10.2	117.2	145.7	10.3	3006.2	< 5.0	71.9	6.9	28.8
TR-SM-13	13	4491.0	32.5	53.3	< 0.2	< 0.5	1.6	2406.2	17.5	25.1	738.5	9844.7	154.2	527.8	29.7	< 5.0	1460.0	1130.6	526.1	11.0	168.4	102.9	11.1	3368.4	< 5.0	78.7	7.0	26.0
TR-SM-14	14	4131.9	31.7	45.9	< 0.2	< 0.5	1.4	2878.3	16.9	20.4	662.8	9345.8	133.6	622.9	40.9	< 5.0	1152.1	1077.1	543.1	11.2	111.5	102.1	10.7	3202.3	< 5.0	73.2	7.3	38.1
TR-SM-15	15	4821.1	27.6	58.2	< 0.2	< 0.5	1.6	2977.9	18.5	22.2	830.5	8073.0	140.1	602.7	32.3	< 5.0	1308.1	1118.4	541.2	12.1	120.8	109.6	12.4	3683.5	< 5.0	90.1	8.3	27.8
TR-SM-16	16	4663.8	26.9	105.5	0.2	< 0.5	2.0	3934.2	11.6	17.9	922.1	7862.9	143.5	447.5	28.8	< 5.0	1028.1	901.5	388.6	11.2	123.6	96.8	17.1	4367.3	< 5.0	85.9	7.5	31.6
TR-SM-17	17	4595.8	27.4	53.2	< 0.2	< 0.5	1.6	3183.9	17.6	21.5	1000.9	7147.9	126.1	542.0	36.4	< 5.0	1306.9	1153.1	653.7	11.4	81.9	126.3	12.2	3954.4	< 5.0	74.4	9.1	26.4

TR-SM-18	18	4098.5	25.6	82.6	< 0.2	< 0.5	2.1	4307.9	10.0	15.3	1014.6	7792.1	127.8	417.3	38.3	< 5.0	919.6	942.3	513.2	9.9	112.8	122.4	16.6	4565.3	< 5.0	60.2	6.9	28.9
TR-SM-20	20	5231.9	15.1	101.6	0.2	< 0.5	2.2	7076.5	5.2	17.0	640.5	6606.9	60.0	404.9	39.6	< 5.0	937.6	859.5	177.9	4.2	84.3	80.6	28.5	5304.2	< 5.0	57.5	6.6	42.2
TR-SM-22	22	5192.5	11.4	85.5	< 0.2	< 0.5	1.9	6886.1	4.3	15.9	341.1	5768.6	24.7	373.6	37.7	< 5.0	851.0	836.1	136.0	2.4	249.4	66.1	27.5	4663.2	< 5.0	51.0	5.9	40.3
TR-SM-24	24	4985.6	6.5	67.9	< 0.2	< 0.5	1.2	6180.2	4.7	12.9	150.4	4392.1	10.3	343.4	34.0	< 5.0	623.3	727.5	100.1	< 2.0	178.8	90.6	23.9	3609.7	< 5.0	43.8	5.6	35.1
TR-SM-26	26	4894.6	3.4	46.0	< 0.2	< 0.5	0.6	5625.6	4.8	10.3	52.9	3186.0	3.4	326.8	31.5	< 5.0	396.7	746.6	75.4	< 2.0	119.7	69.6	21.1	2894.7	< 5.0	43.8	4.9	27.8
TR-SM-28	28	4998.4	2.9	33.2	< 0.2	< 0.5	0.4	5972.8	4.7	9.3	30.1	2486.6	2.4	340.5	32.0	< 5.0	286.0	557.3	23.8	< 2.0	976.9	13.7	21.5	2374.8	< 5.0	30.8	4.4	22.7
TR-SM-30	30	5358.5	3.6	41.4	< 0.2	< 0.5	0.3	6158.6	5.4	9.3	39.5	2366.3	3.4	349.7	32.9	< 5.0	263.6	604.2	99.0	< 2.0	30.0	49.0	22.5	2601.5	< 5.0	42.9	4.3	21.9
TR-SM-32	32	5437.9	3.4	43.5	< 0.2	< 0.5	< 0.2	6584.4	4.6	6.5	29.2	1750.7	2.2	405.4	29.8	< 5.0	122.4	492.7	38.3	2.1	36.1	71.3	23.0	2789.7	< 5.0	51.2	4.5	13.5
TR-SM-34	34	5408.4	3.5	40.8	< 0.2	< 0.5	< 0.2	6644.6	4.2	7.4	32.1	1826.6	3.1	388.1	31.8	< 5.0	133.7	475.9	23.0	< 2.0	70.3	52.2	23.1	2746.5	< 5.0	44.3	5.0	16.8
TR-SM-36	36	5660.1	3.5	39.3	< 0.2	< 0.5	< 0.2	6914.0	4.4	6.7	24.5	1705.9	2.7	406.9	31.9	< 5.0	96.9	411.0	24.6	< 2.0	26.8	43.6	24.0	2557.7	< 5.0	50.1	5.9	14.5
TR-SM-38	38	4727.5	3.1	28.1	< 0.2	< 0.5	< 0.2	5600.5	3.9	4.4	21.4	1185.4	1.5	358.8	24.1	< 5.0	41.8	392.4	21.9	< 2.0	16.1	43.2	19.0	2366.8	< 5.0	49.9	5.4	8.1
TR-SM-40	40	5176.6	3.0	38.3	< 0.2	< 0.5	< 0.2	6427.9	4.1	5.7	26.8	1542.1	2.1	391.9	28.1	< 5.0	96.8	441.5	32.3	< 2.0	11.6	73.8	21.7	2674.4	< 5.0	52.3	4.8	11.9
TR-SM-42	42	5623.1	2.9	43.7	< 0.2	< 0.5	< 0.2	7054.6	4.3	4.1	26.3	1415.6	2.5	436.9	25.7	< 5.0	29.1	342.1	261.3	< 2.0	< 5.0	51.6	24.6	2406.2	< 5.0	46.4	4.7	7.7
TR-SM-46	46	5365.7	3.1	34.2	< 0.2	< 0.5	< 0.2	6276.1	4.4	2.1	21.9	977.8	1.5	441.1	18.4	< 5.0	16.1	353.5	24.4	< 2.0	19.7	53.4	20.8	2473.3	< 5.0	50.3	5.0	2.9
TR-SM-48	48	5941.9	3.7	41.2	< 0.2	< 0.5	< 0.2	6676.3	4.9	1.7	23.0	948.3	< 1.50	479.9	16.4	< 5.0	11.8	340.0	174.2	< 2.0	27.3	104.1	21.7	2522.8	< 5.0	59.0	5.6	1.9
TR-SM-50	50	6240.8	2.9	43.9	< 0.2	< 0.5	< 0.2	6652.8	5.6	1.6	23.6	972.4	2.0	484.8	14.6	< 5.0	9.7	364.8	118.7	2.8	40.0	94.8	21.7	2631.0	< 5.0	61.6	7.0	1.2
TR-SM-52	52	5589.0	3.9	48.0	< 0.2	< 0.5	0.3	6821.4	4.6	3.9	80.7	1708.3	9.9	483.3	17.4	< 5.0	129.9	330.1	39.6	< 2.0	44.0	100.1	22.1	2781.5	< 5.0	67.2	6.0	7.9
TR-SM-54	54	5270.4	2.5	39.9	< 0.2	< 0.5	< 0.2	6142.6	4.3	2.9	57.4	1372.2	6.3	469.1	13.6	< 5.0	86.1	315.5	27.3	2.0	47.6	64.6	20.1	2378.5	< 5.0	60.7	5.4	5.2
TR-SM-56	56	5179.0	2.6	39.2	< 0.2	< 0.5	< 0.2	6742.3	4.2	2.4	50.6	1393.8	5.5	542.2	12.7	< 5.0	74.3	290.9	24.1	2.5	62.5	41.8	21.1	2375.2	< 5.0	57.7	5.8	4.0
TR-SM-58	58	5029.0	2.5	38.8	< 0.2	< 0.5	< 0.2	7109.1	3.9	1.6	42.0	1184.6	3.5	568.3	10.2	< 5.0	30.7	290.2	22.1	< 2.0	25.4	37.4	21.1	2215.7	< 5.0	53.2	5.6	1.2
TR-SM-60	60	5202.4	2.4	39.3	< 0.2	< 0.5	< 0.2	7998.6	3.5	1.5	25.8	1259.4	2.6	699.7	10.8	< 5.0	26.6	227.6	16.6	2.5	72.3	44.8	24.1	2398.5	< 5.0	55.6	4.4	1.6
TR-SM-62	62	6902.8	2.4	65.6	< 0.2	< 0.5	0.3	9903.9	4.5	2.2	24.7	1804.6	5.3	746.4	13.5	< 5.0	24.0	206.9	28.0	< 2.0	39.8	72.6	32.1	2011.9	< 5.0	70.0	8.3	1.1
TR-SM-72	72	3918.1	1.9	46.0	< 0.2	< 0.5	< 0.2	8490.5	2.7	1.5	13.3	1428.0	1.8	757.2	12.6	< 5.0	18.0	189.6	26.7	< 2.0	70.3	83.3	24.1	2094.3	< 5.0	62.9	4.5	0.9
TR-SM-82	82	3397.7	2.3	59.3	< 0.2	< 0.5	< 0.2	10353.5	3.8	2.0	21.4	1910.8	2.3	914.3	17.4	< 5.0	26.6	225.8	30.3	< 2.0	59.3	80.7	27.7	2069.2	< 5.0	50.9	4.6	1.1
TR-SM-92	92	3208.4	1.9	61.2	< 0.2	< 0.5	< 0.2	12721.0	3.2	1.6	15.2	2327.8	1.6	1092.4	23.1	< 5.0	12.3	237.3	27.3	< 2.0	36.1	71.5	31.8	1816.4	< 5.0	49.0	4.8	0.8
TR-SM-98	98	2854.1	2.0	63.5	< 0.2	< 0.5	< 0.2	13528.9	3.1	1.5	15.1	2496.9	< 1.5	1229.3	26.3	< 5.0	11.5	241.1	39.0	< 2.0	47.4	92.0	32.3	1919.1	< 5.0	44.4	4.3	< 0.6
TR-SM-102	102	3860.5	2.9	73.2	< 0.2	< 0.5	0.3	13807.5	4.2	3.0	65.6	3173.8	6.7	1197.3	31.5	< 5.0	84.6	255.0	75.1	< 2.0	8.9	63.5	35.1	2095.1	< 5.0	69.4	5.8	7.8
TR-SM-112	112	2578.8	2.4	67.6	< 0.2	< 0.5	< 0.2	14843.7	2.7	1.7	22.4	2883.8	2.3	1444.6	32.2	< 5.0	24.3	157.8	39.3	< 2.0	66.9	71.2	33.9	1856.6	< 5.0	50.6	4.0	3.0
TR-SM-122	122	2909.5	2.0	79.0	< 0.2	< 0.5	0.2	14792.9	4.0	1.7	16.4	3299.0	1.9	1341.1	35.2	< 5.0	19.4	169.4	27.6	< 2.0	30.6	65.3	34.1	2071.3	< 5.0	65.2	4.6	3.2
TR-SM-132	132	3306.2	2.2	69.9	< 0.2	< 0.5	< 0.2	13396.7	4.5	1.5	15.9	3266.8	2.0	1505.3	37.2	< 5.0	13.1	232.2	134.9	< 2.0	< 5.0	81.6	30.9	1900.1	< 5.0	24.7	5.1	3.3
TR-SM-142	142	2757.8	2.1	75.6	< 0.2	< 0.5	0.2	15491.3	3.0	1.6	16.2	3925.4	1.6	1493.4	42.1	< 5.0	16.0	149.3	24.3	< 2.0	87.8	78.4	33.8	1933.8	< 5.0	35.2	4.8	2.8
TR-SM-148	148	2004.1	2.1	65.8	< 0.2	< 0.5	< 0.2	15771.4	5.5	1.7	22.2	3960.0	1.9	1606.7	46.0	< 5.0	27.9	180.5	25.0	< 2.0	33.5	72.5	32.9	2201.4	< 5.0	26.6	3.3	2.8
TR-SM-151	151	3352.0	3.7	68.2	< 0.2	< 0.5	0.3	11770.4	4.0	3.7	95.7	3601.3	10.3	1067.7	36.1	< 5.0	129.2	281.0	48.1	< 2.0	65.5	87.9	28.7	2685.4	< 5.0	41.4	4.3	6.8
TR-SM-161	161	1925.3	2.7	63.9	< 0.2	< 0.5	0.2	13240.7	3.1	2.0	40.9	3831.8	4.2	1332.7	42.6	< 5.0	47.6	213.9	30.0	< 2.0	34.4	75.8	28.4	2709.6	< 5.0	24.1	3.2	3.8
TR-SM-171	171	1490.8	2.3	51.3	< 0.2	< 0.5	< 0.2	10742.6	3.5	1.6	18.2	3403.4	< 1.5	1241.3	40.2	< 5.0	19.3	252.1	42.4	< 2.0	66.3	85.8	21.7	2606.5	< 5.0	31.1	2.9	4.2
TR-SM-181	181	1213.2	2.2	32.1	< 0.2	< 0.5	< 0.2	9984.9	4.3	1.6	13.8	3038.7	< 1.5	1180.3	38.3	< 5.0	11.9	227.3	36.4	< 2.0	79.1	70.2	16.9	2498.5	< 5.0	23.3	2.9	6.8
TR-SM-191	191	1957.1	3.2	33.2	< 0.2	< 0.5	0.2	8266.6	6.9	2.9	25.6	3028.0	2.0	1055.9	38.7	< 5.0	30.3	288.5	42.3	< 2.0	18.8	67.8	15.7	3383.7	< 5.0	35.6	4.8	11.6
TR-SM-203	203	4355.9	4.0	49.5	< 0.2	< 0.5	0.7	8130.3	14.2	5.6	106.6	4491.9	10.9	1373.6	46.0	< 5.0	121.5	442.2	123.6	< 2.0	< 5.0	71.3	20.2	3017.3	< 5.0	98.3	10.3	35.0
TR-SM-212	212	5100.4	3.5	42.9	< 0.2	< 0.5	0.7	6792.6	23.8	6.9	38.9	5601.4	2.4	2155.7	67.2	< 5.0	24.3	528.9	209.1	< 2.0	< 5.0	117.2	15.3	2804.5	< 5.0	183.0	18.2	67.1
TR-SM-222	222	5779.7	4.2	49.3	< 0.2	< 0.5	0.8	6680.3	29.1	9.0	48.7	5755.5	2.0	2180.9	67.6	< 5.0	36.2	563.1	246.5	< 2.0	< 5.0	152.3	16.1	3200.5	< 5.0	219.5	24.8	70.8
TR-SM-232	232	5138.6	4.1	33.7	< 0.2	< 0.5	0.5	5791.4	31.0	10.7	52.5	5779.5	3.3	2154.3	63.4	< 5.0	44.6	536.8	228.8	< 2.0	< 5.0	132.4	14.7	2587.7	< 5.0	194.3	29.4	52.4
TR-SM-242	242	5049.2	3.8	25.9	< 0.2	< 0.5	< 0.2	2689.5	28.9	7.8	41.1	8667.4	3.2	3293.5	95.9	< 5.0	22.5	433.6	347.1	< 2.0	< 5.0	95.5	9.2	2479.0	< 5.0	362.4	22.0	27.3

TR-SM-246	246	4501.7	< 1.5	28.8	< 0.2	< 0.5	< 0.2	1780.1	19.4	5.9	15.7	7156.0	2.8	2946.3	90.3	< 5.0	14.5	401.9	397.4	< 2.0	357.2	93.1	6.6	234.8	< 5.0	329.0	14.2	16.9			

Appendix Table 8 *ICP-OES geochemical assay for Transplant, which includes the following elements; Aluminum (Al), Arsenic (As), Barium (Ba), Beryllium (Be), Boron (B), Cadmium (Cd), Calcium (Ca), Chromium (Cr), Cobalt (Co), Copper (Cu), Iron (Fe), Lead (Pb), Magnesium (Mg), Manganese (Mn), Molybdenum (Mo), Nickel (Ni), Phosphorus (P), Potassium (K), Selenium (Se), Silicon (Si), Sodium (Na), Strontium (Sr), Sulfur (S), Thallium (Tl), Titanium (Ti), Vanadium (V), Zinc (Zn).*

Appendix 5 Testate Amoebae Supplementary Data

Cartier Testate Amoebae Supplementary Data

Species	Depth (cm)																														
	2	**4**	**6**	**8**	**10**	**12**	**14**	**16**	**17**	**20**	**22**	**24**	**26**	**28**	**30**	**32**	**34**	**36**	**38**	**40**	**42**	**44**	**46**	**48**	**50**	**60**	**70**	**80**	**90**	**100**
Alabasta militaris	31	51	46	30	54	30	49	31	34	6	4	36	24	26	24	36	31	33	14	16	4	6	0	0	2	0	0	0	0	0
Arcella discoides type	0	2	1	0	2	2	3	4	0	0	5	4	12	7	10	10	5	4	10	4	20	4	5	2	5	0	2	2	1	0
Arcella hemispherica type	0	2	0	0	1	0	0	0	0	2	3	0	0	1	0	0	0	0	0	0	0	0	0	4	5	2	4	0	1	1
Archerella flavum	0	0	0	0	0	0	0	0	0	0	0	0	0	0	0	0	0	0	2	0	0	0	0	0	3	9	1	4	0	0
Assulina muscorum type	17	4	11	10	10	9	26	6	0	18	11	32	18	7	1	3	1	2	1	0	0	0	0	0	0	0	0	4	0	0
Assulina seminulum type	0	1	0	0	0	0	0	0	0	0	0	0	0	4	1	2	0	0	0	0	0	0	0	0	0	0	0	0	0	0
Bullinularia indica	0	0	0	0	0	0	0	0	0	0	0	0	0	3	0	0	2	0	1	0	0	0	0	0	1	0	1	0	0	0
Centropyxis aculeata type	0	3	1	1	0	1	0	0	0	0	0	4	0	2	1	0	2	0	0	0	0	0	0	0	0	0	0	0	0	0
Centropyxis cassis type	0	1	0	0	0	0	0	0	0	0	0	0	0	0	1	0	0	0	0	0	0	0	0	0	0	0	0	0	0	0
Centropyxis ecornis type	0	0	0	0	1	0	1	0	0	0	0	0	0	0	0	0	0	0	0	0	0	0	0	0	0	0	0	0	0	0
Centropyxis spp.	6	0	0	0	0	0	0	0	0	0	0	0	0	0	0	0	0	0	0	0	0	0	0	0	0	0	0	0	0	0
Corythion-Trinema type	1	7	1	8	0	1	3	0	0	4	3	0	0	1	2	0	0	0	0	0	0	0	0	0	0	0	0	0	0	0
Cyclopyxis arcelloides type	0	1	0	8	3	1	0	2	0	0	0	0	0	22	22	15	16	15	30	65	22	50	4	0	3	1	0	0	0	1
Difflugia globulosa type	0	0	0	0	0	0	0	0	0	0	0	0	22	0	0	0	1	0	0	0	0	6	0	0	1	0	0	2	1	0
Difflugia pulex	1	5	12	26	47	20	32	18	12	0	6	32	52	7	11	38	46	28	18	51	24	32	4	0	5	0	0	0	0	0
Difflugia spp.	0	0	0	0	0	0	0	0	0	0	0	0	0	0	0	7	5	4	10	4	0	4	0	0	0	0	0	0	0	0
Euglypha strigosa type	0	0	3	3	0	1	0	0	0	0	0	0	0	0	0	0	0	0	0	0	0	0	0	0	0	0	0	0	0	0
Euglypha tuberculata type	1	8	6	11	6	4	3	2	4	2	8	12	2	7	8	2	1	0	0	0	0	0	0	0	1	0	0	0	0	0
Heleopera petricola	3	5	3	6	1	7	1	0	4	0	0	4	0	1	10	2	0	1	0	2	12	4	1	0	1	0	0	0	0	0
Heleopera sylvatica	11	0	7	0	4	0	9	13	4	2	0	0	0	3	0	0	0	1	1	2	0	0	0	0	0	0	0	0	0	0
Hyalosphenia elegans	36	28	0	0	0	0	0	0	0	78	56	16	2	8	3	1	1	2	0	0	0	0	0	0	0	0	0	0	0	0
Hyalosphenia minuta	3	0	0	0	0	0	0	0	0	0	0	0	0	0	0	0	0	0	0	0	0	0	0	0	0	0	0	0	0	0
Hyalosphenia papilio	0	0	0	0	0	0	0	0	4	0	0	0	0	2	0	0	0	15	6	2	18	0	0	1	1	0	1	0	0	0
Hyalosphenia subflava	1	2	23	9	9	21	11	2	6	0	0	0	0	23	44	35	28	22	12	20	12	8	49	72	42	25	82	3	3	12
Nebela tincta type	32	23	15	5	5	15	12	6	6	0	0	8	0	5	11	0	6	6	3	1	20	0	0	0	2	0	0	0	0	0
Padaungiella wailesi type	0	10	1	15	0	15	0	4	22	0	0	0	0	0	2	0	4	2	0	0	0	0	0	0	0	0	0	0	0	0

Phryganella acropodia type	0	0	0	0	0	0	0	0	0	0	0	0	0	3	1	1	0	1	0	0	0	0	0	0	5	0	0	0	0	2
Physochila griseola	0	3	0	6	1	2	0	2	0	6	4	4	2	0	0	0	0	0	0	0	0	0	0	1	0	1	0	0	0	0
*Trigonopyxis arcu*la type	7	3	7	11	9	13	9	8	2	4	1	20	9	9	11	14	7	2	10	10	8	4	1	2	20	13	14	1	4	108
degraded / indent	0	1	4	1	5	1	7	2	8	0	0	0	0	13	0	15	0	16	5	0	0	8	1	1	4	0	0	1	0	0
Total	**150**	**160**	**141**	**150**	**158**	**143**	**166**	**100**	**106**	**122**	**101**	**172**	**143**	**154**	**163**	**181**	**156**	**154**	**123**	**177**	**140**	**126**	**66**	**82**	**102**	**50**	**105**	**17**	**10**	**124**

Appendix Table 9 *Testate amoebae supplementary data for Cartier, including species / complex names, sample depths (cm), species abundance for each sample depth, and total TA abundances for each depth.*

Laurentian Testate Amoebae Supplementary Data

Species	Depth (cm)																													
	0	**3**	**5**	**7**	**10**	**12**	**14**	**16**	**18**	**23**	**25**	**27**	**29**	**31**	**33**	**35**	**37**	**39**	**41**	**43**	**45**	**47**	**49**	**51**	**59**	**69**	**79**	**89**	**99**
Alabasta militaris	0	0	0	0	0	0	0	0	0	11	3	2	16	0	4	1	0	1	0	0	0	0	0	0	0	0	0	0	0
Arcella discoides type	0	0	0	0	0	4	7	3	8	0	1	2	0	0	0	0	1	0	0	0	0	0	0	0	1	1	0	1	0
Arcella hemispherica type	0	0	0	0	0	0	0	0	0	0	3	1	0	0	0	4	0	0	0	0	0	0	0	0	3	6	0	1	1
Arcella spp.	0	0	1	6	12	3	3	12	0	18	0	4	0	5	0	0	0	0	0	0	0	0	0	0	0	0	0	0	0
Archerella flavum	0	0	0	0	0	0	0	0	0	0	2	0	0	4	1	1	0	0	0	0	0	0	0	0	0	0	0	0	0
Assulina muscorum type	12	11	2	0	1	0	0	0	0	14	1	8	0	1	0	1	0	2	0	0	0	0	0	0	0	0	0	0	0
Assulina seminulum type	0	0	0	0	0	0	0	0	3	0	0	0	0	0	0	0	0	0	0	0	0	0	0	0	0	0	0	0	0
Centropyxis aculeata type	0	0	0	0	0	0	1	0	0	5	6	3	9	1	4	1	0	0	0	0	0	0	0	0	1	0	0	0	0
Centropyxis cassis type	25	3	5	0	0	0	3	2	1	3	0	4	0	0	0	0	0	0	0	0	0	0	0	0	0	0	0	0	0
Centropyxis ecornis type	0	0	0	0	0	0	0	2	0	0	0	0	0	0	0	0	0	0	0	0	0	0	0	0	0	0	0	0	0
Centropyxis platystoma type	0	0	0	0	0	0	2	0	0	11	3	0	0	1	4	3	2	0	0	0	0	0	0	0	0	0	7	2	0
Corythion-Trinema type	33	0	6	1	1	0	0	3	0	0	1	0	0	0	0	0	0	0	0	0	0	0	0	0	0	0	0	0	0
Cyclopyxis arcelloides type	1	0	31	20	0	50	53	16	41	12	14	17	16	25	11	9	0	2	1	0	0	0	0	0	0	0	0	0	0
Difflugia globulosa type	0	37	58	36	180	29	3	19	5	109	24	15	6	20	0	1	1	0	0	0	0	0	0	0	0	0	0	0	0
Difflugia kempnyi	1	0	0	0	0	0	0	0	0	0	0	0	0	0	0	0	0	0	0	0	0	0	0	0	0	0	0	0	0
Difflugia oblonga type	0	0	9	0	0	0	0	0	0	2	0	0	0	0	0	0	0	0	0	0	0	0	0	0	0	0	0	0	0
Difflugia pulex	33	0	11	33	0	1	0	2	4	35	15	8	9	7	9	2	2	0	0	0	0	0	0	0	0	0	0	0	0
Euglypha rotunda type	61	0	4	25	0	0	1	0	0	1	0	0	0	0	0	0	0	0	0	0	0	0	0	0	0	0	0	0	0
Euglypha tuberculata type	0	0	0	0	0	0	0	0	0	0	3	0	0	0	0	3	0	0	0	0	0	0	0	0	0	0	0	0	0
Heleopera petricola	42	2	0	0	0	3	0	0	3	0	0	1	0	0	0	0	0	0	0	0	0	0	0	0	0	0	0	0	0
Heleopera rosea	0	0	0	0	0	0	0	0	0	1	1	0	0	0	0	2	1	0	0	0	0	0	0	0	0	0	0	0	0
Heleopera sphagni	0	0	0	0	1	1	0	0	0	2	0	0	0	1	0	0	0	0	0	0	0	0	0	0	0	0	0	0	0
Heleopera sylvatica	0	0	1	0	0	0	0	0	0	1	1	0	0	0	0	0	0	0	0	0	0	0	0	0	0	0	0	0	1
Hyalosphenia elegans	6	0	0	0	0	0	0	0	0	1	0	0	0	0	0	0	0	0	0	0	0	0	0	0	0	0	0	0	0
Hyalosphenia papilio	0	0	0	0	1	1	4	8	4	14	4	4	1	0	1	1	3	1	0	0	0	0	0	0	0	0	0	2	3
Hyalosphenia subflava	0	0	4	4	0	1	6	9	8	3	8	26	16	29	42	41	40	64	9	11	0	0	0	0	5	3	1	2	1
Nebela tincta type	0	0	0	0	4	0	0	1	0	2	2	7	20	1	1	1	0	0	0	0	0	0	0	0	0	0	0	0	0

Padaungiella lageniformis	0	0	0	1	0	0	0	0	0	0	0	0	0	0	0	0	0	0	0	0	0	0	0	0	0	0	0	0	0
Phryganella acropodia type	8	0	70	1	4	39	27	12	11	13	3	0	0	0	0	0	0	0	0	0	0	0	0	0	0	0	0	0	3
Physochila griseola	166	282	180	15	3	1	9	4	4	2	0	0	0	0	0	1	0	0	0	0	0	0	0	0	0	0	0	0	0
Pseudodifflugia fulva type	0	0	11	0	0	0	0	3	0	0	0	0	0	0	0	0	0	0	0	0	0	0	0	0	0	0	0	0	0
Tracheleuglypha dentata	0	0	0	0	0	0	0	0	0	1	0	0	0	0	0	0	0	0	0	0	0	0	0	0	0	0	0	0	0
Trigonopyxis arcula type	0	0	1	0	0	1	0	4	4	3	9	8	8	6	23	24	12	10	1	0	0	0	0	0	0	0	2	2	1
degraded / indent	0	0	7	0	0	9	16	8	4	0	0	5	0	0	0	0	1	0	1	0	0	0	0	0	0	0	0	0	0
Total	**388**	**335**	**401**	**142**	**207**	**143**	**135**	**108**	**100**	**264**	**104**	**115**	**101**	**101**	**100**	**96**	**63**	**80**	**12**	**11**	**0**	**0**	**0**	**0**	**10**	**10**	**10**	**10**	**10**

Appendix Table 10 *Testate amoebae supplementary data for Laurentian, including species / complex names, sample depths (cm), species abundance for each sample depth, and total TA abundances for each depth.*

Transplant Testate Amoebae Supplementary Data

Species	Depth (cm)																												
	0	**2**	**3**	**4**	**5**	**6**	**7**	**8**	**9**	**10**	**12**	**13**	**15**	**18**	**21**	**23**	**25**	**27**	**29**	**31**	**35**	**37**	**42**	**47**	**53**	**59**	**71**	**81**	**91**	**99**
Alabasta militaris	0	0	0	0	0	0	0	0	0	0	0	0	0	0	0	0	0	0	0	0	4	0	0	0	0	0	0	0	0	0
Archerella flavum	0	1	0	0	1	0	0	0	0	0	0	0	0	0	0	0	0	0	1	0	0	0	0	0	0	0	0	0	0	0
Arcella catinus	0	0	0	0	2	0	0	0	0	0	0	0	0	0	0	0	0	0	0	0	0	0	0	0	0	0	0	0	0	0
Arcella discoides type	20	4	16	28	13	11	9	18	0	7	0	3	1	1	1	1	1	0	0	2	2	0	0	0	0	0	0	0	0	0
Arcella hemispherica type	0	0	0	0	0	0	0	0	0	0	0	0	0	0	0	1	0	0	0	0	4	2	0	0	0	0	0	0	0	0
Arcella spp.	0	1	0	0	0	0	0	0	0	0	0	0	0	0	0	0	0	0	0	1	0	0	0	0	0	0	0	0	0	1
Arcella vulgaris	0	0	0	0	0	0	0	0	0	0	0	0	1	1	0	0	0	0	0	0	0	0	0	0	0	0	0	0	0	0
Assulina muscorum type	24	2	12	0	19	11	2	2	0	4	3	0	0	0	0	0	0	0	0	0	2	0	0	0	0	0	0	0	0	0
Bullinularia indica	8	0	0	0	0	0	0	0	0	0	0	0	0	0	0	0	0	0	0	0	0	0	0	0	0	0	0	0	0	0
Centropyxis aculeata type	0	0	0	0	0	0	0	0	0	0	0	0	0	2	1	0	0	1	0	0	0	0	0	0	0	0	0	0	0	0
Centropyxis cassis type	0	0	0	0	79	0	1	0	0	5	0	1	0	1	2	0	0	0	0	0	0	0	0	0	0	0	0	0	0	0
Centropyxis platystoma type	20	0	5	0	0	7	0	2	0	2	0	0	0	2	0	0	0	0	0	0	3	0	0	0	0	0	0	0	0	0
Centropyxis spp.	0	1	0	0	0	0	0	0	0	0	0	0	0	0	0	0	0	0	0	0	0	0	0	0	0	0	0	0	0	0
Corythion-Trinema type	16	15	1	18	20	11	17	0	0	22	0	5	4	0	0	0	0	0	0	0	0	0	0	0	0	0	0	0	0	0
Cyclopyxis arcelloides type	0	0	9	8	6	36	20	24	102	41	82	103	84	60	20	12	0	0	0	1	7	0	0	0	0	0	0	0	0	0
Cyclopyxis eurystoma	0	0	0	0	0	0	0	0	0	0	0	0	0	0	56	25	0	0	0	0	0	0	0	0	0	0	0	0	0	0
Difflugia pulex	0	25	46	68	10	21	6	34	6	6	0	5	0	1	5	3	0	0	0	0	0	0	0	0	0	0	0	0	0	0
Difflugia leidyi	0	0	0	0	0	0	0	0	0	0	0	2	0	1	0	1	0	0	0	0	0	0	0	0	0	0	0	0	0	0
Difflugia globulosa type	0	2	0	0	0	0	0	14	0	3	5	2	2	2	0	0	0	0	0	0	0	0	0	0	0	0	0	0	0	0
Euglypha tuberculata type	56	6	0	8	35	0	9	0	0	4	4	1	1	5	0	0	0	0	0	0	0	0	0	0	0	0	0	0	0	0
Heleopera petricola	8	0	0	4	0	0	1	0	0	0	0	0	0	0	0	0	0	0	0	0	0	0	0	0	0	0	0	0	0	0
Heleopera sylvatica	0	0	0	0	6	0	1	0	0	0	0	0	0	0	0	0	0	0	0	0	0	0	0	0	0	0	0	0	0	0
Hyalosphenia papilio	0	0	0	0	0	0	0	0	0	0	0	0	0	0	0	1	0	0	0	0	0	0	0	0	0	0	0	0	0	0
Hyalosphenia subflava	4	288	145	60	10	61	20	12	2	3	2	2	7	15	16	80	34	68	51	22	22	8	0	6	1	0	0	0	0	0

Nebela tincta type	84	31	73	0	160	78	28	0	4	5	0	0	0	1	0	0	0	2	0	0	0	0	0	0	0	0	0	0	0	0
Phryganella acropodia type	0	4	0	0	2	0	10	0	0	25	0	7	21	6	0	0	0	0	0	0	0	0	0	0	0	0	0	0	0	0
Trigonopyxis arcula type	0	0	2	0	2	9	0	6	12	3	5	0	0	3	5	2	10	3	1	1	6	0	0	4	0	0	0	0	10	2
degraded / indent	0	0	0	0	11	1	5	0	0	8	0	10	2	4	7	6	5	0	0	0	0	0	0	0	0	0	0	0	0	0
Total	**240**	**380**	**309**	**194**	**376**	**246**	**129**	**112**	**126**	**138**	**101**	**141**	**123**	**105**	**113**	**132**	**50**	**74**	**53**	**27**	**50**	**10**	**0**	**10**	**1**	**0**	**0**	**0**	**10**	**3**

Appendix Table 11 *Testate amoebae supplementary data for Transplant, including species / complex names, sample depths (cm), species abundance for each sample depth, and total TA abundances for each depth.*

Appendix 6 Carbon – Nitrogen Chemistry Supplemental Data (C_{org}, LARCA, C_{inorg}, C/N)

Cartier Carbon – Nitrogen Chemistry Supplemental Data

Sample Code	Depth (cm)	Organic C (%)	Inorganic C (%)	Sulfur (%)	Nitrogen (%)	Volume (cc)	Dry Weight (g)	Bulk Density	Organic C Density	Sulfur Density (mg/cc)	Organic C Accumulation Rate	Organic C / Inorganic C	Carbon / Nitrogen
CART-C-2	2	39.45	2.70	0.06	0.48	25.06	0.84	0.03	0.01	0.02	10.58	14.61	82.19
CART-C-3	3	39.04	5.38	0.04	0.41	18.39	0.84	0.05	0.02	0.02	16.19	7.26	95.22
CART-C-4	4	37.85	4.05	0.05	0.45	10.44	0.35	0.03	0.01	0.02	10.56	9.35	84.11
CART-C-6	6	8.28	0.93	0.05	0.36	25.70	0.76	0.03	0.00	0.01	1.74	8.90	23.00
CART-C-7	7	38.96	3.37	0.06	0.75	16.56	0.95	0.06	0.02	0.03	11.15	11.56	51.95
CART-C-8	8	41.27	2.98	0.06	0.69	17.60	1.14	0.07	0.03	0.04	14.90	13.85	59.81
CART-C-10	10	42.95	3.02	0.06	0.78	17.66	1.17	0.07	0.03	0.04	17.27	14.22	55.06
CART-C-11	11	41.40	3.50	0.04	0.57	15.87	0.74	0.05	0.02	0.02	6.90	11.83	72.63
CART-C-12	12	42.30	2.57	0.05	0.73	18.00	0.88	0.05	0.02	0.02	8.66	16.46	57.95
CART-C-13	13	40.09	3.73	0.05	0.68	14.18	0.52	0.04	0.01	0.02	9.84	10.75	58.96
CART-C-14	14	41.44	3.48	0.05	0.70	15.84	0.45	0.03	0.01	0.01	7.80	11.91	59.20
CART-C-15	15	40.91	4.44	0.05	0.74	16.32	0.53	0.03	0.01	0.02	8.23	9.21	55.28
CART-C-16	16	40.52	4.05	0.05	0.66	14.28	0.60	0.04	0.02	0.02	7.71	10.00	61.39
CART-C-17	17	40.94	3.49	0.04	0.63	18.38	0.69	0.04	0.02	0.01	8.50	11.73	64.98
CART-SM-19	19	40.36	2.79	0.10	0.85	3.11	0.15	0.05	0.02	0.05	10.25	14.47	47.48
CART-SM-21	21	40.82	3.45	0.18	1.02	2.38	0.09	0.04	0.01	0.07	6.28	11.83	40.02
CART-SM-23	23	40.88	2.67	0.24	1.28	3.99	0.23	0.06	0.02	0.14	8.21	15.31	31.94
CART-SM-25	25	42.03	2.48	0.33	1.33	4.62	0.26	0.06	0.02	0.18	8.54	16.95	31.60
CART-SM-27	27	41.80	2.49	0.40	1.16	3.96	0.20	0.05	0.02	0.20	8.97	16.79	36.03
CART-SM-29	29	41.62	2.56	0.40	0.99	2.73	0.15	0.05	0.02	0.22	9.18	16.26	42.04
CART-SM-31	31	43.28	2.33	0.48	0.99	1.62	0.18	0.05	0.02	0.24	20.55	18.58	43.72
CART-SM-33	33	42.93	2.87	0.56	1.29	3.06	0.26	0.08	0.04	0.47	16.46	14.96	33.28

CART-SM-35	35	44.01	2.28	0.59	1.34	3.24	0.12	0.04	0.02	0.23	7.00	19.30	32.84
CART-SM-37	37	42.12	2.16	0.40	0.93	4.56	0.17	0.04	0.02	0.15	6.38	19.50	45.29
CART-SM-39	39	42.10	1.90	0.43	1.16	2.80	0.14	0.05	0.02	0.22	11.76	22.16	36.29
CART-SM-41	41	44.58	2.36	0.51	1.28	4.37	0.30	0.07	0.03	0.35	10.67	18.89	34.83
CART-SM-43	43	45.48	2.61	0.45	1.38	4.25	0.34	0.08	0.04	0.36	12.22	17.43	32.96
CART-SM-45	45	45.99	2.12	0.35	1.53	3.80	0.37	0.10	0.04	0.34	29.51	21.69	30.06
CART-SM-47	47	44.90	2.38	0.33	1.36	2.52	0.19	0.08	0.03	0.25	7.33	18.87	33.01
CART-SM-49	49	45.51	2.30	0.32	1.22	3.60	0.26	0.07	0.03	0.23	4.94	19.79	37.30
CART-SM-51	51	48.04	2.54	0.21	1.46	5.28	0.80	0.15	0.07	0.32	11.71	18.91	32.90
CART-SM-53	53	48.89	2.31	0.19	1.52	3.73	0.56	0.15	0.07	0.29	13.86	21.16	32.16
CART-SM-55	55	49.75	2.37	0.17	1.26	3.31	0.67	0.20	0.10	0.35	21.53	20.99	39.48
CART-SM-57	57	48.71	2.28	0.18	1.32	3.60	0.62	0.17	0.08	0.31	16.83	21.36	36.90
CART-SM-59	59	48.63	3.06	0.19	1.39	3.91	0.54	0.14	0.07	0.26	13.41	15.89	34.99
CART-SM-69	69	50.94	2.15	0.16	1.48	4.80	0.50	0.10	0.05	0.17	7.04	23.69	34.42
CART-SM-79	79	51.79	1.59	0.14	1.49	3.40	0.39	0.11	0.06	0.16	10.79	32.57	34.76
CART-SM-89	89	50.67	1.82	0.13	1.77	3.06	0.45	0.15	0.07	0.19	14.63	27.84	28.63
CART-SM-99	99	51.28	1.80	0.16	1.63	3.42	0.39	0.11	0.06	0.18	9.22	28.49	31.46
CART-SM-109	109	51.93	2.21	0.13	1.39	4.40	0.45	0.10	0.05	0.13	11.34	23.50	37.36
CART-SM-119	119	49.94	2.96	0.11	1.34	3.40	0.36	0.11	0.05	0.12	10.73	16.87	37.27
CART-SM-129	129	49.37	2.54	0.15	2.19	2.74	0.27	0.10	0.05	0.15	16.64	19.44	22.54
CART-SM-139	139	49.83	2.44	0.13	2.30	5.00	0.46	0.09	0.05	0.12	17.36	20.42	21.67
CART-SM-149	149	50.37	2.27	0.14	1.70	5.04	0.43	0.09	0.04	0.12	17.68	22.19	29.63
CART-SM-159	159	49.28	2.18	0.15	1.99	5.50	0.52	0.09	0.05	0.14	17.95	22.61	24.76
CART-SM-169	169	48.71	2.49	0.09	1.14	4.50	0.49	0.11	0.05	0.10	24.91	19.56	42.73
CART-SM-179	179	48.98	2.58	0.13	1.42	4.94	0.42	0.08	0.04	0.11	25.90	18.98	34.49
CART-SM-189	189	49.51	2.36	0.10	1.54	3.78	0.43	0.11	0.06	0.11	36.40	20.98	32.15
CART-SM-199	199	47.02	2.39	0.09	1.21	5.70	0.38	0.07	0.03	0.06	20.20	19.67	38.86
CART-SM-209	209	48.08	2.50	0.08	1.16	4.76	0.41	0.09	0.04	0.07	27.55	19.23	41.45
CART-SM-219	219	47.68	2.74	0.14	1.42	4.40	0.34	0.08	0.04	0.11	25.67	17.40	33.58
CART-SM-229	229	48.78	3.08	0.14	1.86	2.79	0.31	0.11	0.05	0.15	44.43	15.84	26.23
CART-SM-239	239	47.29	2.99	0.19	2.42	4.56	0.33	0.07	0.03	0.14	26.86	15.82	19.54
CART-SM-249	249	48.50	3.10	0.16	1.48	4.62	0.43	0.09	0.04	0.15	37.66	15.65	32.77
CART-SM-259	259	47.88	3.15	0.20	1.84	5.08	0.42	0.08	0.04	0.16	24.81	15.20	26.02
CART-SM-269	269	32.49	0.23	0.27	1.62	5.29	0.68	0.13	0.04	0.35	13.47	141.26	20.06
CART-SM-279	279	22.95	1.76	0.23	1.37	4.97	0.58	0.12	0.03	0.27	8.44	13.04	16.75
CART-SM-289	289	20.78	0.68	0.20	1.18	4.62	0.69	0.15	0.03	0.30	9.74	30.56	17.61
CART-SM-299	299	31.83	2.22	0.23	1.38	6.30	0.59	0.09	0.03	0.21	9.91	14.34	23.07
CART-SM-309	309	20.21	2.21	0.24	1.29	5.57	0.76	0.14	0.03	0.33	9.63	9.14	15.67
CART-SM-319	319	15.72	2.31	0.43	1.31	3.40	0.66	0.20	0.03	0.84	9.75	6.81	12.00
CART-SM-329	329	14.02	1.48	0.38	1.08	4.40	0.82	0.19	0.03	0.71	8.52	9.47	12.98

CART-SM-339	339	6.10	0.67	0.21	0.47	3.75	1.52	0.41	0.02	0.85	11.66	9.10	12.98
CART-SM-349	349	10.12	0.85	0.28	0.78	2.89	0.69	0.24	0.02	0.66	16.55	11.91	12.97
CART-SM-359	359	6.11	0.50	0.20	0.51	2.92	1.13	0.39	0.02	0.77	11.46	12.22	11.98
CART-SM-369	369	6.82	0.91	0.32	0.57	3.96	1.32	0.33	0.02	1.07	8.71	7.49	11.96
CART-SM-379	379	4.85	0.22	0.25	0.36	3.99	1.70	0.43	0.02	1.07			
CART-SM-389	389	6.61	0.52	0.22	0.52	3.20	1.18	0.37	0.02	0.81			
CART-SM-399	399	3.85	0.14	0.15	0.31	3.40	1.78	0.52	0.02	0.78			
CART-SM-409	409	3.85	0.17	0.14	0.30	3.80	2.10	0.55	0.02	0.78			
CART-SM-419	419	1.32	0.05	0.05	0.11	2.82	3.19	1.13	0.01	0.57			
CART-SM-429	429	1.42	0.00	0.05	0.10	3.30	3.87	1.00	0.01	0.50			
CART-SM-439	439	1.61	0.00	0.05	0.12	2.31	1.70	0.74	0.01	0.37			

Appendix Table 12 *Carbon – nitrogen chemistry supplementary data for Cartier, including depth (cm), organic C (%), inorganic C (%), sulfur (%), nitrogen (%), sample volume (cc), sample dry weight (g), bulk density, organic C density, sulfur density (mg/cc), organic C accumulation rate, organic C / inorganic C, and C / N.*

Laurentian Carbon – Nitrogen Chemistry Supplemental Data

Sample Code	Depth (cm)	Organic C (%)	Inorganic C (%)	Sulfur (%)	Nitrogen (%)	Volume (cc)	Dry Weight (g)	Bulk Density	Organic C Density	Sulfur Density (mg/cc)	Organic C Accumulation Rate	Organic C / Inorganic C	Carbon / Nitrogen
LAU-C-1	1	43.57	4.84	0.10	1.29	6.96	0.35	0.05	0.02	0.02	27.11	9.00	33.78
LAU-C-2	2	43.67	4.33	0.11	1.27	5.60	0.45	0.08	0.04	0.04	26.51	10.09	34.39
LAU-C-3	3	42.81	4.12	0.14	1.60	5.76	0.46	0.08	0.03	0.05	27.79	10.39	26.76
LAU-C-4	4	43.11	4.33	0.16	1.74	6.17	0.48	0.08	0.03	0.05	40.48	9.96	24.78
LAU-C-5	5	42.12	4.88	0.19	1.95	3.76	0.47	0.12	0.05	0.10	29.66	8.63	21.60
LAU-C-6	6	41.36	4.15	0.23	2.19	6.12	0.53	0.09	0.04	0.08	26.63	9.97	18.89
LAU-C-7	7	39.14	3.72	0.29	2.37	8.80	0.78	0.09	0.03	0.10	31.36	10.52	16.51
LAU-C-8	8	38.66	3.32	0.32	2.29	4.20	0.48	0.11	0.04	0.14	34.07	11.64	16.88
LAU-C-9	9	38.95	3.10	0.37	2.38	8.80	1.00	0.11	0.04	0.16	31.95	12.56	16.37
LAU-C-10	11	40.26	3.77	0.40	2.34	5.88	0.54	0.09	0.04	0.15	28.30	10.68	17.21
LAU-C-11	13	39.62	4.24	0.38	2.38	4.85	0.43	0.09	0.03	0.13	29.20	9.34	16.65
LAU-C-12	14	42.71	4.03	0.42	2.14	5.71	0.40	0.07	0.03	0.12	25.53	10.60	19.96
LAU-C-13	15	44.81	3.94	0.55	2.14	4.80	0.39	0.08	0.04	0.20	20.02	11.37	20.94
LAU-C-14	16	47.34	3.74	0.72	2.09	4.08	0.44	0.11	0.05	0.37	22.10	12.66	22.65
LAU-SM-24	24	48.09	3.18	0.62	1.65	3.04	0.39	0.13	0.06	0.38	8.20	15.12	29.15
LAU-SM-26	26	48.40	2.91	0.53	1.49	3.42	0.45	0.13	0.06	0.33	14.15	16.63	32.48
LAU-SM-28	28	48.70	3.15	0.46	1.41	3.06	0.47	0.15	0.07	0.34	14.62	15.46	34.54
LAU-SM-30	30	48.61	3.09	0.49	1.48	3.42	0.38	0.11	0.05	0.26	7.28	15.73	32.84
LAU-SM-32	32	49.04	3.01	0.47	1.38	3.42	0.35	0.10	0.05	0.24	4.86	16.29	35.54

LAU-SM-36	36	49.37	2.59	0.37	1.53	3.42	0.53	0.16	0.08	0.28	6.13	19.06	32.27
LAU-SM-38	38	49.90	2.68	0.32	1.62	3.42	0.56	0.16	0.08	0.26	7.50	18.62	30.80
LAU-SM-40	40	49.83	2.94	0.33	1.67	3.60	0.67	0.19	0.09	0.31	8.95	16.95	29.84
LAU-SM-42	42	50.18	2.88	0.30	1.77	2.88	0.53	0.18	0.09	0.28	30.33	17.42	28.35
LAU-SM-44	44	50.43	2.82	0.32	1.51	3.78	0.67	0.18	0.09	0.28	29.33	17.88	33.40
LAU-SM-46	46	50.83	2.54	0.32	1.41	3.36	0.42	0.13	0.06	0.20	24.79	20.01	36.05
LAU-SM-48	48	50.91	2.76	0.27	1.47	3.60	0.71	0.20	0.10	0.27	13.39	18.45	34.63
LAU-SM-50	50	51.07	2.49	0.23	1.48	2.34	0.53	0.23	0.12	0.27	13.61	20.51	34.51
LAU-SM-52	52	51.13	2.43	0.19	1.29	3.06	0.51	0.17	0.09	0.16	14.25	21.04	39.64
LAU-SM-54	54	50.12	2.72	0.32	1.36	3.02	0.59	0.19	0.10	0.31	12.69	18.43	36.85
LAU-SM-56	56	50.09	2.53	0.24	1.32	2.88	0.62	0.22	0.11	0.26	12.13	19.80	37.95
LAU-SM-58	58	52.13	3.06	0.21	1.41	4.00	0.80	0.20	0.10	0.22	13.13	17.04	36.97
LAU-SM-60	60	52.17	2.51	0.24	1.42	4.20	0.82	0.20	0.10	0.25	13.97	20.78	36.74
LAU-70	70	51.33	3.10	0.16	1.36	4.40	0.54	0.12	0.06	0.10		16.56	37.74
LAU-80	80	50.79	3.01	0.14	1.54	3.86	0.47	0.12	0.06	0.09		16.87	32.98
LAU-90	90	49.27	2.80	0.15	1.68	4.37	0.39	0.09	0.04	0.07		17.60	29.33
LAU-100	100	47.26	3.12	0.16	1.73	3.42	0.32	0.09	0.04	0.07		15.15	27.32
LAU-110	110	48.80	3.32	0.18	1.80	3.78	0.43	0.11	0.06	0.10		14.70	27.11
LAU-120	120	48.71	4.20	0.16	1.76	4.36	0.34	0.08	0.04	0.06		11.60	27.68
LAU-131	131	48.85	3.58	0.17	2.02	5.28	0.49	0.09	0.05	0.08		13.65	24.18
LAU-141	141	49.84	3.40	0.17	1.85	3.78	0.28	0.07	0.04	0.06		14.66	26.94
LAU-151	151	47.75	3.38	0.19	1.73	2.88	0.19	0.07	0.03	0.06		14.13	27.60
LAU-163	160	44.37	2.70	0.28	1.94	6.86	0.69	0.10	0.04	0.13		16.43	22.87
LAU-173	170	40.70	2.73	0.29	2.16	3.68	0.36	0.10	0.04	0.12		14.91	18.84
LAU-183	180	37.57	3.37	0.29	2.35	3.84	0.34	0.09	0.03	0.10		11.15	15.99
LAU-193	190	31.93	4.60	0.28	2.13	4.41	0.54	0.12	0.04	0.11		6.94	14.99
LAU-203	200	25.38	4.19	0.30	1.89	4.56	0.75	0.16	0.04	0.12		6.06	13.43
LAU-213	210	23.88	2.10	0.27	1.71	3.59	0.59	0.16	0.04	0.11		11.37	13.96
LAU-223	220	16.20	1.84	0.25	1.32	4.36	0.92	0.21	0.03	0.09		8.80	12.27
LAU-233	228	3.21	0.24	0.14	0.25	4.84	3.02	0.62	0.02	0.03		13.38	12.84
LAU-243	243	1.06	0.03	0.07	0.10	3.36	4.79	1.03	0.01	0.01		35.33	10.60
LAU-253	253	0.53	0.38	0.06	0.03	1.93	4.23	1.43	0.01	0.00		1.39	17.67
LAU-264	264	0.47	0.52	0.02	0.02	3.24	2.95	2.19	0.01	0.00		0.90	23.50
LAU-274	274	0.70	0.22	0.01	0.04	3.74	4.05	0.91	0.01	0.00		3.18	17.50
LAU-284	284	0.70	0.44	0.01	0.04	3.52	4.06	1.08	0.01	0.00		1.59	17.50
LAU-294	294	0.71	0.45	0.01	0.03	4.00	3.79	1.15	0.01	0.00		1.58	23.67
LAU-304	304	0.66	0.38	0.02	0.03	2.79	3.23	0.95	0.01	0.00		1.74	22.00

Appendix Table 13 *Carbon – nitrogen chemistry supplementary data for Laurentian, including depth (cm), organic C (%), inorganic C (%), sulfur (%), nitrogen (%), sample volume (cc), sample dry weight (g), bulk density, organic C density, sulfur density (mg/cc), organic C accumulation rate, organic C / inorganic C, and C / N.*

Sample Code	Depth (cm)	Organic C (%)	Inorganic C (%)	Sulfur (%)	Nitrogen (%)	Volume (cc)	Dry Weight (g)	Bulk Density	Organic C Density	Sulfur Density (mg/cc)	Organic C Accumulation Rate	Organic C / Inorganic C	Carbon / Nitrogen
TR-SM-2	0	43.16	2.31	0.14	1.43	11.09	0.70	0.06	0.03	0.09	16.01	18.68	30.18
TR-SM-3	3	40.85	3.54	0.14	1.56	8.60	0.54	0.06	0.03	0.09	15.97	11.54	26.19
TR-SM-5	5	42.69	2.83	0.14	1.45	10.35	0.94	0.09	0.04	0.13	24.21	15.08	29.44
TR-SM-6	6	42.34	2.59	0.13	1.47	8.68	0.50	0.06	0.02	0.07	18.61	16.35	28.80
TR-SM-7	7	41.28	3.95	0.15	1.69	6.30	0.69	0.11	0.04	0.16	32.08	10.45	24.43
TR-SM-9	9	39.35	3.19	0.21	2.08	6.55	1.09	0.17	0.07	0.35	43.51	12.34	18.92
TR-SM-10	10	40.31	1.87	0.24	2.15	6.16	0.72	0.12	0.05	0.28	33.50	21.56	18.75
TR-SM-12	12	36.83	3.83	0.29	2.17	9.35	1.27	0.14	0.05	0.39	23.31	9.62	16.97
TR-SM-13	13	37.41	3.34	0.32	2.10	2.12	0.76	0.36	0.14	1.16	42.25	11.20	17.81
TR-SM-14	14	38.53	2.49	0.35	2.25	7.50	0.77	0.10	0.04	0.36	14.73	15.47	17.12
TR-SM-15	15	38.2	2.47	0.35	2.28	7.98	0.65	0.08	0.03	0.28	12.92	15.47	16.75
TR-SM-16	16	40.9	4.14	0.39	2.02	3.36	0.43	0.13	0.05	0.50	18.81	9.88	20.25
TR-SM-17	17	41.4	3.11	0.45	2.14	6.12	0.61	0.10	0.04	0.45	18.81	13.31	19.35
TR-SM-18	18	42.61	2.44	0.50	2.10	6.48	0.89	0.14	0.06	0.68	20.11	17.46	20.29
TR-SM-20	20	45.16	2.36	0.48	2.19	3.15	0.49	0.16	0.07	0.75	24.85	19.14	20.62
TR-SM-22	22	45.21	2.56	0.42	2.29	3.40	0.54	0.16	0.07	0.67	15.67	17.66	19.74
TR-SM-24	24	46.08	2.58	0.33	2.14	3.73	0.63	0.17	0.08	0.56	17.53	17.86	21.53
TR-SM-26	26	48.32	2.41	0.25	2.03	3.73	0.70	0.19	0.09	0.47	14.40	20.05	23.80
TR-SM-28	28	48.34	1.87	0.23	1.93	3.80	0.66	0.17	0.08	0.40	11.20	25.85	25.05
TR-SM-30	30	48.77	2.24	0.22	1.86	3.40	0.61	0.18	0.09	0.39	11.67	21.77	26.22
TR-SM-32	32	49.87	1.88	0.23	1.74	3.60	0.51	0.14	0.07	0.32	4.21	26.53	28.66
TR-SM-34	34	49.28	2.17	0.24	1.78	3.78	0.70	0.19	0.09	0.44	5.68	22.71	27.69
TR-SM-36	36	49.85	1.66	0.22	1.69	3.60	0.70	0.19	0.10	0.43	7.39	30.03	29.50
TR-SM-38	38	51.4	2.19	0.20	1.54	3.42	0.72	0.21	0.11	0.42	10.83	23.47	33.38
TR-SM-40	40	50.1	1.82	0.22	1.61	3.60	0.73	0.20	0.10	0.45	9.80	27.53	31.12
TR-SM-42	42	50.77	1.20	0.21	1.63	2.92	0.58	0.20	0.10	0.42	6.23	42.31	31.15
TR-SM-46	46	51.01	1.72	0.22	1.58	3.78	0.64	0.17	0.09	0.37	5.40	29.66	32.28
TR-SM-48	48	49.46	2.87	0.25	1.40	2.26	0.54	0.24	0.12	0.60	9.15	17.23	35.33
TR-SM-50	50	50.59	1.59	0.23	1.53	1.80	0.24	0.14	0.07	0.31	6.59	31.82	33.07
TR-SM-52	52	52.3	1.85	0.23	1.53	3.24	0.75	0.23	0.12	0.53	9.35	28.27	34.18
TR-SM-54	54	52.89	1.54	0.23	1.36	4.41	0.91	0.21	0.11	0.48	8.97	34.34	38.89
TR-SM-56	56	51.22	1.86	0.22	1.45	4.37	0.72	0.16	0.08	0.36	7.64	27.54	35.32
TR-SM-58	58	50.68	1.61	0.20	1.66	4.18	0.66	0.16	0.08	0.32	5.48	31.48	30.53
TR-SM-60	60	51.55	1.46	0.22	1.12	4.83	0.90	0.19	0.10	0.41	5.05	35.31	46.03
TR-SM-62	62	49.66	0.92	0.19	1.59	4.79	1.12	0.23	0.12	0.44	12.18	53.98	31.23
TR-SM-72	72	52.46	1.70	0.17	0.90	5.06	0.83	0.16	0.09	0.28	11.16	30.86	58.29
TR-SM-82	82	49.84	1.42	0.17	1.28	4.00	0.52	0.13	0.07	0.22	11.32	35.10	38.94
TR-SM-92	92	47.18	3.37	0.16	1.26	4.16	0.44	0.11	0.05	0.17	7.92	14.00	37.44
TR-SM-98	98	45.4	3.09	0.15	1.17	3.36	0.32	0.10	0.04	0.14	5.41	14.69	38.80

TR-SM-102	102	46.07	1.78	0.17	1.16	5.29	0.53	0.10	0.05	0.17	6.65	25.88	39.72
TR-SM-112	112	43.59	2.56	0.15	0.89	5.29	0.38	0.07	0.03	0.11	6.02	17.03	48.98
TR-SM-122	122	44.12	2.21	0.17	1.20	6.88	0.57	0.08	0.04	0.14	29.54	19.96	36.77
TR-SM-132	132	40.3	2.54	0.16	1.27	4.42	0.42	0.10	0.04	0.15	28.55	15.87	31.73
TR-SM-142	142	44.59	2.30	0.15	1.09	4.40	0.32	0.07	0.03	0.11	25.96	19.39	40.91
TR-SM-148	148	44.14	2.69	0.17	1.12	5.08	0.36	0.07	0.03	0.12	26.49	16.41	39.41
TR-SM-151	151	47.22	2.07	0.21	1.32	5.32	0.62	0.12	0.06	0.25	47.32	22.81	35.77
TR-SM-161	161	46.18	2.45	0.22	1.40	4.41	0.41	0.09	0.04	0.21	31.68	18.85	32.99
TR-SM-171	171	46.83	2.60	0.21	1.88	4.03	0.45	0.11	0.05	0.23	36.71	18.01	24.91
TR-SM-181	181	47.42	3.03	0.21	2.01	4.13	0.30	0.07	0.03	0.15	29.40	15.65	23.59
TR-SM-191	191	46.58	3.37	0.29	2.46	4.61	0.29	0.06	0.03	0.18	21.60	13.82	18.93
TR-SM-203	203	41.86	0.64	0.27	1.58	5.20	0.44	0.09	0.04	0.23	6.36	65.41	26.49
TR-SM-212	212	21.25	1.34	0.26	1.52	3.23	0.72	0.22	0.05	0.58	6.60	15.86	13.98
TR-SM-222	222	22.27	0.22	0.30	1.64	3.99	0.64	0.16	0.04	0.48	4.40	101.23	13.58
TR-SM-232	232	16.51	1.41	0.24	1.39	3.24	0.55	0.17	0.03	0.41		11.71	11.88
TR-SM-242	242	3.46	0.52	0.23	0.33	4.16	2.19	0.53	0.02	1.21		6.65	10.48
TR-SM-246	246	0.41	0.09	0.02	0.04	2.24	2.78	1.24	0.01	0.25		4.56	10.25

Appendix Table 14 *Carbon – nitrogen chemistry supplementary data for Transplant, including depth (cm), organic C (%), inorganic C (%), sulfur (%), nitrogen (%), sample volume (cc), sample dry weight (g), bulk density, organic C density, sulfur density (mg/cc), organic C accumulation rate, organic C / inorganic C, and C / N.*

Appendix 7 CCA Analysis Raw Data

Predictor	Df	ChiSquare	F	Pr(>F)
tmm_pc1	1	0.380	6.477	0.001
s_percent	1	0.202	3.439	0.001
base_nut_pc1	1	0.120	2.050	0.008
carbon_pc1	1	0.209	3.556	0.001
other_pc1	1	0.190	3.234	0.001
Residual	75	4.398	NA	NA

Appendix Table 15 *CCA anova by term. Including predictor, Df, ChiSquare, F, Pr(>F).*

	Df	ChiSquare	F	Pr(>F)
Model	5	1.100	3.751	0.001
Residual	75	4.398	NA	NA

Appendix Table 16 *CCA anova global. Including Df, ChiSquare, F, Pr (>F).*

CCA1	CCA2	Taxa	Taxa Acronym	abs_score
0.470	-0.995	*Alabasta militaris*	ala_mil	1.465
-0.058	-0.045	*Arcella discoides* type	arc_dis	0.104
-1.595	-0.179	*Arcella hemispherica* type	arc_hem	1.774
-0.914	-0.107	*Archerella flavum*	arc_fla	1.021
0.291	-0.783	*Assulina muscorum* type	ass_mus	1.074
0.668	0.477	*Assulina seminulum* type	ass_sem	1.145
0.047	-0.089	*Bullinularia indica*	bul_ind	0.136
-0.119	0.148	*Centropyxis aculeata* type	cen_acu	0.267
0.752	0.597	*Centropyxis cassis* type	cen_cas	1.350
0.711	0.417	*Centropyxis ecornis* type	cen_eco	1.128
0.348	-2.096	*Centropyxis sp.*	cen_spp	2.444
0.833	-0.145	*Corythion-trinema* type	cor_tri	0.978
0.602	0.818	*Cyclopyxis arcelloides* type	cyc_arc	1.419
0.643	0.842	*Difflugia globulosa* type	dif_glo	1.485
0.465	-0.294	*Difflugia pulex*	dif_pul	0.759
0.032	0.277	*Difflugia spp.*	dif_spp	0.308
0.436	-0.954	*Euglypha strigosa* type	eug_str	1.390
0.483	-0.911	*Euglypha tuberculata* type	eug_tub	1.394
0.560	-0.657	*Heleopera petricola*	hel_pet	1.217
0.266	-1.448	*Heleopera sylvatica*	hel_syl	1.714
0.712	-1.659	*Hyalosphenia elegans*	hya_ele	2.371
0.302	-2.204	*Hyalosphenia minuta*	hya_min	2.505
-0.693	0.060	*Hyalosphenia papilio*	hya_pap	0.753
-0.555	0.155	*Hyalosphenia subflava*	hya_sub	0.710
0.590	-0.468	*Nebela tincta* type	neb_tin	1.058
0.742	-1.387	*Padaungiella wailesi* type	pad_wai	2.129
0.466	0.856	*Phryganella acropodia* type	phr_acr	1.322
1.117	-0.205	*Physochila griseola*	phy_gri	1.322
-0.835	-0.162	*Trigonopyxis arcula type*	tri_arc	0.997
0.345	0.414	Degraded / indent	deg_ind	0.759
-0.165	0.308	*Arcella spp.*	arc_spp	0.474
-1.198	-0.398	*Centropyxis platystoma* type	cen_pla	1.596
1.306	-1.425	*Difflugia kempnyi*	dif_kem	2.731
1.180	0.480	*Difflugia oblonga* type	dif_obl	1.660
1.259	0.034	*Euglypha rotunda* type	eug_rot	1.293
-0.512	0.368	*Heleopera rosea*	hel_ros	0.880
0.500	0.872	*Heleopera sphagni*	hel_sph	1.372
1.238	1.226	*Padaungiella lageniformis*	pad_lag	2.463
1.203	1.119	*Pseudodifflugia fulva* type	pse_ful	2.323
0.349	0.799	*Tracheleuglypha dentata*	tra_den	1.149
0.695	0.893	*Arcella catinus*	arc_cat	1.587
0.635	1.546	*Arcella vulgaris*	arc_vul	2.182
0.179	1.258	*Cyclopyxis eurystoma*	cyc_eur	1.437
0.736	1.353	*Difflugia leidyi*	dif_lei	2.088
0.728	0.186	*Eugylpha tuberculata* type	eug_tub	0.914
0.107	1.169	*Hyalosphenia papilio*	hya_pap	1.276

Appendix Table 17 *CCA species scores, scaling 2. Including CCA1, CCA2, Taxa name, Taxa acronym, abs_score.*

Appendix 8 PERMANOVA Data

	Df	Sum Sq	Mean Sq	F Value	Pr(>F)
Groups	2	0.00194	0.0009691	0.0583	0.937
Residuals	78	1.29619	0.0166179	NA	NA

Appendix Table 18 *Permutation test for homogeneity of multivariate dispersions.*

	Df	Sum Sq	R2	F	Pr(>F)
Phase	2	2.4372	0.1032	5.0360	0.001
Core	2	2.9428	0.1246	6.0808	0.001
Residual	76	18.390	0.7788	NA	NA
Total	80	23.612	1	NA	NA

Appendix Table 19 *PERMANOVA global*

	Df	Sum Sq	R2	F	Pr(>F)
Model	2	2.2789	0.0965	4.1663	0.001
Residual	78	21.333	0.9034	NA	NA
Total	80	23.612	1	NA	NA

Appendix Table 20 *PERMANOVA phase stratified by core.*

Appendix 9 PCA Loadings

	PC1	PC2	PC3	PC4	PC5
calcium_geo	0.5193	0.4018	0.1004	-0.3711	-0.6488
strontium_geo	0.4805	0.4772	-0.0924	-0.0999	0.7230
magnesium_geo	0.4124	-0.3006	0.7869	0.3392	0.0717
phosphorus_geo	-0.5005	0.2476	0.5850	-0.5641	0.1661
percent_n_geo	-0.2805	0.6775	0.1408	0.6472	-0.1533

Appendix Table 21 *PCA loadings base_nut_pc1*

	PC1	PC2
percent_corg_geo	0.7071	0.7071
percent_cinorg_geo	-0.7071	-0.7071

Appendix Table 22 *PCA loadings carbon_pc1*

	PC1	PC2	PC3	PC4	PC5	PC6	PC7	PC8
aluminum_geo	0.3845	0.2931	-0.0677	-0.2957	-0.6501	0.3095	-0.3931	-0.0348
titanium_geo	0.4031	0.3330	-0.0765	-0.1712	0.1985	-0.4158	0.0677	0.6887
iron_geo	0.4001	-0.2770	0.2521	0.4027	0.0821	-0.3907	-0.0589	-0.1738
manganese_geo	0.0318	-0.5958	0.0576	-0.7465	-0.0513	-0.2767	0.0111	-0.0631
chromium_geo	0.4268	-0.1177	0.0981	-0.1581	0.6000	0.6370	-0.0585	-0.0038
cobalt_geo	0.3603	-0.3474	0.3694	0.2888	-0.3967	0.1351	0.5561	0.2111
vanadium_geo	0.4128	0.3278	-0.0795	-0.0912	0.0904	-0.2768	0.4223	-0.6664
silicon_geo	0.2143	-0.3595	-0.8775	0.2166	-0.0550	0.0351	0.0450	0.0374

Appendix Table 23 *PCA loadings other_pc1*

	PC1	PC2	PC3	PC4	PC5	PC6
copper_geo	0.4576	0.2613	0.2082	-0.2492	-0.2126	-0.7560
nickel_geo	0.4332	0.3030	-0.3283	-0.4905	-0.3098	0.5254
lead_geo	0.4448	-0.0110	0.3141	0.6882	-0.4152	0.2388
zinc_geo	0.3534	-0.4991	-0.7251	0.2014	0.0504	-0.2388
cadmium_geo	0.2833	-0.7068	0.4687	-0.4034	0.1137	0.1573
arsenic_geo	0.4470	0.3012	0.0686	0.1422	0.8191	0.1164

Appendix Table 24 *PCA loadings tmm_pc1*